Conformational flexibility and complex formation of biologically relevant molecules studied with high-resolution broadband rotational spectroscopy

Dissertation
zur Erlangung des Doktorgrades
des Fachbereichs Chemie
der Universität Hamburg

Angefertigt am
Max-Planck-Institut
für Struktur und Dynamik der Materie
Hamburg

vorgelegt von
Sabrina Zinn
Hamburg, März 2016

Abstract

"Dem Anwenden muss das Erkennen vorausgehen." (Max Planck)

The motivation to understand intermolecular interactions on a fundamental level encourages natural scientists for more than 120 years. In 1894, Emil Fischer developed the key-lock principle to describe the binding process between an enzyme and a corresponding substrate. As simple and understandable this picture is in general, as complicated and complex is the understanding of it on a molecular level.

Countless examples exist that demonstrate the importance of this key-lock principle, from the interaction between neurotransmitter and receptor or the antigen recognition to the interaction of carbohydrates on the cell surface. All of these examples have in common that large biomolecular systems are involved, built up by long chains of amino acids, monosaccharides or nucleotides. The folding of these chains into a three-dimensional structure, for example in enzymes, often reveals an active site, where the interaction takes place. At the active site only a few molecules might be involved in the so called molecular recognition process. In this work, model systems of biologically relevant molecules and complexes are studied, modeling the active side of a biological system.

For a fundamental understanding of recognition processes in nature it is important to study the interplay between different intermolecular forces, like hydrogen bonding or dispersion interaction. Additionally, it is also essential to gain information about the conformational flexibility of the molecule itself, which allows for structural changes during the recognition process. This can be referred to the induced fit picture, an extension of the key-lock principle, postulated by Daniel E. Koshland in 1958, whereby the substrate induces a structural change in the enzyme upon binding, to fit into the active site.

High-resolution microwave spectroscopy is perfectly suited to study conformational flexibility and intermolecular interactions of biologically relevant molecules. The exceptional accuracy of the obtained spectroscopic constants allows for precise structure determination of gas-phase molecules from only the experimental data. Furthermore, even subtle changes of the structure can be identified in the rotational spectrum, since the spectrum is like a fingerprint of the molecule. The recently developed broadband technique, used in this study, allows for measuring a broad part of the microwave spectrum in a very time efficient way. Different conformers,

isomers or complexes can all be studied in one spectrum.

In the framework of this thesis a broadband microwave spectrometer with an implemented laser ablation source was built up and put into operation. A precise structure determination was achieved for the odorant molecule cinnamaldehyde, which is the main component of cinnamon oil. Furthermore, the widespread drug ibuprofen was studied, which is a highly flexible molecule. Interesting insight into the structural properties, like the preferred orientation of the substitutions of its aromatic ring, could be obtained. Additionally, the interplay of different intermolecular forces was studied on two different complexes. The aggregation of the small sugar glycolaldehyde and the interaction in the diphenylether methanol complex gave information about the competition and cooperativity of hydrogen bonding and dispersion interactions. The second complex is the start of a series of studies of similar complex systems with an increasing size of the alcohol, where it is expected that the dominance of dispersion will be increase.

Zusammenfassung

"Dem Anwenden muss das Erkennen vorausgehen." (Max Planck)

Das Ziel intermolekulare Wechselwirkungen auf einem grundlegenden Niveau zu verstehen motiviert Naturwissenschaftler seit mehr als 120 Jahren. Bereits 1894 entwickelte Emil Fischer das Schlüssel-Schloss-Prinzip, dass den Bindungsprozess zwischen einem Enzym und dem zugehörigen Substrat beschreibt. So verständlich dieses Bild im allgemeinen ist, so kompliziert und komplex ist das fundamentale Verständnis auf molekularer Ebene.

Zahlreiche Beispiele verdeutlichen die Wichtigkeit des Schlüssel-Schloss-Prinzips, von der Wechselwirkung zwischen Neurotransmitter und Rezeptor oder der Antigenerkennung zu den Wechselwirkungen von Sacchariden auf der Zelloberfläche. All diese Beispiele haben gemeinsam, dass große biomolekulare Systeme involviert sind, die aus langen Ketten aus Aminosäuren, Sacchariden oder Nukleotiden aufgebaut sind. Die Faltung der Ketten in eine dreidimensionale Strukturen, wie zum Beispiel in Enzymen, bildet oft ein aktives Zentrum aus, an dem der Prozess der molekularen Erkennung stattfindet. In dieser Arbeit wurden Modellsysteme von biologisch relevanten Molekülen und Komplexen untersuchet, die das aktive Zentrum eines biologischen Systems nachbilden.

Um molekulare Erkennungsprozesse in der Natur fundamental zu verstehen, ist es wichtig das Zusammenspiel verschiedener intermolekularer Wechselwirkungen, wie zum Beispiel Wasserstoffbrückenbindungen oder Dispersion zu untersuchen. Zusätzlich ist es essentiell, die Rolle der Flexibilität der Moleküle an sich zu beleuchten, die auch strukturelle Änderungen während des Erkennungsprozesses ermöglichen. Dies nimmt Bezug auf die *"Induced-fit"* Theorie, die eine Erweiterung des Schlüssel-Schloss-Prinzips darstellt und 1958 von Daniel E. Koshland postuliert wurde, wonach die Annäherung des Substrats eine strukturelle Änderung des Enzyms induziert und die Bindung an das aktive Zentrum damit ermöglicht.

Hochaufgelöste Mikrowellenspektroskopie ist perfekt geeignet um die Flexibilität von biologisch relevanten Molekülen und deren intermolekulare Wechselwirkungen zu untersuchen. Die außerordentliche Genauigkeit der gemessenen spektroskopischen Konstanten erlaubt es, eine präzise Struktur der untersuchten Moleküle in der Gasphase zu bestimmen und dies einzig aus den experimentellen Daten. Zudem können sogar kleinste Änderungen in der Molekülstruktur im Rotationsspektrum identifiziert werden, da das

Spektrum wie ein Fingerabdruck des Moleküls ist. Die kürzlich entwickelte Breitband-Technik, die in dieser Arbeit verwendet wurde, erlaubt es einen breiten Teil des Mikrowellenspektrums in kürzester Zeit aufzunehmen. Unterschiedliche Konformere, Isomere oder Komplexe können so in einem Spektrum untersucht werden.

Im Rahmen dieser Arbeit wurde ein Breitband-Mikrowellenspektrometer mit integrierter Laserablationsquelle aufgebaut und in Betrieb genommen. Damit gelang es die präzise Struktur des Duftstoffes Zimtaldehyd, dem Hauptbestandteil des Zimtöls, zu bestimmen. Des Weiteren wurde das weit verbreitete Schmerzmittel Ibuprofen untersucht, welches ein sehr flexibles Molekül ist. Interessante Einblicke in die strukturellen Möglichkeiten, wie die bevorzugte Orientierung der Substituenten des aromatischen Ringes, konnten erlangt werden. Zusätzlich wurde das Zusammenspiel verschiedener intermolekularer Kräfte anhand zweier Molekülkomplexe untersucht. Die Aggregatbildung des kleinsten Zuckers, Glycolaldehyd, und die Wechselwirkung im Diphenylether-Methanol-Komplex haben Informationen über Konkurrenz- und Kooperativitätsverhalten von Wasserstoffbrückenbindungen und Dispersions-Wechselwirkungen ergeben. Der zweite Komplex ist der Start einer Serie von Studien an ähnlichen Komplexen mit wachsender Alkoholgröße, bei der ein Anstieg der Dominanz von Dispersions-Wechselwirkungen erwartet wird.

Publications

1) Thomas Betz, Sabrina Zinn, Jack B. Graneek and Melanie Schnell. *Nuclear quadrupole coupling constants of two chemically distinct nitrogen atoms in 4-aminobenzonitrile.* Journal of Physical Chemistry A, **118**(28):5164-5169, 2014.

2) Thomas Betz, Sabrina Zinn and Melanie Schnell. *The shape of ibuprofen in the gas phase.* Physical Chemistry Chemical Physics, **17**:4538-4541, 2015.

3) Sabrina Zinn, Thomas Betz, Chris Medcraft and Melanie Schnell. *Structure determination of trans-cinnamaldehyde.* Physical Chemistry Chemical Physics, **17**:16080-16085, 2015.

4) Sabrina Zinn, Chris Medcraft, Thomas Betz and Melanie Schnell. *High-resolution rotational spectroscopy study of the smallest sugar dimer: Interplay of hydrogen bonds in the glycolaldehyde dimer.* Angewandte Chemie International Edition, **128**:6079-6084, 2016.

5) Chris Medcraft, Sabrina Zinn, Melanie Schnell,
Anja Poblotzki, Jonas Altnöder, Matthias Heger, Martin A. Suhm,
Dominic Bernhard, Anke Stamm, Fabian Dietrich, Markus Gerhards
Aromatic embedding wins over classical hydrogen bonding - a multi-spectroscopic approach for the diphenyl ether-methanol complex, submitted May 2016

Contents

Acknowledgment

Chapter 1

Introduction

Intermolecular interactions are of fundamental interest for chemical, physical and biological scientists. They are especially intriguing when it comes to processes in nature, such as molecular recognition, as our whole life is based on these important principles.

A prominent example for molecular recognition can be found in the terminal step of the synthesis of the blood group antigens A and B. Both antigens only differ in the terminal monosaccharide unit, which is galactosamine in the case of blood group A antigens and unsubstituted galactose in the case of blood group B antigens [1, 2]. The terminal transfer of this monosaccharide to an acceptor (the H-antigen) is catalyzed by the highly specific enzymes galactosyltransferases, in which the recognition of the small change in the monosaccharide unit leads to a specific binding (or no binding) to the enzyme [3, 4]. This important biomolecular process is studied, for example, with protein nuclear magnetic resonance (NMR) spectroscopy but the mechanism of the transfer of the monosaccharide, depicted in Figure 1.1, which keeps its configuration at the anomeric center upon the transfer, is still not completely understood [5–8]. This points out the importance of studying molecular recognition also on smaller model complexes, modeling for example the active site of an enzyme, to expand the gained information to larger systems.

The catalysis of the blood group antigens is also an example for the importance of saccharides in nature [9, 10]. Their occurrence, for example on the cell surface, and their conformational flexibility can lead to highly specific recognition processes by forming various intermolecular interactions like hydrogen bonding or dispersion interactions [11–13]. A precise knowledge of the structure, the internal dynamics and the intermolecular interactions involved is needed to get a fundamental understanding of biological processes and is essential, for example, in drug development.
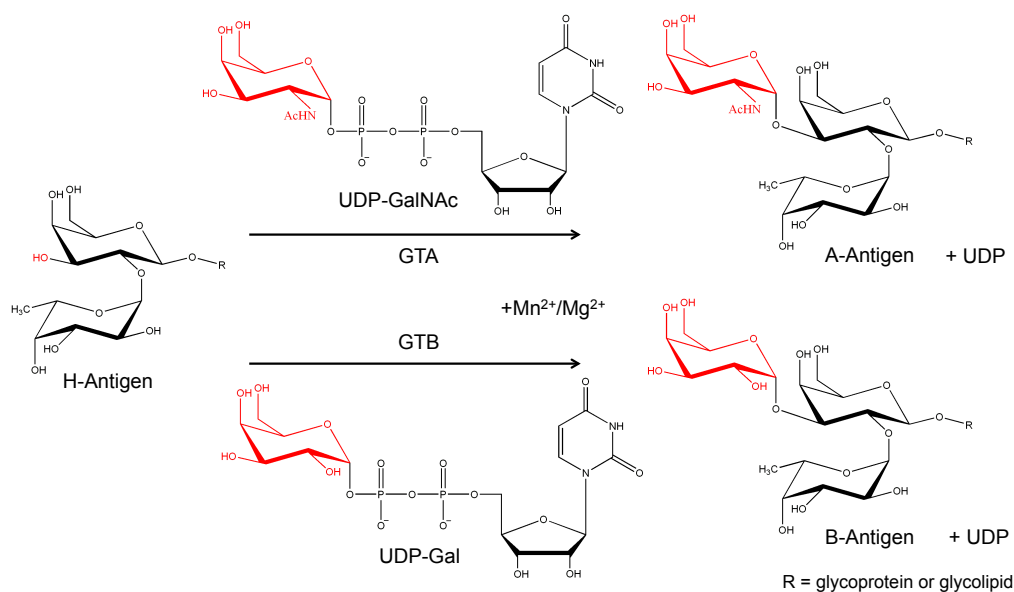
Figure 1.1: *Terminal step of the synthesis of the blood group antigens A and B, catalyzed by the enzymes galactosyltransferase A (GTA) and galactosyltransferase B (GTB). The galactosyl unit (red) is transferred from the activated donor molecule, uridindiphosphate (UDP), to the acceptor molecule, the H-antigen (antigen of the blood group 0). The transfer is highly selective towards a change in the galactosyl unit.*

Spectroscopic investigations of biologically relevant systems can be performed in the solid, the liquid or in the gas phase. In the liquid phase large molecules can be studied using NMR spectroscopy [14, 15]. Richard R. Ernst was awarded with the Nobel Prize for his contribution to the development of high-resolution NMR spectroscopy (1991)[16]. This technique can require a time consuming sample preparation and a large number of NMR spectra have to be measured before the structure can be evaluated. Beside solid state NMR, a common technique to study solid state molecules is X-ray diffraction. Even large molecules like proteins or enzymes can be studied if they can be crystallized. The corresponding structure can be calculated from the patterns of the diffracted X-ray radiation, which is scattered by the electron cloud of the molecules in the crystal. A huge number of protein structures were identified with this method, and famous scientists were awarded with the Nobel Prize for their work , for example Max von Laue (1904, Physics) and Dorothy C. Hodgkin (1964, Chemistry) [17]. Furthermore, in 1951 Bijvoet et al. demonstrated for the first time that the absolute configuration of chiral molecules can be determined using x-ray diffraction [18]. Ongoing attempts to improve this method in

combination with the new x-ray free-electron laser light sources led to the possibility to study dynamics of chemical processes since they provide a time resolution on the order of a femtosecond [19, 20] and in addition no large crystals are needed any more [21].

The method used in this work is high-resolution rotational spectroscopy of molecules in the gas phase, revealing insights to the structure of a sample in a solvent-free environment eliminating any solvent effects. Furthermore, structural changes upon complex formation with one or more water molecules in the gas phase can be studied as well, bridging the results of gas-phase spectroscopy and studies of liquid samples [22–26].

The collection of various techniques described above, covering different phases, points out that an overall knowledge of molecular processes can only be achieved by gathering information from various fields of natural science.

Rotational spectroscopy is based on the excitation of molecules using microwave radiation, covering a frequency range from the centimeter to the millimeter wave region. The use of microwave radiation dates back to military use in World War II, where the RADAR technique became common and the development of electronics for using microwave radiation expanded. The first that time microwave radiation was used for molecular spectroscopy was for measuring absorption spectra of molecules in the early 1940's, and a first review of microwave spectroscopy was already published by Gordy in 1948. [27]. In 1951, Townes and coworkers studied ammonia molecules using microwave radiation in a quadrupole focuser [28–30]. By first selecting ammonia states using an inhomogeneous electric field they created a population inversion, which they afterwards excited using the lowest inversion transition of ammonia, at a wavelength of 12.7 mm, leading to an amplification of the spontaneous emission in the molecule. This resulted in the development of the MASER (Microwave Amplification by Stimulated Emission of Radiation), which was the precursor of the LASER (Light Amplification by Stimulated Emission of Radiation) [31, 32]. For the invention of the MASER Townes, Bassow and Prochonorow were awarded with the Nobel Prize for physics in 1964. Since then a large development of microwave spectroscopy was made and is still ongoing today.

A major step towards the recent high-resolution spectrometers was made by Balle and Flygare who combined emission spectroscopy in the time domain with the supersonic expansion technique [33]. By changing the experimental setup to a coaxial arrangement of the molecular beam and the microwave field Grabow et al. could increase the resolution significantly [34]. The cavity technique used for these experiments reveals a high resolution but has the drawback of a small frequency bandwidth in a sin-

gle measurement. A huge breakthrough in the bandwidth limitations was recently made in the Pate group [35]. They developed the chirped pulse microwave technique, allowing for measuring a broadband microwave spectrum covering several GHz within a single experiment. This improvement led to a fast increase of studies of large and flexible molecules using microwave spectroscopy. Since the rotational spectrum is like a fingerprint of a molecule and the observed rotational lines are narrow and well resolved, it is possible to identify different molecules, isomers, conformers and isotopologues within the same measured broadband spectrum. The only limitations of the technique are that the molecule needs a permanent dipole moment and that it can be brought into the gas phase. This barrier was lowered by combining a Fourier transform microwave spectrometer with a laser ablation source, to bring fragile molecules into the gas phase [36]. Various biologically relevant molecules, like monosaccharides, amino acids, nucleobases, neurotransmitters and drugs could be measured due to this development [37–47].

The information obtained from a microwave spectrum are many-fold. A main advantage is that the measured rotational constants are directly related to the structure of the molecule, since they only depend on the moments of inertia of the molecule. Kraitchman developed specific formulas for calculating the precise atom position from the rotational constants of the molecule and its isotopically substituted species [48]. Modern broadband microwave spectrometers allow to measure the isotopically substituted species of larger molecules and complexes in natural abundance in a very short time due to the high sensitivity. This provides a direct way to determine the precise structure of a molecule only from the experimental data and thus it is possible to benchmark quantum chemical calculations. Furthermore, molecules containing an atom with a nuclear spin larger than $\frac{1}{2}$ show an additional splitting of the transitions due to nuclear quadrupole coupling. The analysis of this coupling provides information of the electronic surrounding of the corresponding nuclei. Hyperfine structure in the spectrum can also be caused by large amplitude motions and internal rotation in the molecule. Their analysis provides information on internal dynamics occurring in the molecule.

Further studies towards reaction dynamics of large molecules were recently undertaken by performing double resonance experiments [49, 50]. The combination of broadband rotational spectroscopy and IR light to excite vibrational motions in the molecule, called dynamic rotational spectroscopy, was successfully used to study the isomerization dynamics in cyclopropane carboxaldehyde and pentenyne. This opens another field of applications for broadband microwave spectroscopy as it enables for exam-

ple a direct determination of reaction rates.

Recently, the ongoing attempt to extend the applications of microwave spectroscopy led to a promising series of studies of chiral molecules [51]. Chiral molecules have almost the same physical properties but can show different chemical and biological behavior. Using conventional spectroscopy, they cannot be differentiated because they have the same rotational constants showing the same spectrum. Due to a small modification of the broadband microwave setup and by applying a second pulse in a perpendicular arrangement, the chiral species can be differentiated in the time domain by their phases in the free-induction decay [52, 53]. The development of this technique was a major breakthrough and a large step towards the goal of the determination of the absolute configuration.

Finally, microwave spectroscopy also is very important in the field of astrochemistry. The high amount of molecular signals from dense gas clouds, measured for example with the new Atacama Large Millimeter/Submillimeter Array (ALMA) radiotelescope [54], needs to be compared to spectroscopic data measured in the laboratory [55–58]. In both cases the molecules, radicals or ions are in the gas phase supporting a direct comparison of the transition frequencies. The astrochemical species can, for example, be produced by using a discharge nozzle, which gives also insight towards the question of how molecules are formed in space [59].

The molecules studied within this work cover a broad part of the features mentioned above. The study of the well known painkiller ibuprofen, for example, gave interesting insights to the conformational behavior of this class of drugs, which can be directly related to their pharmacological function to inhibit the origination of pain. In the rotational spectrum of 4-aminobenzonitrile a complex splitting caused by two distinct nitrogen atoms is analyzed. The results allow for determining the electronic surrounding of the nitrogen atoms, which is additionally compared to structurally related molecules. Furthermore, the precise structure of the odorant molecule *trans*-cinnamaldehyde is studied by recording the rotational spectrum of its isotopologues in natural abundance.

The results for the glycolaldehyde dimer, where the monomer unit is the first and so far only sugar detected in interstellar space, improved our understanding of the interplay of intermolecular interactions for this kind of molecular systems. Since molecular recognition is still not well understood on a molecular level [60], studies of complex systems can improve our knowledge how the different non-covalent interactions reinforce or compete with each other. For the same purpose the complex formed by the aromatic molecule diphenylether and the small alcohol methanol was studied. Diphenylether provides several opportunities for building up

intermolecular interactions with methanol. The two aromatic rings with their delocalized π-electron system might lead to a dominance of dispersion interaction in the complex formation. Furthermore, diphenylether is a rather flexible molecule, revealing a complex splitting in the monomer spectrum caused by large amplitude motions. The change of the flexibility of the molecule upon complex formation is another interesting aspect of this study. This is the first part of a series of studies of complexes formed by diphenylether-like molecules and aliphatic alcohols with increasing complexity. This series will provide insight towards the understanding of molecular recognition driven by intermolecular forces.

In the following chapter the theoretical background for this work is explained in detail and a description of the experimental setup is given thereafter. The obtained experimental results are presented in the Chapters 4 - 8.

Chapter 2

Theoretical background

2.1 Fundamentals of rotational spectroscopy

2.1.1 Rotational Hamiltonian

Rotational spectroscopy involves the excitation and probing of rotational degrees of freedom in a molecule using microwave radiation. The different energy levels in a molecule are represented in Figure 2.1. The molecular energy is mainly influenced by the translational, the electronic, the vibrational and the rotational motions. As these motions happen on different timescales, they can be treated separately. This assumption is known as the Born Oppenheimer approximation, which is an important theory for molecular spectroscopy [61].

The Born Oppenheimer approximation also allows us to separate the electronic and the nuclear energy, since the heavy nuclei barely move on the timescale of the electron motion (attoseconds). This means, that the molecular Hamiltonian can be written as the sum of the electronic ($\hat{H}_{el}$), the vibrational ($\hat{H}_{vib}$), the rotational ($\hat{H}_{rot}$) and the translational ($\hat{H}_{trans}$) contribution [62]:

$$\hat{H}_{total} = \hat{H}_{el} + \hat{H}_{vib} + \hat{H}_{rot} + \hat{H}_{trans} \tag{2.1}$$

The molecular energy and the total wavefunction follow with:

$$E_{total} = E_{el} + E_{vib} + E_{rot} + E_{trans} \tag{2.2}$$

$$\psi_{total} = \psi_{el}\psi_{vib}\psi_{rot}\psi_{trans} \tag{2.3}$$
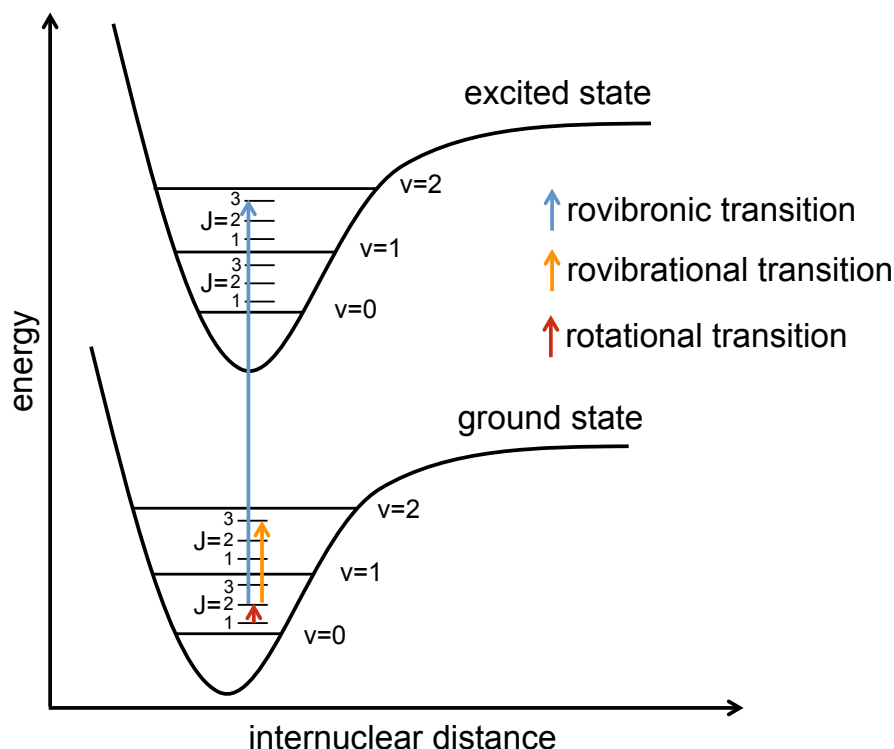
Figure 2.1: *Potential energy curves of the electronic ground state and an electronically excited state in a molecule. The electronic states contain several vibrational states and each vibrational state contains several rotational states. Different types of transitions are depicted.*

In this work only the rotational energy of a system in the electronic and vibrational ground states will be evaluated and for this the time-independent rotational Schrödinger equation has to be solved:

$$\hat{H}_{rot}\psi_{rot} = E_{rot}\psi_{rot} \tag{2.4}$$

To determine the rotational energy of a molecule it is important to know its mass distribution, which is described by the moments of inertia. The moment of inertia in a molecule along an axis a is defined by:

$$I_a = \sum_i m_i r_i^2 \tag{2.5}$$

If we adjust a Cartesian coordinate system such that its origin is placed at the center of mass of the molecule, the corresponding diagonalized inertia

tensor

$$\mathbf{I} = \begin{pmatrix} I_{xx} & 0 & 0 \\ 0 & I_{yy} & 0 \\ 0 & 0 & I_{zz} \end{pmatrix} \tag{2.6}$$

with

$$I_{xx} = \sum_i m_i(y_i^2 + z_i^2) \tag{2.7}$$

$$I_{yy} = \sum_i m_i(z_i^2 + x_i^2) \tag{2.8}$$

$$I_{zz} = \sum_i m_i(x_i^2 + y_i^2) \tag{2.9}$$

is in the principle axis system of the molecule. The axes are label with a, b and c and oriented such that $I_a \leq I_b \leq I_c$.

Due to the symmetry of a molecule and the corresponding moments of inertia, molecules can be sorted into different groups:

Linear Molecules: $I_a = 0$ and $I_b = I_c$; examples are CO_2, OCS or HCN.

Spherical-Top Molecules: All three moments of inertia are equal, $I_a = I_b = I_c$, examples for this group are SF_6 and CH_4.

Symmetric-Top Molecules: Two moments of inertia are equal. Two cases can be differentiated. If $I_a = I_b < I_c$ the molecule is called oblate symmetric-top, for example like benzene or NH_3 and if $I_a < I_b = I_c$ the molecule is called prolate symmetric-top, as in CH_3Cl or in $HCCCH_3$.

Asymmetric-Top Molecules: All three moments of inertia are unique, $I_a \neq I_b \neq I_c$. This is the largest class and all molecules studied within this work belong to this group. Examples for this case are ethanol or all amino acids. A special subgroup are planar asymmetric-top molecules in which $I_c - I_a - I_b = 0$, as for example in H_2O or NO_2.

According to Table 2.1 different representations can be used to transfer the molecular axis system (a, b, c) into the axis system of the laboratory frame (x, y, z).

The rotational energy in a molecule is quantized and the total angular momentum quantum number J is introduced to describe the rotational energy levels.

For linear molecules the energy of a rigid rotor is described as:

$$E(J) = BJ(J+1) \tag{2.10}$$

with the rotational constant

$$B = \frac{\hbar^2}{2I} \tag{2.11}$$

The reduced Planck constant $\hbar$ is defined as:

$$\hbar = \frac{h}{2\pi} \tag{2.12}$$

Table 2.1: *Possible representations of the molecular axis system. The I^r representation is best suited for symmetric and slightly asymmetric prolate tops, whereas the III^r representation should be used to describe symmetric and slightly asymmetric oblate tops.*

	I^r	I^l	II^r	II^l	III^r	III^l
x	b	c	c	a	a	b
y	c	b	a	c	b	a
z	a	a	b	b	c	c

Since a rotating system is not rigid and the atom positions move upon rotation due to centrifugal forces, centrifugal distortion constants are added to Equation 2.10 to correct the energy of rotational levels:

$$E(J) = BJ(J+1) - DJ^2(J+1)^2 + HJ^3(J+1)^3.... \tag{2.13}$$

where D is the quartic and H the sextic centrifugal distortion constant.

For the description of the energy levels of a symmetric-top molecule two rotational constants, A and B, are used and a second quantum number K is established, which is the projection of the total angular momentum along the symmetry axis. The energy levels including centrifugal distortion are given by:

$$\begin{aligned} E_{J,K} = {} & BJ(J+1) + (A-B)K^2 - D_J[J(J+1)]^2 \\ & -D_{JK}[J(J+1)]K^2 - D_K K^4 + H_{JJJ}[J(J+1)]^3 \\ & +H_{JJK}[J(J+1)]^2 K^2 + H_{JKK}[J(J+1)]K^4 \\ & +H_{KKK}K^6 + ... \end{aligned} \tag{2.14}$$

For an asymmetric-top molecule the rotational energy levels cannot be calculated analytically anymore, since the asymmetric-top Hamiltonian does not commute with the projection of the total angular momentum on any of the molecule-fixed axes. The matrix representation of the molecular Hamiltonian has to be evaluated to determine the rotational energy levels. The two-fold K-degeneracy of a symmetric top is lifted in an asymmetric top and each line is split into $2J+1$ components. The degree of asymmetry in an asymmetric top molecule is defined by the asymmetry parameter κ, with

$$\kappa = \frac{2B - A - C}{A - C} \tag{2.15}$$

which can vary between the limiting cases of the prolate symmetric top ($B = C$) with $\kappa = -1$ and the oblate symmetric top ($A = B$) with $\kappa = 1$ [63] (Fig. 2.2). The highest degree of asymmetry will be reached at $\kappa = 0$. The quantum number K is not suited anymore to label the rotational energy levels of an asymmetric molecule, therefore it is replaced by the two quantum numbers K_a and K_c, which describe the projection of K on the a and c inertial axes in the limiting cases of the prolate and oblate symmetric top molecule. The correlation of the energy levels is displayed in Figure 2.3.

Rotational emission or absorption is observable when a molecule has a permanent electric dipole moment. The selection rules for transitions in an asymmetric-top molecule can be listed according to its dipole moment components, listed in Table 2.2.

Table 2.2: *Selection rules for an asymmetric-top molecule.*

| dipole	transition type	ΔJ	ΔK_a	ΔK_c
μ_a	a-type	$0, \pm 1$	$0, \pm 2, ...$	$\pm 1, \pm 3, ...$
μ_b	b-type	$0, \pm 1$	$\pm 1, \pm 3, ...$	$\pm 1, \pm 3, ...$
μ_c	c-type	$0, \pm 1$	$\pm 1, \pm 3, ...$	$0, \pm 2, ...$
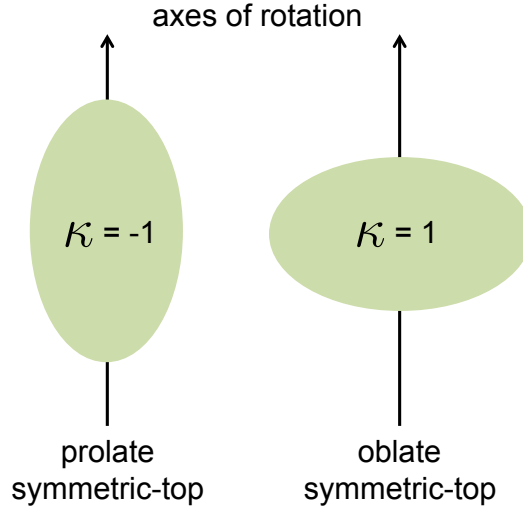
Figure 2.2: *Schematic drawing of the mass distribution in a prolate and in an oblate symmetric-top molecule.*

According to the change in J, transitions with $\Delta J = -1$ form a P-branch, transitions with $\Delta J = 1$ a R-branch and transitions with $\Delta J = 0$ belong to a Q-branch.

In order to simplify the complex molecular Hamiltonian for an asymmetric top molecule, Watson demonstrated that due to symmetry properties the number of terms can be reduced significantly [65–67]. The two established reduction schemes are the A-reduction, suited for most of the asymmetric top molecules and the S-reduction, suited for slightly asymmetric molecules. Using the I_r representation (Tab. 2.1) and including the five quartic centrifugal distortion constants Δ_J, Δ_{JK}, Δ_K, δ_J and δ_K, the A-reduced Hamiltonian has the form:

$$
\begin{aligned}
H^{(A)} = {} & \frac{1}{2}(B^{(A)} + C^{(A)})\hat{J}^2 + [A^{(A)} - \frac{1}{2}(B^{(A)} + C^{(A)})]\hat{J}_z^2 \\
& + \frac{1}{2}(B^{(A)} - C^{(A)})(\hat{J}_x^2 - \hat{J}_y^2) - \Delta_J \hat{J}^4 \\
& - \Delta_{JK}\hat{J}^2\hat{J}_z^2 - \Delta_K\hat{J}_z^4 - 2\delta_J\hat{J}^2(\hat{J}_x^2 - \hat{J}_y^2) \\
& + \delta_K[\hat{J}_z^2(\hat{J}_x^2 - \hat{J}_y^2) + (\hat{J}_x^2 - \hat{J}_y^2)\hat{J}_z^2] + O(6) + ... \quad (2.16)
\end{aligned}
$$

where $\hat{J}_x, \hat{J}_y, \hat{J}_z$ are the angular momentum vectors along the molecular axes and $\hat{J}^2 = \hat{J}_x + \hat{J}_y + \hat{J}_z$.
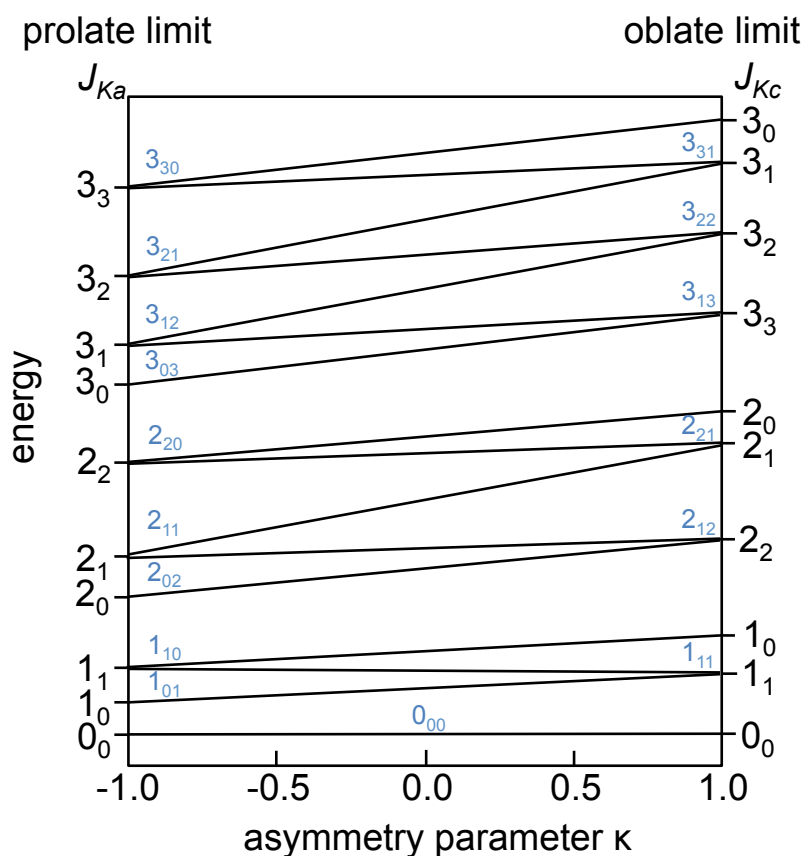
Figure 2.3: *Correlation diagram between the energy levels of a prolate symmetric-top (left) and an oblate symmetric-top (right). The rotational energy levels of an asymmetric-top molecule are plotted as a function of the asymmetry parameter κ and labeled using the King-Hainer-Cross notation $J_{K_a K_c}$ [64].*

The corresponding matrix elements for the A-reduced Hamiltonian are:

$$
\begin{aligned}
\langle JKM|\hat{H}^{(A)}|JKM\rangle &= \frac{1}{2}(B^{(A)} + C^{(A)})(J(J+1) - K^2) \\
&\quad + A^{(A)}K^2 - \Delta_J J^2(J+1)^2 \\
&\quad - \Delta_{JK}J(J+1)K^2 - \Delta_K K^4 \\
&\quad + O(6) + ... \tag{2.17}
\end{aligned}
$$

$$
\begin{aligned}
\left\langle JKM|\hat{H}^{(A)}|JK\pm 2M\right\rangle \;=\; & \frac{1}{4}(B^{(A)}+C^{(A)}) \\
& -\delta_J J(J+1) + \frac{1}{2}\delta_{JK} \\
& [K^2+(K\pm 2)^2]\times[(J(J+1) \\
& -K(K\pm 1))(J(J+1) \\
& -(K\pm 1)(K\pm 2))]^{\frac{1}{2}}+O(6)+... \quad (2.18)
\end{aligned}
$$

The complete S-reduced Hamiltonian with the corresponding matrix elements can be found in Reference [67].

2.1.2 Nuclear quadrupole splitting

Molecules containing one or more atoms with a nuclear spin larger than $I=\frac{1}{2}$ show additional hyperfine splitting in the rotational spectrum. This is caused by the coupling between the nuclear quadrupole moment and the electric field gradient of the molecule, which is induced by the electronic charge distribution. The charge distribution in a nucleus with a nuclear spin of 0 or $\frac{1}{2}$ is spherical and no quadrupole moment exists but for $I=\frac{1}{2}$ spin-rotation coupling can occur, which leads to rather small splittings, typically on the order of less than 1 kHz [68]. Nuclei with $I\geq 1$ have a non-spherical charge distribution and thus a quadrupole moment Q. The spin angular momentum for this nucleus is given by

$$
\mathbf{I} = [I(I+1)]^{\frac{1}{2}}\hbar^2 \qquad (2.19)
$$

Due to the electric field gradient in the molecule this spin angular moment is coupled to the rotational angular momentum $\mathbf{J}$. The coupling of these two vectors results in the total angular momentum $\mathbf{F}$ and the new quantum number F describes the energy levels of the hyperfine structure, which can take the values

$$
F = J+I, J+I-1, ..., |J-1| \qquad (2.20)
$$

by following the selection rule:

$$
\Delta F = 0 \pm 1 \qquad (2.21)
$$

The expression for the energy levels depends again on the type of the rotor. In the case of an asymmetric rotor it is defined by the electric field

gradient, the angular momentum operators and the asymmetry parameter κ.

Each rotational transition is split into several components. The splitting decreases with increasing J and depending on the resolution it starts to coincide for higher J transitions. The width of the splitting depends on the number of quadrupole nuclei, on the spin-angular momentum $\mathbf{I}$ and the nuclear quadrupole moment Q.

The hyperfine splitting is fit by determining the nuclear quadrupole coupling constants χ, which is defined as,

$$\chi = eqQ \tag{2.22}$$

where e is the elementary charge, Q is the atomic nuclear quadrupole moment, which is a known constant depending on the atom, and q is the electric field gradient. The electric field gradient provides information about the electronic surrounding of the quadrupole nucleus and thus can characterize chemical bonding and the degree of hybridization [69].

The nuclear quadrupole coupling constants are a tensor of the form

$$\chi = \begin{pmatrix} \chi_{aa} & \chi_{ab} & \chi_{ac} \\ \chi_{ab} & \chi_{bb} & \chi_{bc} \\ \chi_{ac} & \chi_{bc} & \chi_{cc} \end{pmatrix} \tag{2.23}$$

with the relationship

$$\chi_{aa} + \chi_{bb} + \chi_{cc} = 0. \tag{2.24}$$

In order to compare the nuclear quadrupole coupling constants of different molecules, the nuclear quadrupole tensor has to be transferred from the principle axis system of the molecule (a, b, c) into the principle axis system of the quadrupolar axes (x, y, z). This is done by a rotation of the axis system about a certain angle θ [67, 69].

An example of the analysis of a complex hyperfine splitting caused by two disparate nitrogen atoms in the molecule 4-aminobenzonitrile and how it can be used to determine the electron distribution of the nitrogen atoms is discussed in Chapter 4.

2.1.3 Large amplitude motions and internal rotation

Flexible molecules often show large amplitude motions (LAM). If these motions are on the order of a bond length the structure can change significantly or can even tunnel from one equilibrium position to another one. Different kinds of LAM can be differentiated. A well known one is the

inversion motion of ammonia molecules, which is also known as umbrella motion. The structure changes by tunneling through the planar configuration to its energetically equivalent but inverted, pyramidal configuration. A similar kind of motion is seen in molecules containing an amino group (NH_2-). In these cases the large amplitude motion can be described by a double-well potential for the two minima positions separated by a potential barrier. Tunneling will lift the vibrational degeneracy of these states, which leads to a splitting of the rotational transitions. The size of the splitting of the rotational transitions is directly related to the barrier height of the internal motion.

Beside proton tunneling, ring puckering and structural isomerization, one of the most common large amplitude motions is caused by internal rotation around single bonds. For example, a methyl group (CH_3) can rotate with respect to the rest of the molecule, which can lead to three energetically equivalent minimum positions in the case of an asymmetric top molecule. The coupling between the internal rotation and the overall rotation of the molecule leads two a splitting of the rotational transitions into a nondegenerate A state and a doubly degenerate E state (Fig. 2.4). Due to the hindered internal rotation the rotational Hamiltonian has to be extended including the kinetic and potential energy of the internal rotor. The extended Hamiltonian for an asymmetric molecule including internal rotation is

$$\hat{H}_R = \hat{H}^{(A)} + \hat{H}_I \qquad (2.25)$$

where $\hat{H}^{(A)}$ is the A-reduced rotational Hamiltonian and $\hat{H}_I$ is the Hamiltonian of the internal rotation defined as

$$\hat{H}_I = F(\hat{j}_\alpha - \hat{J})^2 - V(\alpha) \qquad (2.26)$$

where F is the rotational constant for the internal rotor, $\hat{j}$ is the angular momentum operator of the internal rotation, $\mathbf{J}$ is the total angular momentum operator and $V(\alpha)$ is the potential energy with the internal rotation angle α.

In the case of the C_{3v}-symmetric methyl group, the methyl top has a $2\pi/3$, periodicity and the potential energy $V(\alpha)$ can be expressed in the following manner

$$V(\alpha) = \frac{1}{2}V_3(1 - \cos 3\alpha) + \frac{1}{2}V_6(1 - \cos 6\alpha) + ... \qquad (2.27)$$

In most cases, $V_3 \gg V_6$ so that only the first term of the expansion is important. The equation represents then a three-fold potential, which is

depicted in Figure 2.4.
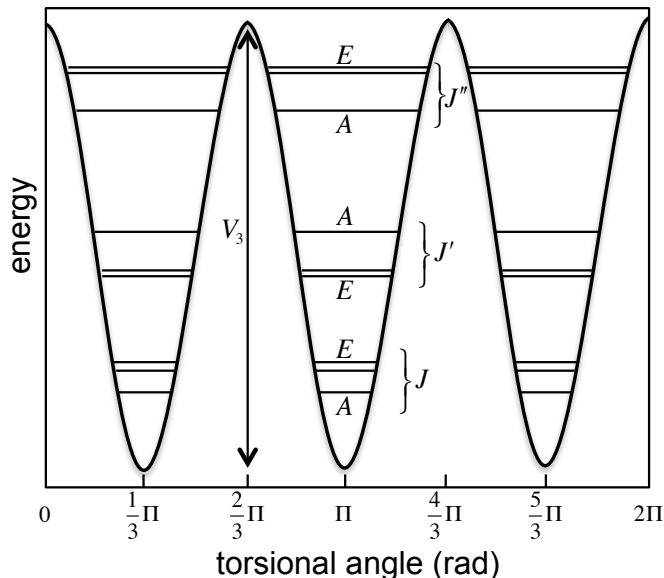
Figure 2.4: *Three fold barrier for the internal rotation of a C_{3v}-symmetric rotor, like a methyl group. The energy levels are split into a doubly degenerate E state and a nondegenerate A state.*

Straightforward solutions for the rotational Hamiltonian can be obtained for the two extreme cases of the potential barrier height. In the case of the very low barrier ($V_3 \rightarrow 0$) it can be regarded as a free rotor where each level is twofold degenerate, which corresponds to the two different possible directions of the rotation in the classical picture. In the limiting case of an infinite barrier ($V_3 \rightarrow \infty$) the solutions for the Hamiltonian are the harmonic oscillator wavefunctions. Each level is then threefold degenerate corresponding to the three-well potential [67].

For internal rotors with finite barrier heights, tunneling through the barrier becomes possible, which leads to a splitting of the triply degenerate levels into an E and an A state, as mentioned above.

The Hamiltonians required for the analysis of rotational spectra featuring internal rotation or other kinds of large amplitude motions and also of molecules containing several internal rotation tops are implemented in a number of fitting programs, such as SPFIT, XIAM or ERHAM. All of them are developed for the analysis of rotational spectra, and a detailed description of their properties can be found in the corresponding literature [70–72]. Additional programs for analyzing rotational spectra are available on the PROSPE homepage [73].

2.1.4   Structure determination methods

High-resolution microwave spectroscopy provides the unique possibility to determine the precise atom position of a molecule solely from the experimental data. The obtained rotational constants contain structural information as shown in Section 2.1.1. They depend on the mass of the molecule, and thus by changing the mass, for example by isotopic substitution, the spectrum of the molecule changes and another set of rotational constants can be determined. The high sensitivity of modern microwave spectrometers allows for the measurement of even rare isotopologues in natural abundance. To a first approximation, the respective atom position is unchanged due to this small mass change, and the rotational constants of the isotopologues increase the structural information obtained from the spectrum.

To describe a molecule containing N atoms in a Cartesian system, 3N coordinates are needed. This correspond to $3N - 6$ independent internal parameters, containing $N - 1$ bond lengths, $N - 2$ bond angles and $N - 3$ dihedral angles. In planar molecules this number is reduced to $2N - 3$ independent internal parameters. The number of independent parameters required for the description of the molecular structure can be obtained by determining the rotational constants of the parent and the singly substituted species of a molecule.

The ground state structure of the molecule, which is measured using microwave spectroscopy, is called the effective structure (r_0) and includes zero point motions of the molecule. The structure with the best comparability between experimental and calculated structures and also between different molecules, is the equilibrium structure (r_e) of the molecule. It describes the distances between vibrationless nuclei in a static system, which are isotopically invariant. This hypothetical structure is obtained at the global minimum of the potential energy surface (Fig. 2.5).

The differences of the equilibrium rotational constants (B_e) and the rotational constants of the molecule in the ground state (B_0) can be described as the sum of the normal modes in the molecule, expressed as

$$B_e = B_0 + \sum_i \alpha_i \frac{d_i}{2} \tag{2.28}$$

with the vibrational degeneracy d_i and the rovibration constant α. In a molecule with N atoms, $3N - 6$ vibrational normal modes are present, resulting in the same number of singly excited vibrational states that need to be studied to correct the ground state constants for their zero point contribution and to obtain the equilibrium constants. This was done so
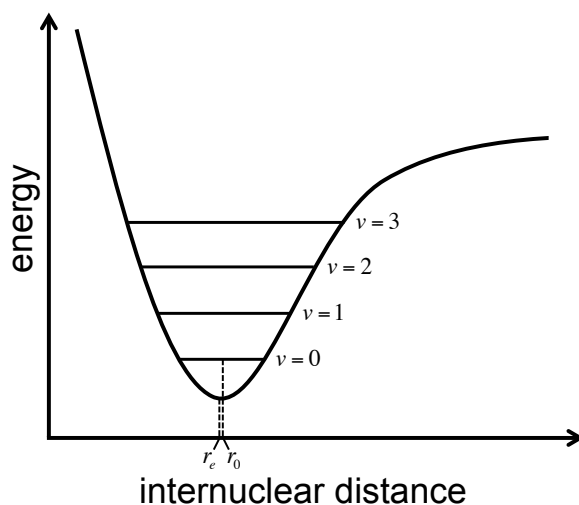
Figure 2.5: *Potential energy curve of the electronic ground state in a molecule. The r_e value describes the equilibrium internuclear distance of the hypothetically vibrationless nuclei and r_0 is the internuclear distance of nuclei in the absolute ground state.*

far only for small, linear molecules for benchmarking purposes, as it implies an immense effort for larger molecules.

Different methods to calculate the precise atom position from the obtained ground state rotational constants have been developed. An overview of the most common methods is given in the following, regarding also their aim to compensate for zero point motions in order to get closer to the equilibrium geometry.

Least square fit of the effective structure (r_0)

A first approximation of the structure of a molecule is obtained by determining the effective structure (r_0) (Fig. 2.5). In this case the structural parameters are fit in a least square manner to get a good reproduction of the experimentally obtained B_0 ground-state rotational constants of all isotopologues. In this method structural changes caused by isotopic substitution are neglected, which leads to a deviation of the effective structure from the equilibrium structure. Especially in the case of lighter atoms the mass change can significantly affect the zero-point motions and the determined atom position of a hydrogen atom is less reliable than the one of a heavier atom.

The differences between the equilibrium structure and the effective

structure increase even more if the molecule contains large amplitude motions or low-lying out-of-plane motions, as shown in Section 6.3.

In this work the effective r_0-structure of *trans*-cinnamaldehyde was fit using the STRFIT-program, which is available from the PROSPE homepage [73].

Substitution structure (r_s) using Kraitchman's equations

Another method to determine the geometry of a molecule from the experimental rotational constants was developed by Kraitchman [48]. Explicit formulas for linear, symmetric and asymmetric top molecules were established to calculate the atom position of an isotopically substituted atom from the moment of inertia of the substituted species. The obtained structure is called substitution structure (r_s). The calculations also consider the change of the moment of inertia upon isotopic substitution, which leads to a partial cancellation of the rovibrational contribution, since they are mass-dependent. This partial cancellation reveals a structure which is supposed to be closer to the equilibrium structure than the effective r_0-structure discussed before.

Larger errors in the calculated structure can occur for atoms with positions close to a principle axis of the molecule. Furthermore, for a complete structure determination, isotopic substitution of every single atom in the molecule is required, which can be challenging or even experimentally unfeasible.

Mass-dependent structure determination (r_m)

In this method a mass-scaling is used to get equilibrium-quality geometries. To determine the structure of the molecule, a least square fit of the structural parameters to the ground-state rotational constants is performed, in principle similar to the r_0-structure. However, in this method two adjustable parameters are fit simultaneously, which account for the rovibrational contribution. The first parameter accounts for the mass dependence of the rovibrational contribution by scaling its moments of inertia according to the mass change upon substitution. The second parameter corrects the structure for deviations caused by atoms close to the principle axis system of the molecules. These two parameters do not have a physical meaning but they correct the fitted structure and provide a geometry close to the equilibrium geometry.

An example of a structure determination using the mass-dependent method and a comparison of other methods in the case of the odorant

molecule *trans*-cinnamaldehyde is shown in Chapter 6.

Semi-experimental equilibrium structure determination (r_e^{SE})

The determination of a semi-experimental structure became more sensible with the increasing availability of high level computational methods. Using quantum chemical calculations the rovibrational constant α (see equation 2.28) can be calculated and used to correct the experimentally obtained ground-state rotational constants. From the obtained semi-experimental equilibrium rotational constants (B_e^{SE}) the structure is calculated again in a least-square manner. These semi-experimental r_e^{SE}-structures are very close to the equilibrium structures, as for example shown in Reference [74].

So far, this method was only used for relatively small molecules, since high level quantum chemical calculations of larger molecules still consume a large amount of computational time.

2.2 Quantum chemical calculations

In the following section a brief description of the quantum chemical calculations performed to support the spectroscopic analysis is given. For all calculations the GAUSSIAN 09 program suite was used.

In high-resolution rotational spectroscopy, quantum chemical calculations are performed for different reasons. As a first step it facilitates the assignment to get an approximate idea of the rotational constants of a molecule and of the size and direction of its dipole moment components. Furthermore, it is relevant to search for different minimum positions of the molecular structure. For this a scan of the potential energy surface of the molecule can be done. If a complete experimental structure determination is not possible, for example due to a low intensity of the measured spectrum, quantum chemical calculations can be used to compare the experimentally determined constants with calculated ones and to draw a conclusion to the molecular structure. Additionally, the vibrational modes of the molecule can be calculated and spectroscopic constants like distortion constants can be predicted.

In this work the *ab initio* method MP2 and the DFT methods B3LYP and M06 are mainly used. The second order Møller-Plesset perturbation theory (MP2) [75] is based on the Hartree-Fock (HF) method [76–78] but also includes electronic correlation and thus inherently consider dispersion. In density functional theory (DFT) the distribution of the electrons in the molecule is parameterized as a molecular density [79]. The hybrid-functional B3LYP (Becke, three parameter, Lee-Yang-Parr) uses a linear combination of the exact Hartree-Fock functional and the electron-electron exchange-correlation to describe the system [80]. Another member of these functionals is the M06 series of the Minnesota functionals, which takes dispersion interactions into account in an empirical manner [81]. An advantage of the DFT methods compared to *ab initio* methods is the shorter computational time required. For the DFT methods, further developments correct for dispersion interactions, which are especially important for weakly bound complexes. In this work, the M06-2X functional and Grimme's dispersion corrected B3LYP-D3 functional are used [82].

A linear combination of basis functions make up the basis set, which models the orbitals of the molecule. The size and type of the basis set have to be chosen regarding the type of the molecule and the computational time and data storage space available. Two different classes of basis sets were used in this work. For the DFT methods commonly the Pople-type triple split (6-311) basis sets are used, which can be adjusted for the use of polarization functions or diffuse orbitals, for example [83, 84]. The

Dunning-type basis sets (cc-pVnZ) are designed for *ab initio* methods including correlation correction. The basis set can be augmented by adding diffuse functions, which model the outer electron orbitals [85].

A comparison of calculations, using different methods and basis sets, to experimental rotational constants and molecular parameters on various molecules and complexes is demonstrated in Chapters 4-8.

2.3 Spectrum analysis and fitting

The analysis of a rotational spectrum is an iterative process. The choice of an appropriate Hamiltonian to fit the measured rotational spectrum is important. This depends on symmetry properties or the degree of asymmetry of the molecule and the occurrence of splittings caused by large-amplitude motions or quadrupole coupling. Several programs were developed to assist the analysis of the spectrum. In this work the PGOPHER program suite [86] was mainly used. Both the S- and A-reduction of the molecular Hamiltonian are implemented in this program. The rotational constants and up to the hextic distortion constants can be fit to define the rotational Hamiltonian. Furthermore, the nuclear quadrupole coupling constants of several quadrupole containing nuclei can be fit simultaneously.

The program offers a graphical user interface (GUI) to display a comparison between the measured and a simulated spectrum using calculated rotational constants. The user can then assign rotational quantum numbers to the experimental transitions, and the spectroscopic constants are fit to the assigned transitions in a least-square manner. The rotational spectrum should be fit with a minimum number of constants, leading to an error of the fit of a few kHz, which is then in the order of the experimental accuracy [87]. If a large number of transitions could be assigned, also higher-order centrifugal distortion constants can be fit. This is particularly true for transitions including higher J quantum numbers.

For the assignment process it is helpful to recognize characteristic patterns in the rotational spectrum [88]. A regular pattern can, for example, be found for a-type transitions, which arises from molecules with a large dipole moment in the direction of the a-axis (Tab. 2.2). The spectrum shows groups of transitions with a harmonic pattern. An example of an a-type spectrum is depicted in Figure 6.3 for the case of *s-trans-trans*-cinnamaldehyde. Transitions with $\Delta J = 0$ form a Q-branch, an example for the obvious pattern is depicted in Figure 2.6. It can be seen that it consists of many congested rotational transitions. A challenging analysis of a congested Q-branch is discussed in further detail in Section 7.3 for the

case of the glycolaldehyde dimer.
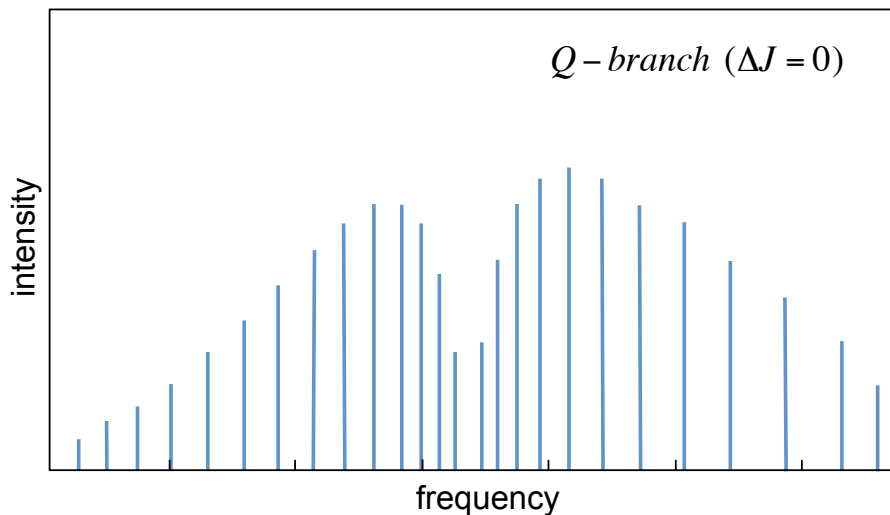
Figure 2.6: *An example for a Q-branch appearing in a b-type spectrum. Transitions of the type $J_{2,J-2} \leftarrow J_{1,J-1}$ occur for $J = 2$ at a frequency of $3(A - B)$, while higher J transitions of this type spread out to lower frequencies. Related transitions of the type $J_{2,J-1} \leftarrow J_{1,J}$ appear for $J = 2$ at a frequency of $3(A - C)$. More transitions of this type are shifted to higher frequencies with increasing J [88].*

A recently developed tool to support the spectral assignment is the AUTOFIT program [89]. Within this program triplets of rotational transitions are assigned automatically, and an overlap of the simulated and the measured spectrum is calculated. Millions of different possible triplets can be calculated using fast computational power. A list of the top 100 sets of rotational transitions, with preferentially small differences between the calculated and measured frequencies, is provided by the program and can be used as a starting point for spectral fitting. This method was used for the analysis of the glycolaldehyde dimer reported in Chapter 7.

Chapter 3

Experimental details

In the following chapter the experimental setup developed within this work is explained in detail. The main part of the experiments was performed using the "BEAMSPEC" instrument, depicted in Figure 3.1. This newly designed vacuum chamber assembles a useful combination of spectroscopic tools.
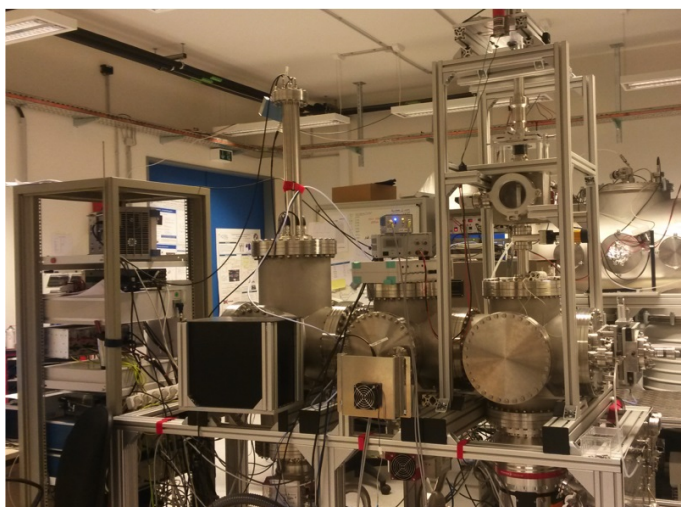
Figure 3.1: *Photograph of the experimental setup in the laboratory. The three vacuum cross-chambers contain a molecular source, a microwave spectrometer and a time-of-flight mass spectrometer (from the right to the left).*

The spectrometer is composed of three vacuum cross-chambers, dividing the experiment into three parts (Fig. 3.2). The first part is the source chamber, where the supersonic expansion takes place (Sec. 3.1). To bring the molecules into the gas phase they can be heated or laser ablated from

a solid sample bar (Sec. 3.4) and afterwards they are coexpanded with a carrier gas. In the second part, excitation and detection of microwave radiation takes place. The chirped-pulse Fourier transform microwave spectroscopy technique (CP-FTMW) is used here to record rotational spectra. The technical details of the method are explained in Section 3.2. The third part of the vacuum chamber hosts a time-of-flight (TOF) mass spectrometer, which can be used for beam diagnostics (Sec. 3.3).
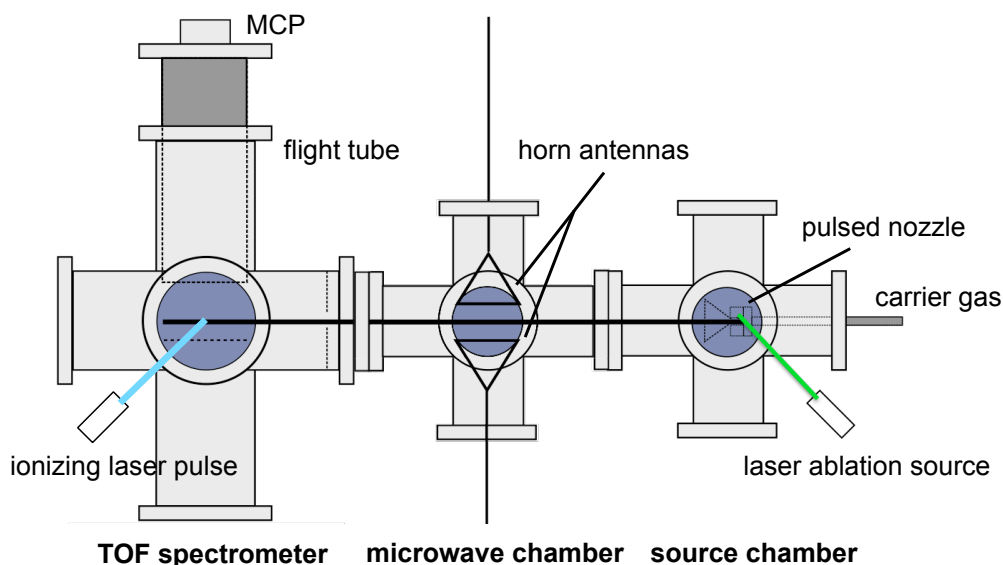
Figure 3.2: *Schematic drawing of the three vacuum cross-chambers.*

The source chamber and the terminal TOF part of the vacuum chamber are pumped with two turbo molecular pumps (Pfeiffer HiPace 1200 and HiPace 700) connected to prepumps (Pfeiffer Xtra Dry 150-2 and MVP 070-3). This leads to a pressure in the chamber during the measurement of approximately 10^{-6} mbar in the source chamber and 10^{-7} mbar in the TOF part of the chamber.

For the study of the diphenylether-methanol complex the "COMPACT" instrument, located in the same laboratory, was used, as discussed in Section 3.2.

3.1 Molecular beam experiments

Molecular beam techniques are a useful tool in various fields of physical chemistry and high-resolution spectroscopy in particular benefits from their advantages. A molecular beam is produced when a gas is expanded

from a high pressure area into a vacuum through a very small opening. Within this process the atoms or molecules can be cooled very efficiently. Due to the low vibrational and rotational temperature only a small number of energy levels in the system are populated, which leads to an increase of the intensity of the populated energy levels. The molecular beam also features a narrow velocity distribution, which leads to narrow line shapes. Furthermore, the molecules are not interacting with each other, since the molecular beam is very diluted [90], so that there is basically no collisional broadening.

The most common way to produce a molecular beam is to seed the molecules into an inert atomic carrier gas, for example helium, neon or argon. The molecules collide with the atoms in the carrier gas and thermalize with their surrounding. Within this work, a molecular beam is always a mixture of carrier gas atoms and the molecular sample of interest but since the fraction of molecules in the beam is very low it can be characterized like a pure atomic beam.

In our experimental setup the high-pressure area and the vacuum chamber are separated by a pulsed nozzle, and defined molecular packages are expanded into the chamber. The width of the packages is related to the opening time of the nozzle. The sample of interest can be heated in a reservoir in the high pressure area. The velocity distribution can be calculated according to the Maxwell-Boltzmann distribution:

$$P(\nu) = 4\pi \left(\frac{m}{2\pi k_B T} \right)^{\frac{3}{2}} \nu^2 e^{-\frac{m\nu^2}{2k_B T}} \tag{3.1}$$

In Figure 3.3 the velocity distribution of neon at different temperatures is depicted.

Two kinds of molecular beams are differentiated. If the mean free path lengths of the atoms is much larger than the diameter of the container opening, an effusive beam results. In this case no collisions between the atoms happen during the expansion and no energy is transferred [91]. As a result the atoms will not be cooled during the expansion but the atoms are non interacting.

In the second case the opening of the container is larger than the mean free path lengths of the atom and a supersonic beam results, where the atoms can be cooled. Due to many collisions with other atoms during the expansion, the internal and external degrees of freedom of the atoms and molecules are cooled very efficiently.

The maximum velocity of the beam can be calculated using
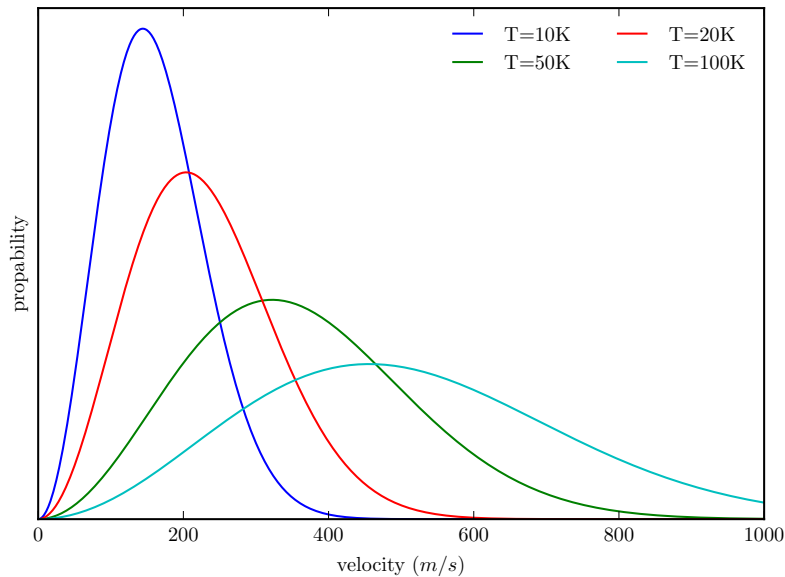
Figure 3.3: *The Maxwell-Boltzmann velocity distribution of neon calculated for different temperatures.*

$$\nu_{max} = \sqrt{\frac{5k_B T_0}{m}} \qquad (3.2)$$

This equation is only true for an ideal gas with an isentropic and adiabatic behavior during the expansion. It thus only provides an approximation for the velocity of a real system, which depends on the temperature of the reservoir before the expansion and on the mass of the expanded atoms or molecules [92]. Figure 3.4 shows the velocity distribution of neon inside the reservoir compared to the terminal velocity of the expanded beam under ideal conditions.

The characteristics of the expansion itself are depicted in Figure 3.5. Different areas of the expanded beam can be described with the Mach number M, giving the ratio of the velocity ν of the molecular beam at a certain point compared to the sound velocity c [93].

$$M = \frac{\nu}{c} \qquad (3.3)$$

The Mach number in the container is smaller than one ($M < 1$) because the atoms collide frequently, which gives a much slower velocity than the sound velocity. During the expansion the density of atoms decreases and the mean velocity increases quickly. In this part of the expansion the
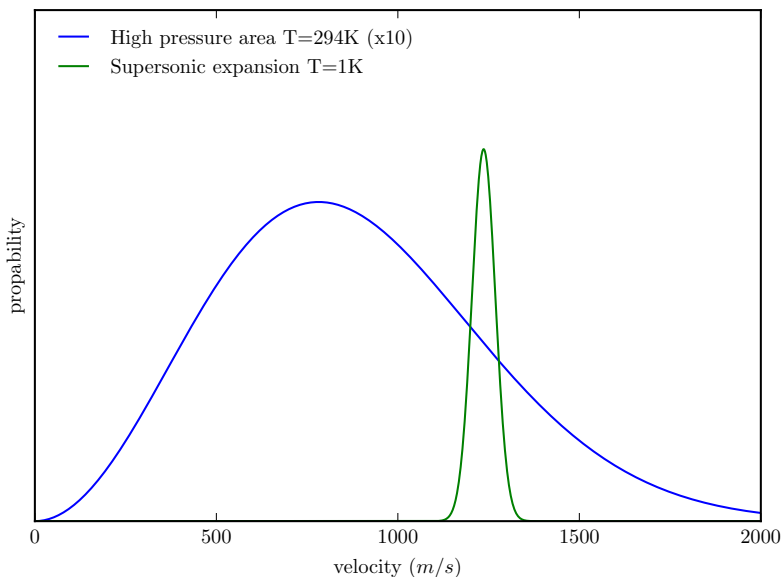
Figure 3.4: *Comparison of the velocity distribution of neon in the high pressure area at room temperature to the terminal velocity of neon reached during the supersonic expansion at 1 K.*

Mach number is much larger than one and the expansion can be described as supersonic. This area is also called the zone of silence, since the beam in this area is so dilute that no collisions take place any more. The length x of this zone depends on the pressure difference between the carrier gas (p_0) and the vacuum chamber (p_B) and on the diameter D of the container opening [92]. It can be calculated by

$$x = 0.67D\sqrt{\frac{p_0}{p_B}} \tag{3.4}$$

and it shows that the required pumping speed, which ultimately determines p_B, is an important parameter for the experimental performance. The microwave excitation should take place in the zone of silence, since the beam temperature is lowest in this area. At the boundaries of the expansion, shock waves are occurring due to collisions with warmer background gas. The terminal shock wave is called Mach disc, which is also known from supersonic aircraft or bullets. At this point the velocity suddenly drops and the Mach number decreases below one.
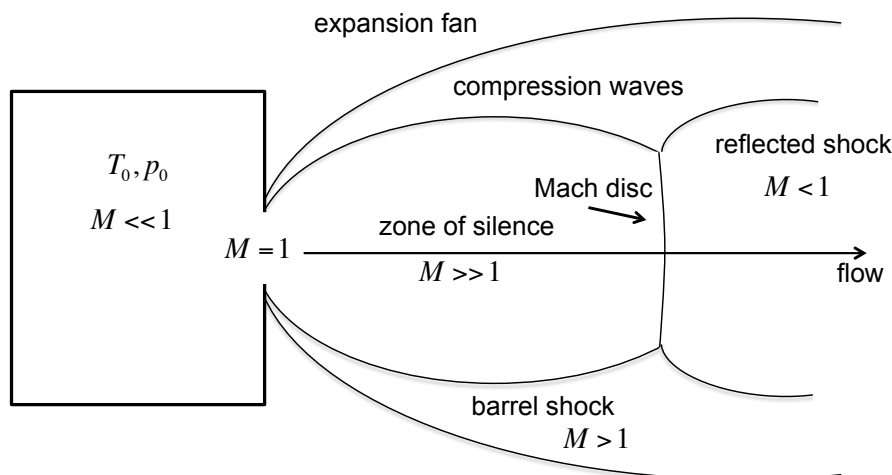
Figure 3.5: *Schematic overview of the different areas in a supersonic expansion.*

The intensity of transitions in the experimental spectrum benefits strongly from lower achieved temperatures in the molecular beam, because at a low rotational temperature less states are populated and thus the populated states gain intensity. A comparison of a simulated spectrum at different temperatures is depicted in Figure 3.6.

Additionally, different carrier gases show different cooling behaviors. Since the exchange of energy during the collision of two particles is more efficient using heavier carrier gases, argon would be a good choice for reaching low beam temperatures. On the other hand argon shows the tendency to form clusters with the molecules of interest, by forming van-der-Waals complexes, and thus the monomer would lose intensity. The choice of the best carrier gas is therefore a compromise between optimal cooling, the tendency to form complexes and also the costs, since some noble gases are fairly expensive. For our measurements the best results are obtained by using neon as a carrier gas, because it reveals a good cooling behavior without the tendency to form complexes with the molecules.

The expansion is a dynamic process, revealing the opportunity to influence and also to optimize the process for the experimental conditions needed for a certain task. A main goal in this work was to study complexes and dimers formed by biologically relevant molecules, and an expansion has to be created to support this formation. For a formation of dimers a three-body collision has to take place. This event scales with $p_0^2 D$, and thus a higher pressure of the carrier gas supports the formation of complexes [92].
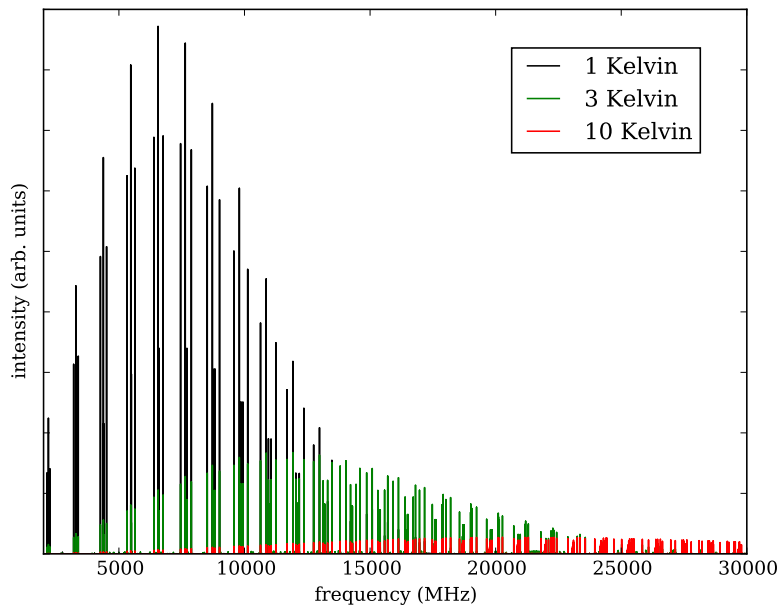
Figure 3.6: *Simulated rotational spectra of cinnamaldehyde at different temperatures. At higher temperatures more energy levels are populated, which leads to a decrease of the intensities in the spectrum.*

Consequently, the ideal parameters for the expansion have to be adjusted for each measurement. This was done, for example, by varying the pressure or the choice of the carrier gas.

3.2 Chirped-pulse Fourier transform microwave spectrometer

The "BEAMSPEC" vacuum chamber is equipped with a chirped-pulse Fourier transform microwave spectrometer (CP-FTMW) for recording the rotational spectra in a broadband manner. This newly developed technique was pioneered by the Pate group in 2008 [35] and provides a fast alternative to the cavity based Balle-Flygare- or Fabry-Perot microwave spectrometers [33, 94–96].

CP-FTMW spectroscopy is based on a fast passage excitation using a linear microwave chirp. The excitation pulse needs to be faster than the relaxation time of the excited states and is typically 1-4 μs long [35]. Our spectrometer covers the frequency range from 2 - 8.5 GHz and was

built to investigate large biomolecules and biologically relevant complexes, revealing small rotational constants and thus low transition frequencies. A comparison of simulated spectra of molecules with different masses is depicted in Figure 3.7. It shows the mass dependence of the frequencies of maximum intensity for molecules at a rotational temperature of 1 K.
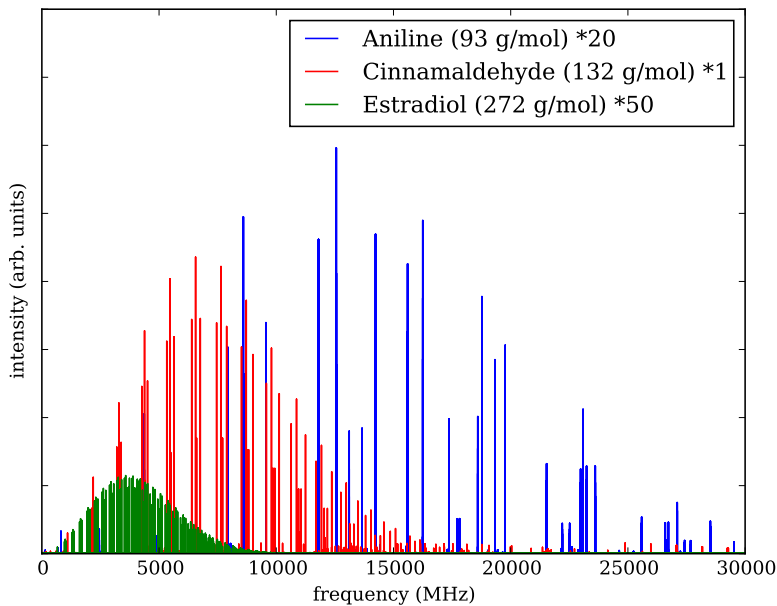
Figure 3.7: *Simulated rotational spectra of molecules with different masses at a rotational temperature of 1 K, showing that the rotational transitions of heavier molecules are shifted towards lower frequencies and show a more congested spectrum. The intensity of the aniline and the estradiol spectrum are scaled to provide a better comparability with the cinnamaldehyde spectrum.*

Furthermore, the intensity S of the obtained signal depends on several parameters. It is proportional to the number of molecules N, the transition frequency ω, the square of the transition dipole moment μ, the amplitude of the excitation radiation ε_0, the population difference of the two states involved in the transition ΔN_0 (which depends on the rotational temperature), and the inverse square root of the chirp rate α [35]:

$$S \propto N \cdot \omega \cdot \mu^2 \cdot \varepsilon_0 \cdot \Delta N_0 \cdot \sqrt{\frac{\pi}{\alpha}} \tag{3.5}$$

The chirp rate α is defined by the difference of the end frequency ω_e

and the start frequency ω_s divided by the pulse duration τ_{AWG} [35]:

$$\alpha = \frac{\omega_e - \omega_s}{\tau_{AWG}} \tag{3.6}$$

A schematic overview of the electronic parts of the microwave spectrometer is shown in Figure 3.8.
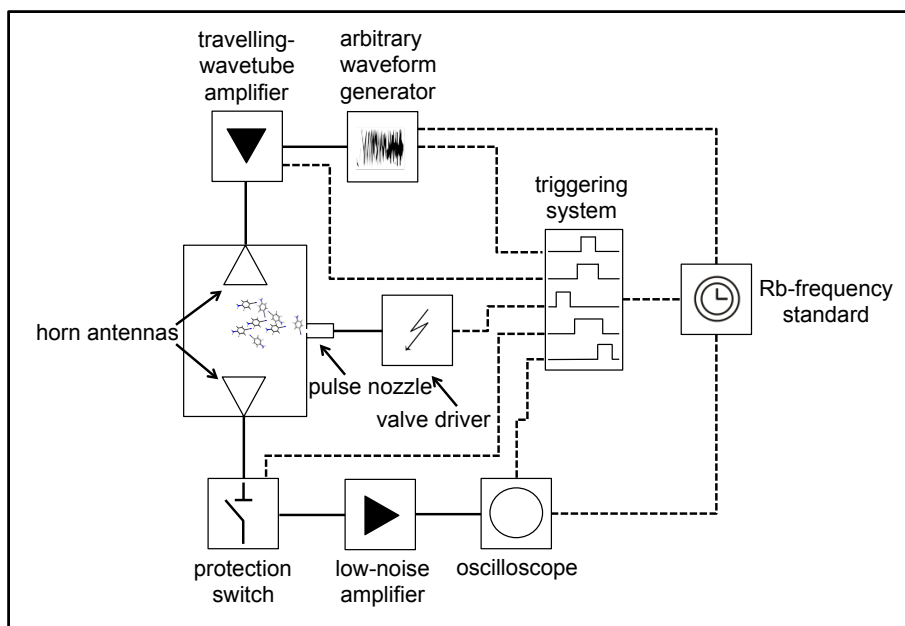
Figure 3.8: *Experimental setup of the "BEAMSPEC" microwave spectrometer. The arbitrary waveform generator (AWG) produces the microwave chirp, which is amplified with a traveling wavetube (TWT) amplifier and transmitted into the chamber with a horn antenna. A second horn antenna receives the molecular response of the excited molecules, which is amplified with a low noise amplifier and recorded with an oscilloscope. A protection switch is used to protect the detection part from the high energy radiation. The control system of triggers, the AWG and the oscilloscope are connected to a Rb-frequency standard to synchronize their phases.*

The microwave chirp is created by a fast arbitrary waveform generator (Tektronix AWG 7122A, 24 GS/s) and amplified using a 300 W traveling wave tube amplifier (TWTA, Amplifier Research 300T2G8). The radiation is transmitted into the vacuum chamber through a microwave horn antenna (Advanced Technical Materials 250-441EM-NF), which is directly mounted to the vacuum flange (Fig. 3.9). The molecules are supersonically expanded into the chamber, as explained in Section 3.1. A pulsed nozzle (Parker General Valve, Series 9) in a perpendicular arrangement to

the horn antenna is used for the expansion of the molecular packages. The microwave chirp excites all resonant transitions of the internally cooled molecules in the covered frequency range, and a macroscopic dipole moment is formed due to the polarization of the molecular ensemble. The free-induction decay (FID) of this macroscopic polarization is received using a second microwave horn antenna and amplified with a low-noise microwave amplifier (Miteq Amplifier AMF-5F-0200080-15-10P). A switch protects the sensitive low-noise amplifier and the oscilloscope from the high-power excitation pulse. The molecular response is recorded by an oscilloscope (Tektronix DPO 71254A, 100 GS/s), and the length of the recorded FID determines the resolution of the spectrum. To obtain the spectrum in the frequency domain, a Fourier transformation (FT) is performed. The frequency span of the spectrometer is limited by the TWTA, the horn antennas and the low-noise amplifier (LNA).
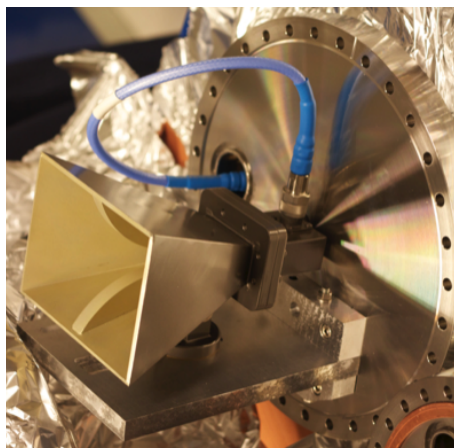
Figure 3.9: *Microwave horn antenna of the "BEAMSPEC" setup, mounted to a vacuum flange.*

In this experiment up to 50 μs of the FID are recorded resulting in a resolution of about 20 kHz. To increase the signal-to-noise ratio of the rotational spectrum the microwave experiment is performed with a repetition rate of 2 - 10 Hz and the data is digitally averaged with the oscilloscope. The repetition rate is limited by the speed of the oscilloscope and the pumping speed. Averaging of the molecular signal requires phase stability which is ensured by phase-locking the AWG and the oscilloscope to a 10 MHz Rb frequency standard. Furthermore the oscilloscope is directly triggered by a marker channel of the AWG. Additional triggers, mandatory for running the experiment, are generated by a National Instruments PXI system (PXIe-1065). The complete trigger scheme is depicted in Figure

3.10. To control the experimental sequence the FTMW++ program written by Jens-Uwe Grabow (Leibniz-Universität Hannover) is used. At time zero the valve is triggered and its opening time τ_{valve} defines the lengths of the gas pulse (Fig. 3.10). The molecular ensemble expands into the chamber and reaches the horn antennas after an expansion time t_{exp}. In the next step, the protection switch is triggered to protect the low-noise amplifier during the excitation process. For generating and amplifying the microwave chirp, the AWG and the TWTA are triggered subsequently, with a short delay for the AWG to account for the ramp up time of the TWTA. Finally the AWG triggers the oscilloscope to record the resulting FID for the duration τ_{osci}.
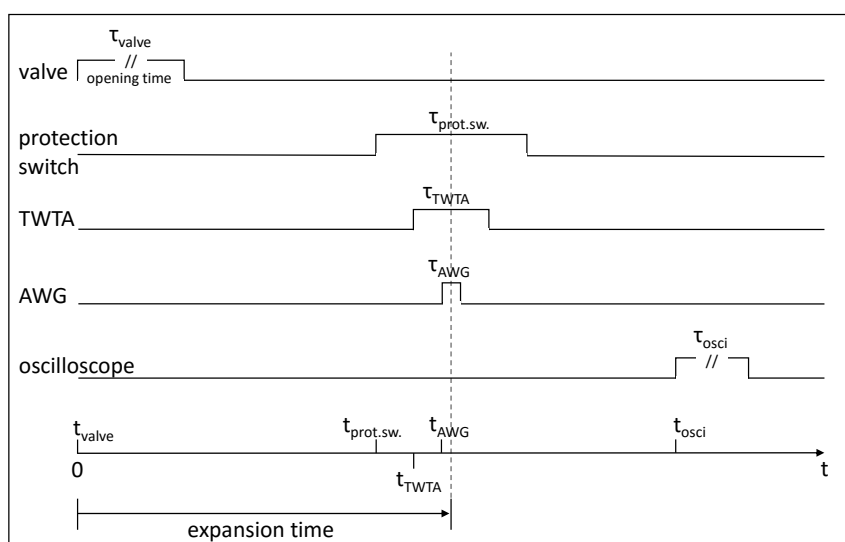
Figure 3.10: *Trigger scheme for recording a microwave spectrum using the "BEAMSPEC" and the "COMPACT" spectrometer.*

The experimental performance of the "COMPACT" chamber [97] used for measuring the diphenylether-methanol complex (Chap. 8) is similar to the one described above. Nevertheless, due to recent improvements the sensitivity of this spectrometer was increased, which is advantageous especially for measuring weakly bound complexes. First, the use of larger horn antennas increased the sensitivity of this experimental setup compared to the "BEAMSPEC" spectrometer. Second, an improved way to perform the experiment, called the fast-frame setup, was implemented, which makes the experiment much faster and with this it gives a good signal-to-noise ratio in a shorter time.

In the fast-frame setup, within one gas-pulse of about 600 μs, up to eight microwave chirps of 4 μs duration are fired with a certain distance as depicted in Figure 3.11. The resulting FIDs are summed up. The fast-frame setup can be performed with a repetition rate of 4 Hz for the gas pulse, giving a total repetition rate of 32 Hz. This is mainly limited by the pumping speed of the roughing pump. This setup can record 1 million averages in approximately 9 hours, while the former setup would have needed about 140 hours, using a repetition rate of 2 Hz.
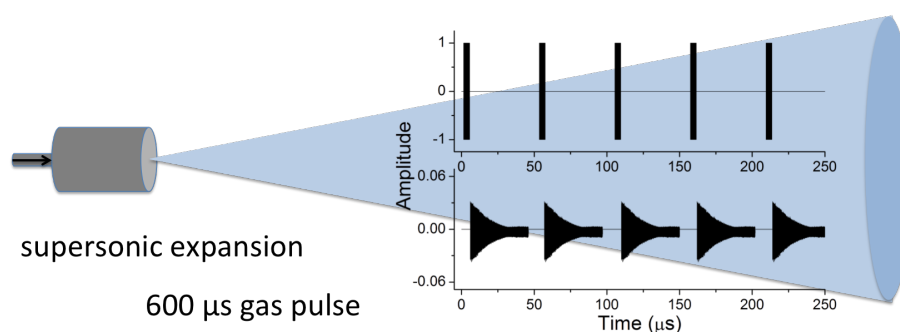
Figure 3.11: *Overview of the fast-frame setup. Several microwave chirps can be used during one gas pulse, and the corresponding FIDs are digitally averaged, which provide a fast repetition rate.*

In general the performance of the spectrometer is very stable. The whole microwave spectrometer only depends on a few electronic components. Beside the nozzle there are no mechanically moving parts used, which allows us to run the experiment over night and for several days, with the only requirement to refill the sample.

To be able to record the whole broadband spectrum at once is one of the major advantages of the chirped-pulse technique. Mixtures of molecules, different conformers, clusters and isotopically substituted species can be studied within one spectrum.

3.3 Time-of-flight mass spectrometer

For analyzing the molecular beam a commercial time-of-flight mass spectrometer (Jordan TOF Product, Inc.) is installed into the "BEAMSPEC" vacuum chamber. Since the main purpose of the instrument is to study complexes of biomolecules and fragile carbohydrates, it is supportive to record a mass spectrum of the molecular beam and it allows us to optimize the experimental condition such that the favored mass peak, for

example of the complex of interest, is increased. The major advantage of the time-of-flight supported beam analysis is its high sensitivity. Compared to microwave spectroscopy, where an ensemble of molecules is needed, even single ions can be detected. Changes in the mass spectrum when optimizing the experimental conditions can be seen directly at the oscilloscope, which is a helpful tool to find the optimum conditions for measuring the rotational spectrum. Fragmentation products, caused by heating of the sample, by the laser ablation process (Sec. 3.4) or also by the ionization can be identified as well and changed if possible. A recorded mass spectrum of an ablated sample is depicted in Figure 3.12.

The time-of-flight mass spectrometer is arranged in the third and terminal cross of the vacuum chamber. When the beam package reaches this part, it is ionized by a UV-laser pulse, using the (2+1) resonance-enhanced multiphoton ionization (REMPI) method. For this a tunable dye-laser (Sirah Lasertechnik, Pulsed Dye Laser, CSTR-LG-2400) is used, which is pumped with a Nd-YAG laser (Innolas Laser, SpitLight 500). The accessible wavelength range of the laser is determined by the dye. For this work mainly the Pyrromethene 580 dye was used, covering the wavelength range between 544 nm and 585 nm. In this case the energy of the UV-laser pulse, after a frequency doubling crystal, is between 8 mJ and 18 mJ and features a line width of $0.06\,\mathrm{cm}^{-1}$. The resulting ions are guided into a 1 m long flight tube by several voltage plates with different electric voltages applied. The ions are detected with a multi-channel plate (MCP) and the signal is recorded with an oscilloscope (Rohde & Schwarz, HMO1002). According to their mass m and their charge q, the ions arrive at different times at the MCP, since the acceleration of the ions, due to the electric field gradient, is proportional to the mass. Lighter molecules are accelerated more and arrive earlier at the MCP, so that a mass-selective spectrum can be recorded (Eq. 3.7) [98].

$$T \propto \sqrt{\frac{m}{q}} \tag{3.7}$$

If the vibronic resonance frequencies of the molecules are not known, an electronic spectrum can be recorded by scanning the frequency of the laser and simultaneously recording only the one mass channel of the molecule of interest. An example of an electronic spectrum is given in Section 4.3. The obtained electronic spectrum can be used to identify resonance frequencies in the molecule and vibrational overtones caused by excited vibrational states can be identified as well.

3.4 Laser ablation source

One of the restrictions of microwave spectroscopy is that the molecules need to be in the gas phase. This can be challenging especially for large and fragile molecules like carbohydrates, which typically cannot be heated sufficiently to evaporate them. A method to bring fragile molecules into the gas phase is laser ablation, which was already successfully applied to study carbohydrates and large biomolecules in the recent past [36, 37, 39].

In general, a laser pulse is used to ablate the molecules from a solid sample. This ablation process happens directly downstream of the nozzle so that the ablated molecules can be seeded into the expansion of a carrier gas. Within the expansion the ablated molecules are cooled before they would be destroyed by the laser power, since the internal energy is transferred very fast and efficiently into translational energy during the expansion. The solid sample is moved permanently during the ablation to deliver a new part of the sample for the next laser pulse.

Within this work a laser ablation source was implemented into the "BEAMSPEC" chamber. The motorization for the sample movement is outside of the vacuum chamber, providing simple maintenance of the system. A ten centimeter long sample bar was constructed, which can be moved up and down in front of the nozzle. In a perpendicular arrangement to the molecular beam a laser pulse, using the second harmonic of a Nd:YAG laser (Continuum, Minilite I, at 532 nm with up to 12 mJ), is focused onto the sample bar to ablate the sample. The ablated molecules are seeded into the expansion and interact with the microwave chirp or the UV laser for mass spectrometry further downstream.

The mass spectrum of an ablated sample was measured successfully within this work. By consequently improving the setup and timing of the experiment, the intensity and stability of the signal was increased several orders of magnitude. The mass spectrum of laser ablated tryptophan is depicted in Figure 3.12. The ionizing laser was kept to a resonance frequency of tryptophan at 286.63 nm (8 mJ per pulse) and the ablation laser was set an output power of 10 mJ per pulse at 532 nm. For this measurement 1500 acquisitions were averaged and a clear mass peak for tryptophan (204 g/mol) was recorded. However, the amount of ablated molecules within one laser pulse was still too low to record a microwave spectrum of an ablated sample. Major changes of the experimental setup, like moving the ablation setup and the nozzle much closer to the microwave horn antennas to prevent the molecules from transversally spreading out too much, would be required in the future to increase the density of molecules. Furthermore, a change from a nanosecond to a picosecond laser could improve

the ablation process.

Consequently, the focus of this work was changed to molecules, which can be brought into the gas phase by heating. This includes already a huge variety of interesting biomolecules and carbohydrates.
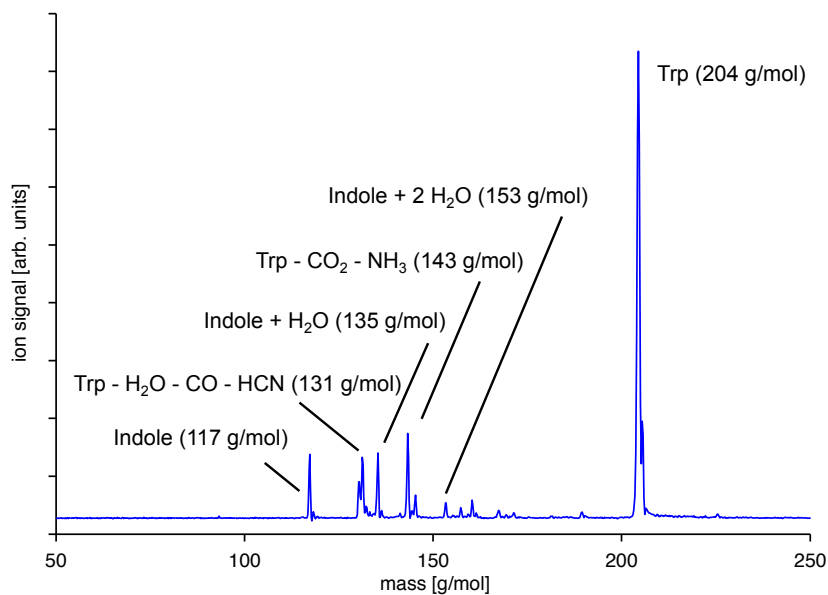
Figure 3.12: *Mass spectrum of laser ablated tryptophan (Trp) in a test measurement. To adjust the parameters of the ablation source, indole was mixed into the carrier gas. Fragments and clusters of tryptophan and indole occur in the mass spectrum. Peaks are labeled with the added or substituted groups and the corresponding parent molecule. For each point 1500 acquisitions are averaged.*

Chapter 4

Nuclear quadrupole coupling constants of two chemically distinct nitrogen atoms in 4-aminobenzonitrile*

4.1 Introduction

One of the first molecules studied with the new "BEAMSPEC" setup is 4-aminobenzonitrile (ABN), depicted in Figure 4.1. The study of this molecule provides an overview of the manifold spectroscopic options the new instrument provides.

ABN belongs to a group of para-substituted benzonitrile molecules. This class of molecules has received much attention because some of its members show dual fluorescence, revealing a solvent-dependent appearance of a second emission at a different frequency from a charge-transfer state upon local excitation [99]. A well studied example for this effect is dimethylaminobenzonitrile (DMABN) [100–104]. In contrast to this molecule, ABN shows no dual fluorescence [105, 106]. This difference was explained by the additional electron-donating character of the alkylated amino group in DMABN [102], compared to the amino group in ABN. Thus, the electronic environment at the amino-group nitrogen can be decisive for the existence of charge-transfer states and hence dual fluorescence (see for example References [107] and [108]).
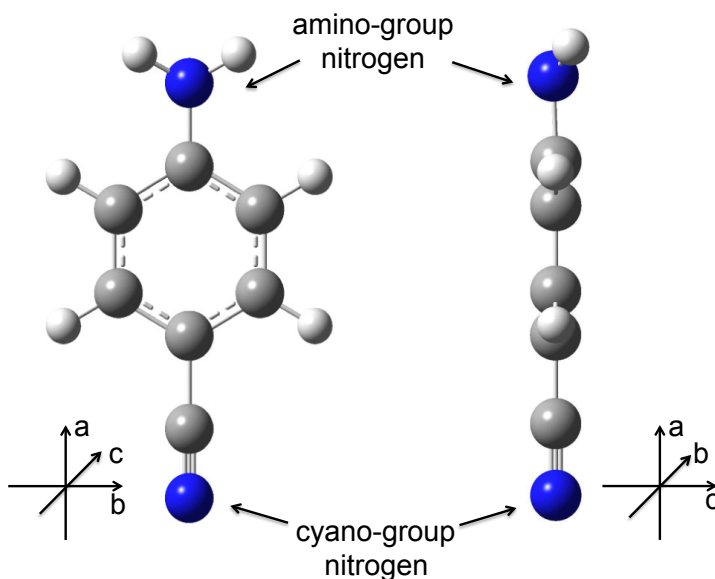
Figure 4.1: *Geometry of 4-aminobenzonitrile. The nitrogen atoms of the nitrile and the amino group lead to a complicated hyperfine structure of rotational transitions. The principal inertial axes are labeled with a, b and c.*

Within this study the complex splitting due to nuclear quadrupole coupling of two chemically distinct nitrogen atoms could be resolved and the quadrupole coupling constants could be determined. The local electronic environment can be characterized using these information, as explained in Section 2.1.2. Furthermore, a mass spectrum and an electronic spectrum were recorded and analyzed using the time-of-flight mass spectrometer (Sec. 3.3).

The rotational spectrum of ABN in the frequency range between 2 to 8.5 GHz was measured with broadband microwave spectroscopy in this thesis. The rotational constants of the asymmetric rotor ABN were determined earlier from rotationally resolved electronic spectra [109, 110]. Due to the lower resolution and higher rotational transitions, and therefore smaller hyperfine splittings involved, the quadrupole coupling constants were not accessible. The frequency range of our spectrometer (2-8.5 GHz) together with the high resolution provided by microwave spectroscopy facilitate their identification. The two non-vanishing dipole moment components of ABN are 5.46 D along the direction of the weakest moment of inertia (μ_a) and 1.45 D in the direction orthogonal to the benzene ring (μ_c) [110], hence the spectrum is dominated by a-type asymmetric rotor

transitions.

The two chemically distinct nitrogen atoms of the respective amino and nitrile groups of this molecule lead to a hyperfine structure of each rotational transition due to nuclear quadrupole coupling. Determining their individual quadrupole interactions is challenging, due to the complicated, combined splitting effect of the two nuclei. The respective nuclear quadrupole coupling constants are presented here. They allow for the investigation of the electronic environment of the molecule in the vicinity of the nitrogen atoms, which is of particular interest when comparing ABN to other para-substituted benzonitriles showing dual fluorescence. Previous microwave spectroscopy studies investigated the differences between dimethylaniline (DMA) and DMABN [111], depicted in Figure 4.2. Here we extend this comparison to include ABN as well.
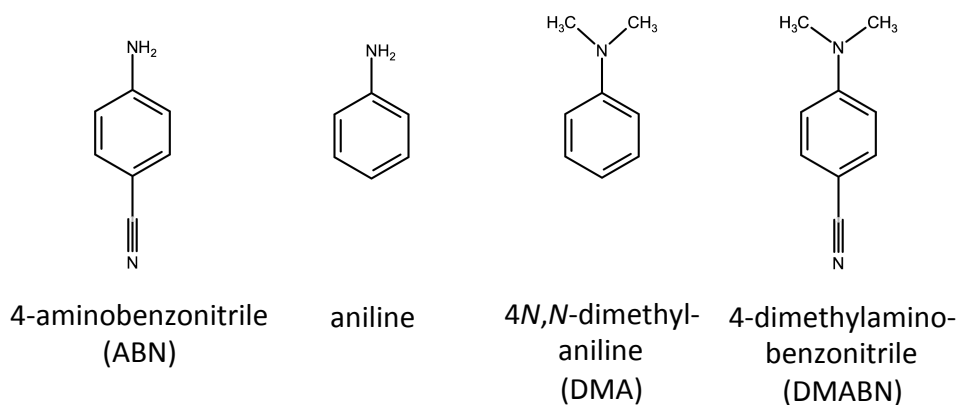
Figure 4.2: *Schematic structures of the molecules used for comparison with 4-aminobenzonitrile.*

4.2   Experimental details

ABN was purchased from Sigma-Aldrich (98 % purity) and used without further purification. The sample was heated to $113\,°C$ in a reservoir and the carrier gas neon, with a backing pressure of 2.5 bar, was flown over it to create a gas mixture. Subsequently, this mixture was expanded into vacuum through a pulse nozzle with an opening time of approximately $400\,\mu s$ and a repetition rate of 2 Hz (compare Sec. 3.2). After an expansion time of $775\,\mu s$ the ABN molecules were excited by a $1\,\mu s$ long microwave pulse, which was linearly frequency chirped from 2 to 8.5 GHz. The resulting free

induction decay (FID) was recorded for $50\,\mu\mathrm{s}$ starting $5\,\mu\mathrm{s}$ after the excitation pulse and then amplified and converted into a digital signal. The complete trigger scheme is depicted in Figure 3.10. In total $337\,000$ FIDs were recorded and digitally averaged. The rotational spectrum was obtained by Fourier transforming the experimental data using a fast Fourier transform algorithm, without any filters or other treatments. The length of the recorded FID set our frequency resolution to $20\,\mathrm{kHz}$, whereas the full width at half maximum of our transitions was on the order of $30\,\mathrm{kHz}$. The experimental rotational spectrum of ABN is depicted in the top trace of Figure 4.3, together with the results of a fit displayed in the bottom trace. The remaining unassigned lines can neither be attributed to the ABN monomer nor to its isotopologues. The signal-to-noise ratio of the spectrum is less than 50:1 and thus no transitions of isotopic substituted species can be identified. The unassigned lines might arise from clusters of ABN or complexes with water.

As mentioned in Section 3.3, the experimental setup allows us to analyze the molecular beam with the TOF mass spectrometer. The recorded mass spectrum, using the resonance frequency of the ABN monomer at a wavelength of $291.5\,\mathrm{nm}$, is depicted in Figure 4.4 and confirms the existence of ABN complexes. Besides the dominant monomer peak, at the mass of $118.4\,\mathrm{g/mol}$, the dimer, trimer and tetramer of ABN are clearly visible. Also the complex of the ABN dimer with water could be identified. Interestingly, no complex of the ABN monomer and water was observed. To obtain the mass spectrum of ABN, the molecules were first ionized with a $8\,\mathrm{ns}$ long light pulse with a pulse energy of $6\,\mathrm{mJ}$ from a tunable Nd:YAG-pumped dye laser (featuring a line width of $0.06\,\mathrm{cm}^{-1}$ at a wavelength of $570\,\mathrm{nm}$). During the experiment, the ionization laser frequency was kept resonant for the ABN monomer. Ionization of the complexes was possible, since the resonances do not shift much upon complex formation and the laser is also rather broad in frequency. For the final spectrum, displayed in Figure 4.4, $36\,000$ mass spectra were averaged.

With the same setup it is possible to study the vibrational structures of electronic levels by a combination of TOF mass spectrometry and ionization techniques, such as resonance enhanced multi-photon ionization (REMPI). The one-color two-photon REMPI spectrum of ABN in the range from 290 to $300\,\mathrm{nm}$ is shown in Figure 4.5.

The frequency was varied in steps of $0.01\,\mathrm{nm}$, and for each point 180 acquisitions were averaged. The line positions were determined by fitting a Lorentzian line shape to each peak. Their assignment was carried out in agreement with References [107] and [112] and also agrees well with more recent results, as compared in Table 4.1 [115, 116] .
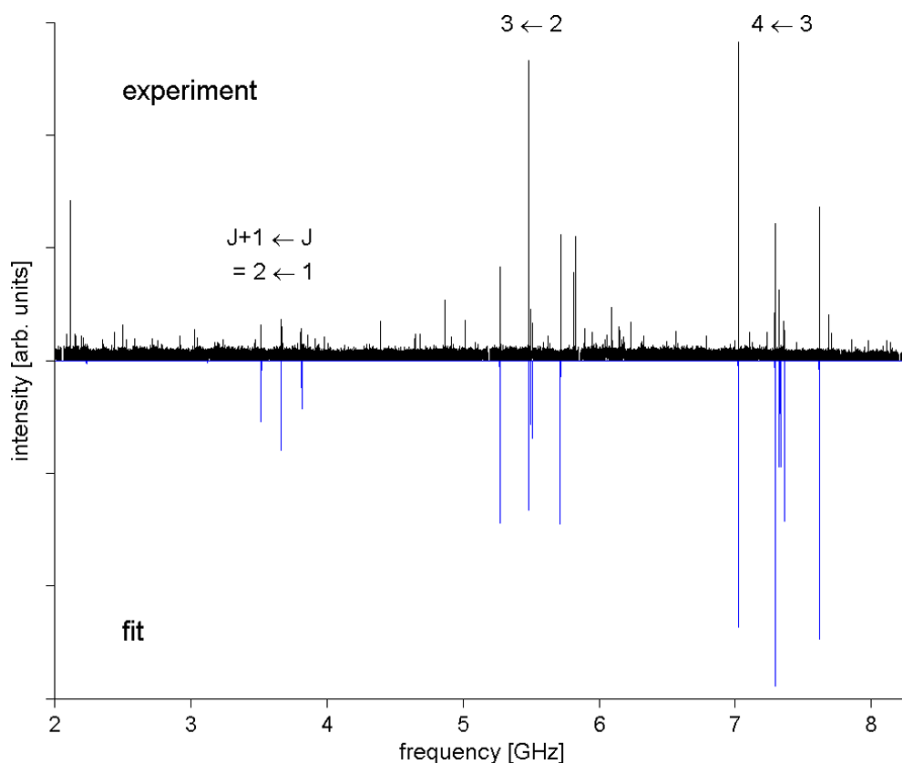
Figure 4.3: *Rotational spectrum of 4-aminobenzonitrile: The upper trace shows the experimental data and the lower trace represents the result of fitting an asymmetric rotor Hamiltonian to it. Known background lines have been removed. Remaining unidentified lines might belong to clusters of ABN or complexes with water.*

4.3   Results and Discussion

In the following, the analysis of the microwave spectrum of ABN and especially the results on the nuclear quadrupole coupling in this molecule are discussed in more detail and compared to related systems. The differences to DMABN are highlighted and presented with the help of analyzing the occupation numbers of the atomic orbitals of the nitrogen in the amino group.

   The microwave spectrum was fit using an asymmetric rotor Hamiltonian (Watson S-Reduction in I^r representation) as implemented in the program PGOPHER [86]. The fitting results are shown in the lower trace of Figure 4.3. Rotational quantum numbers involved in the assigned transitions range from $J = 1$ to $J = 4$. For the corresponding energy levels the influence of distortion constants was found to be small and thus has been
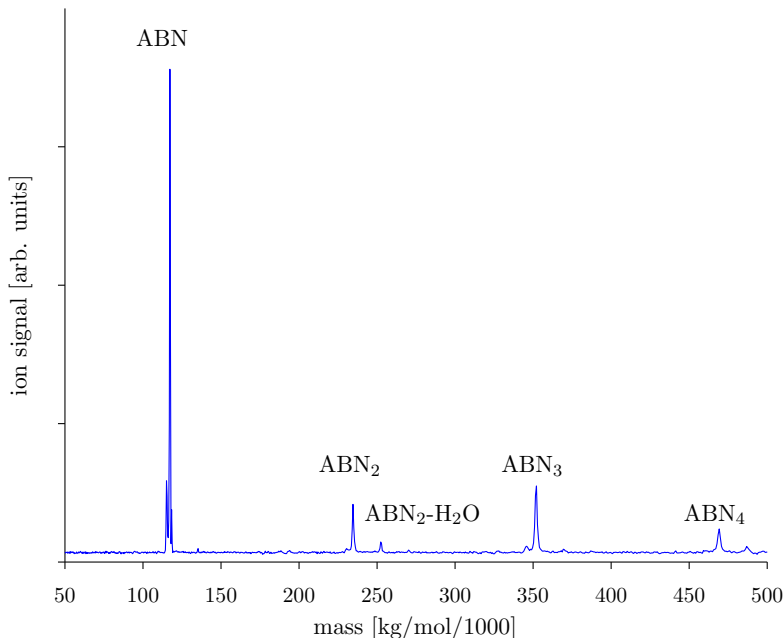
Figure 4.4: *Ion fragments obtained from the molecular beam of ABN analyzed with the TOF mass spectrometer. For each point 36 000 acquisitions were averaged.*

neglected in the fitting procedure. As expected from the dipole moment components, the spectrum of ABN is dominated by a-type transitions. Despite the still significant dipole moment along the c direction, no corresponding transitions were observed. Also no signatures from ^{13}C- or other isotopologues of the molecule could be found in the data.

The obtained rotational and nuclear quadrupole constants are listed in Table 4.2. They show good agreement with the previously reported rotational constants and predictions from quantum-chemical calculations. The overall best agreement is obtained by density functional theory using the M06-2X functional and a 6-31+G(d,p) basis set. The differences in the results obtained at the MP2 level of theory, compared to the M06-2X calculations, mainly arise from different equilibrium positions of the hydrogen atoms in the amino group.

Note that no line splittings arising from the inversion motion of the amino group is observed under the cold conditions of a molecular jet. Similar to the related molecule aniline, the splittings of the respective energy levels are so large that the thermal population of the excited modes becomes negligible at low temperatures (compare e.g. References [117]
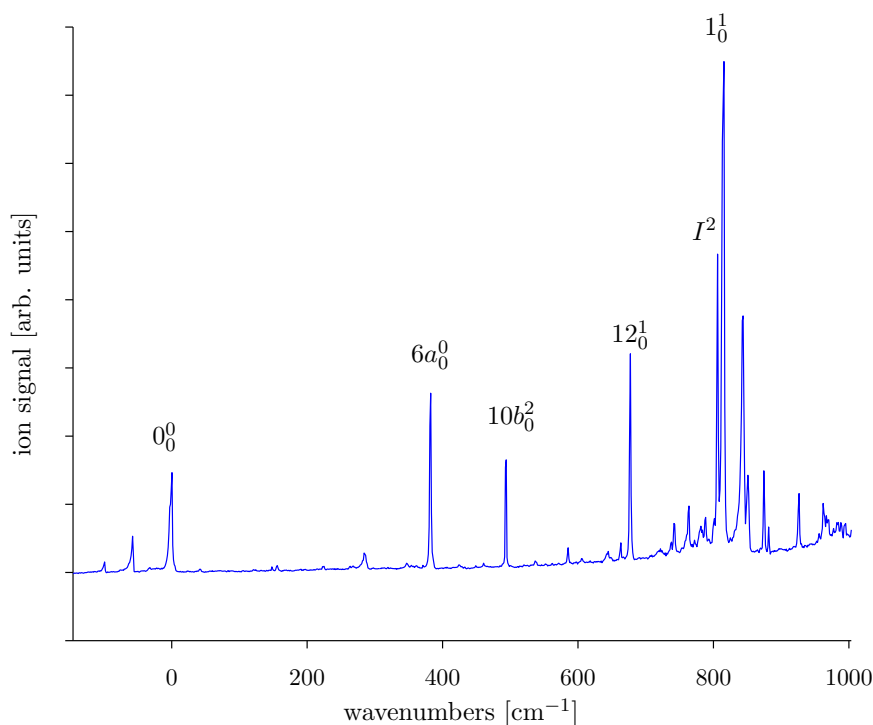
Figure 4.5: *The one-color two-photon REMPI spectrum of 4-aminobenzonitrile. The different lines represent resonances of different vibrational levels of the same excited electronic level. The origin was set to the known value of 33 493 cm^{-1} and the line assignment followed previous work using Varsányi notation [112–114].*

and [118]).

The nuclear quadrupole splitting of the rotational transitions arising from the different nitrogen nuclei is nicely resolved for the two lower J transitions ($J + 1 \leftarrow J = 3 \leftarrow 2$ and $2 \leftarrow 1$), whereas for the transitions corresponding to $J + 1 \leftarrow J = 4 \leftarrow 3$ the groups of lines become quite congested. This underlines the need for observations in this low-frequency range. Typical nuclear quadrupole splitting patterns are presented in Figure 4.6.

The nuclear quadrupole coupling in molecules is sensitive to the local electric field gradient, and thus a comparison of the results with a series of related molecules highlights their differences. In order to relate the nuclear quadrupole coupling constants measured in the inertial principal axis system of ABN (a, b, c) to other molecules, the nuclear quadrupole coupling tensors have to be transferred to their principal axis system (x, y, z). In

Table 4.1: *Line positions of the one-color two-photon REMPI spectrum of 4-aminobenzonitrile. Errors in parentheses represent the 95 % confidence interval of the fit parameters.*

Transition[a]	this work	Ref. [107],[113]
0_0^0 [cm^{-1}]	$33\,493^b$	$33\,493$
$6a_0^0$ [cm^{-1}]	382.9(4)	382
$10b_0^2$ [cm^{-1}]	494.3(3)	494
12_0^1 [cm^{-1}]	678.0(5)	678
I^2 [cm^{-1}]	806.9(3)	807
1_0^1 [cm^{-1}]	815.2(2)	815

[a] Varsányi notation [114];
[b] set to reported value of Reference [107];

Table 4.2: *Spectroscopic constants of 4-aminobenzonitrile.*

parameter	this work	Ref. [109]	M06-2X[a]	B3LYP[a]	MP2[a]
A [MHz]	5581.0(4)	5579.3(5)	5589.84	5565.3	5572.2
B [MHz]	990.3627(7)	990.26(9)	990.5	984.7	981.1
C [MHz]	841.4827(6)	841.39(8)	841.8	837.0	834.9
χ_{aa}^1 [MHz]	2.48(1)		2.315	2.416	2.225
χ_{bb}^1 [MHz]	1.87(2)		2.038	2.115	1.800
χ_{cc}^1 [MHz]	-4.352(2)		-4.389	-4.531	-4.024
χ_{aa}^2 [MHz]	-4.138(9)		-3.712	-3.476	-2.868
χ_{bb}^2 [MHz]	2.40(2)		2.259	2.172	1.464
χ_{cc}^2 [MHz]	1.74(2)		1.475	1.304	1.405
no. lines	114				
error [kHz]	11.64				

[1] amino nitrogen [2] nitrile nitrogen [a] 6-31+G(d,p) basis set
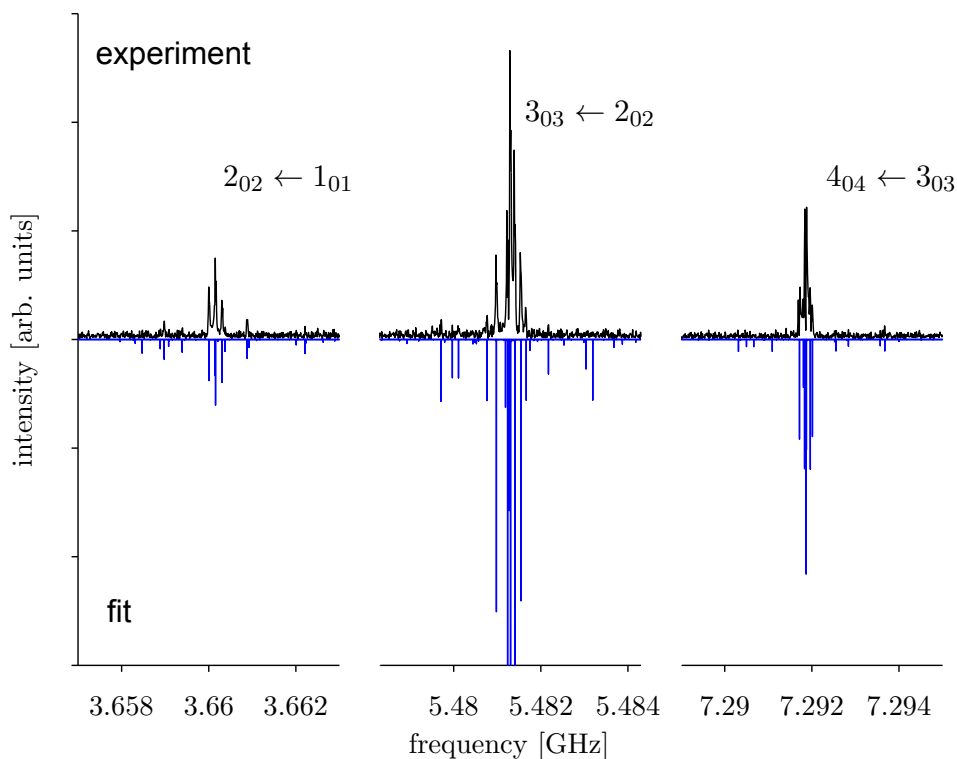
Figure 4.6: *Nuclear quadrupole coupling splitting due to the two nitrogen atoms in ABN for three different rotational transitions. For higher rotational quantum numbers the splitting decreases and gets more congested and thus more difficult to resolve. The transitions are labeled according to the scheme $J'_{K'_a K'_c} \leftarrow J_{K_a K_c}$.*

the case of the molecules described herein, the transformation between the two coordinate systems is given by a rotation around the b axes by an angle θ [111]. Since the off-diagonal elements of the nuclear quadrupole coupling tensors are not determined in the experiment, this angle was estimated from quantum chemical calculations at the M06-2X/6-31+G(d,p) level of theory. For this purpose, the eigenvectors of the calculated nuclear quadrupole tensor were expressed in the coordinates of the inertial principal axis system. θ is then given by the angle between the axes x and a or equivalently between the axes z and c. The axes y and b coincide. The transformed values of the nuclear quadrupole coupling components are then derived from the experimental results by a coordinate rotation, as discussed in Reference [111].

Table 4.3: *Nitrile quadrupole coupling in ABN, DMABN and benzonitrile.*

parameter	ABN	DMABN [111]	benzonitrile [119]
χ_{aa} [MHz]	-4.138(9)	-4.11(30)	-4.2574(4)
χ_{bb} [MHz]	2.40(2)	2.40(13)	2.289(1)
χ_{cc} [MHz]	1.74(2)	1.71(13)	1.949(1)

Table 4.4: *Nuclear quadrupole coupling constants of the nitrogen in the amino group. The values are given in the principle axis system of χ.*

parameter	aniline [118, 120]	ABN	DMABN [111]	DMA [111]
χ_{xx} [MHz]	2.72	2.69	2.56	2.61
χ_{yy} [MHz]	1.86	1.87	2.80	2.80
χ_{zz} [MHz]	-4.59	-4.559	-5.35	-5.41
θ [MHz][a]	13.3	9.7	2.8	3.6

[a] rotation angle

For the nuclear quadrupole coupling constants of the nitrile-nitrogen atom, the corresponding corrections are very small and thus have been neglected. In Table 4.3, the obtained nuclear quadrupole coupling constants for ABN, DMABN and benzonitrile are compared. Both the amino and the dimethylamino group are known to have a strong electron-donating effect on the aromatic ring. The very similar nuclear quadrupole coupling constants for ABN and DMABN compared to the reference molecule benzonitrile confirm this result.

The comparable nuclear quadrupole coupling constants of the amino-nitrogen resulting from these rotations are presented in Table 4.4. In molecules with methylated amino groups (DMABN, DMA), the nuclear quadrupole coupling of the amino-nitrogen atom is enhanced because of the electron-donating character of the methyl groups. However, the nitrile group is known to be electron withdrawing. This property leads to a reduction of the amine nuclear quadrupole coupling, as can be seen for DMABN when compared to DMA. ABN features significantly lower nuclear quadrupole coupling constants than DMA or DMABN. Together these results indicate a lower electron density close to the nitrogen atom in the amino group and thus a lower tendency for the existence of charge-transfer states. In addition the similarity between ABN and aniline is strengthened by the comparison in Table 4.4.

To further support this argument, a population analysis of the amino-nitrogen p-orbitals was carried out according to the Townes-Dailey model [67, 69] and in close analogy to References [111] and [121]. It allows for the estimation of the following indicators from the nuclear quadrupole coupling constants: The ionic character of the amino group N-H bonds, $i_\sigma(NX)$, the ionic character of the N-C bond between the amino group and the aromatic ring, $i_\sigma(NC)$, and the covalent character of the latter, $\pi_c(NC)$. From these quantities, the orbital occupancies of the nitrogen p-orbitals (N_x, N_y, N_z) can be calculated.

The ionic character of the amino group N-H bonds can be calculated using

$$i_\sigma(NX) = \frac{\cos\varphi}{\cos\varphi - 1} \equiv a^2 \tag{4.1}$$

where φ is the angle between the two N-H bonds. It is linked to the amount of s-type hybridization and thus to $i_\sigma(NX)$ (see References [69] and [63], page 234 ff). $i_\sigma(NC)$ can be estimated using the following equation:

$$\frac{\chi_{xx} - \chi_{yy}}{\chi_{210}} = 3a^2 \left[i_\sigma(NX) - i_\sigma(NC)\right] \tag{4.2}$$

χ_{210} has a known value of -10 MHz and describes the coupling of one unpaired p-orbital electron of a nitrogen atom to the electric field gradient [67]. The quadrupole coupling constants were determined from the experimental data. The covalent character of the N-C bond $\pi_c(NC)$ is linked to the values described above via:

$$\frac{\chi_{zz}}{\chi_{210}} = \frac{[1 - (1 - a^2)i_\sigma(NX) - a^2 i_\sigma(NC) - \pi_c(NC)]}{[1 + .3(2i_\sigma(NX) + i_\sigma(NC) - \pi_c(NC))]} \tag{4.3}$$

Finally, the orbital occupancies of the nitrogen p-orbitals (N_x, N_y, N_z) can be calculated:

$$N_x = 1 + \frac{1}{2}\left[i_\sigma(NX) + i_\sigma(NC)\right] \tag{4.4}$$

$$N_y = 1 + i_\sigma(NX) \tag{4.5}$$

$$N_z = 2 - \pi_c \tag{4.6}$$

N_z corresponds to the lone-pair occupation of the nitrogen atom. The value for φ is needed for the calculations above and was taken from quan-

Table 4.5: *Bond characters and nitrogen p-orbital occupancies.*

parameter	aniline	ABN	DMA	DMABN
φ	113.1	113.9	114.7	118
$i_\sigma(\mathrm{NC})$	0.38	0.36	0.27	0.30
$i_\sigma(\mathrm{NX})$ X=H, X=CH$_3$	0.28	0.29	0.29	0.32
$\pi_c(\mathrm{NX})$	0.12	0.15	0.04	0.09
N_x	1.33	1.32	1.28	1.31
N_y	1.28	1.29	1.29	1.32
N_z	1.88	1.85	1.96	1.91

tum chemical calculations for ABN and from the corresponding references for the compared molecules.

The interpretation of the resulting numbers, listed in Table 4.5, follows closely the arguments given in Reference [111]. It stands out that ABN has the lowest occupation of the lone-pair orbital N_z of the amino nitrogen and a high covalent character π_c of the amino group bonds. The combination of the high ionic character of the nitrogen aromatic carbon bond $i_\sigma(\mathrm{NC})$ in ABN and the low ionic character of this bond in DMABN suggests that less charge is concentrated at this location. This could represent a barrier for charge-transfer states and thus could explain the absence of dual fluorescence in ABN. In general, this finding adds microscopic details of the electron distribution to the discussion of dual emission in aminobenzonitrile-like molecules, which can be related to the dynamics of the molecule upon electronic excitation [108].

4.4   Conclusions

We investigated the broadband rotational and the REMPI spectrum of ABN with our broadband microwave spectrometer and the connected mass spectrometer device.

The assigned rotational constants were determined to higher precision and agree very well with previous findings from rotationally resolved electronic spectra. These high-resolution results were used to benchmark quantum chemical calculations. We find that for ABN density functional theory using the M06-2X functional showed the best agreement.

The hyperfine structure due to the nuclear quadrupole coupling of the two chemically distinct nitrogen atoms in ABN was resolved. The experimentally determined nuclear quadrupole coupling constants allowed for

the analysis of the electronic environment of the nitrogen locations. It was found that DMABN and ABN have a similar electronic environment at the nitrile-nitrogen atom and hence that the influence of the methyl groups through the aromatic ring is negligible compared to the effect of the amino group itself.

By calculating the occupancies of the hybrid orbitals of the amino-group nitrogen, we showed that there is a significantly lower charge density in ABN compared to other para-substituted benzonitriles like DMABN. This result is particularly interesting with respect to the occurrence of dual fluorescence because it can be interpreted as a possible barrier to charge-transfer states.

Chapter 5

The shape of ibuprofen in the gas phase*

5.1   Introduction

Ibuprofen (from **i**so-**bu**tyl-**pro**panoic-**phen**olic acid), depicted in Figure 5.1, is of high relevance in medical applications because of its anti-flammatory, pain-relieving effect and is today a widespread non-prescriptive drug. The World Health Organization lists it as one of the essential drugs needed in a basis health care system [122]. It belongs to the class of non-steroidal anti-inflammatory drugs (NSAIDs), which inhibit the enzyme cyclooxygenase (COX) by interacting with and thus competitively blocking its active site (e.g. see References 123–126). Cyclooxygenase has a key role in the production chain of pain, inflammation and fever mediators, such as the class of prostaglandins.

From a structural point of view, ibuprofen (IUPAC name (RS)-2-(4-(2-methylpropyl)phenyl)propanoic acid) consists of an aromatic ring connecting an isobutyl and a propanoic acid group (see Fig. 5.1). It features a stereogenic center at the α-methyl carbon site connecting the carboxyl group and the aromatic ring. Interestingly, only the S-enantiomer has a pharmaceutical effect [127, 128]. The main conformational degrees of freedom are the orientation of the carboxyl group and the positioning of the isobutyl group with respect to the aromatic ring. Previous studies of ibuprofen include vibrational spectroscopy and theoretical calculations of the conformations, which predict a large number of low-energy conformers [129–132].
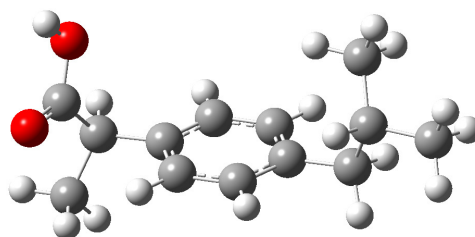
Figure 5.1: *Scheme of the molecular structure of ibuprofen, consisting of a phenyl ring (middle), and an isobutyl group (right), and a propanoic acid group (left).*

Studies of the enzyme-inhibitor complex structures in crystals revealed that the inhibiting effect of ibuprofen is achieved by inserting the carboxyl group into the hydrogen bond network of the active site of the COX enzyme and thus blocking the molecular recognition mechanisms needed for its catalyzing effect [133]. The binding of ibuprofen to the active site of the enzyme is depicted in Figure 5.2. The nature of the active site of the COX enzyme has been studied with NMR spectroscopy [134, 135] and an overview on the structural basis of the inhibition effect is given in Reference [136]. These studies suggest that conformational flexibility of the inhibitor and at the same time a stable configuration of the carboxyl group are a prerequisite for successfully establishing the enzyme-inhibitor complex. The elucidation of the structures of the ibuprofen conformers presented in this work can help to identify the interactions and conformational changes accompanied with the molecular recognition of the inhibitors.

Rotational spectroscopy provides detailed and unambiguous information on the molecular structure and it supports the characterization of larger, conformationally flexible molecules, such as strawberry aldehyde ($C_{12}H_{14}O_3$) for which five low-energy conformers have been observed [137]. The structurally related pain-relieving molecules aspirin [43] and paracetamol [46] have been studied recently by rotational spectroscopy as well. Both molecules also show conformational flexibility.

5.2   Experimental details

For the experiments described here, ibuprofen was purchased from Sigma-Aldrich (98 % purity) and used without further purification. The sample was heated to 110 °C in a reservoir and the carrier gas neon, with a backing pressure of 1.5 bar, was flowed over it to create a gas mixture. Sub-
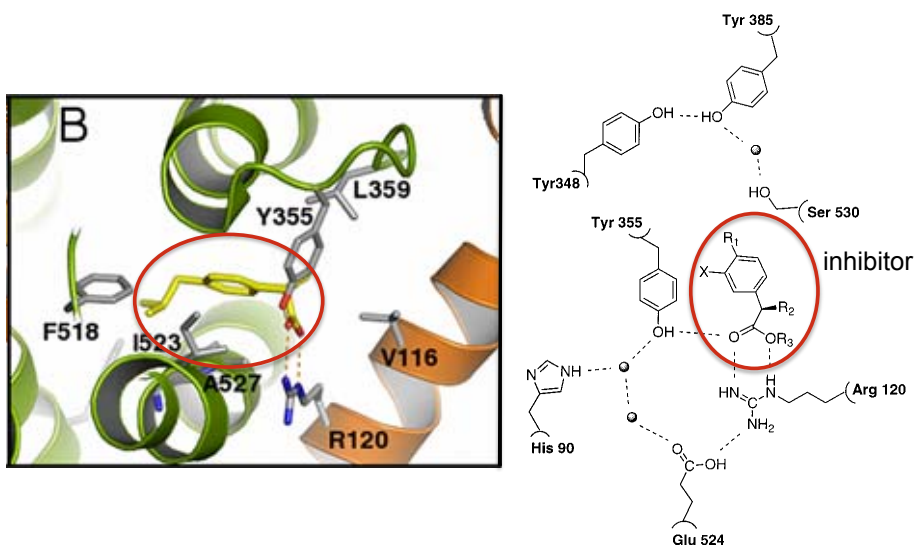
Figure 5.2: *Binding position of ibuprofen or related drugs (red circles) to the active site of the COX enzyme. The figures are taken from References [133] and [135].*

sequently, this mixture was expanded into vacuum through a pulse nozzle (Sec. 3.1). The ibuprofen molecules were excited by a $1\,\mu$s long microwave pulse, which was linearly frequency chirped from 2 to 8.5 GHz. $10\,\mu$s of the resulting free induction decay (FID) were recorded, starting $5\,\mu$s after the excitation pulse and then amplified and converted into a digital signal. The length of the recorded FID sets the frequency resolution to 100 kHz, whereas the full width at half maximum of observed lines was on the order of 30 kHz. 650 000 FIDs have been recorded and averaged for the final rotational spectrum depicted in Figure 5.3. More experimental details can be found in Chapter 3.

5.3   Results and Discussion

In total, four conformers of ibuprofen were observed with similar intensities (see Fig. 5.5). Each spectrum was fit using an asymmetric rotor Hamiltonian (Watson S-Reduction in I^r representation) as implemented in the program PGOPHER [86] (Sec. 2.1). The obtained spectroscopic parameters are listed and compared to density-functional values in Table 5.2. In total 52 - 77 lines per conformer were assigned and the average error of the fits is on the order of 50 kHz. Transitions from $J + 1 \leftarrow J = 4 \leftarrow 3$ up

to 15 ← 14 are present in the spectrum. In our frequency (2 to 8.5 GHz) and temperature range (approximately 1-3 K) c- and b-type transitions are predicted to be much weaker and are thus not observed in the data. Including distortion constants does not further improve the accuracy of the fit and thus they are not accessible in this frequency range for ibuprofen. As apparent from Figure 5.3 there are unassigned lines left in the recorded rotational spectrum. They are not connected to additional conformers of ibuprofen and most likely arise from unidentified complexes or fragments.
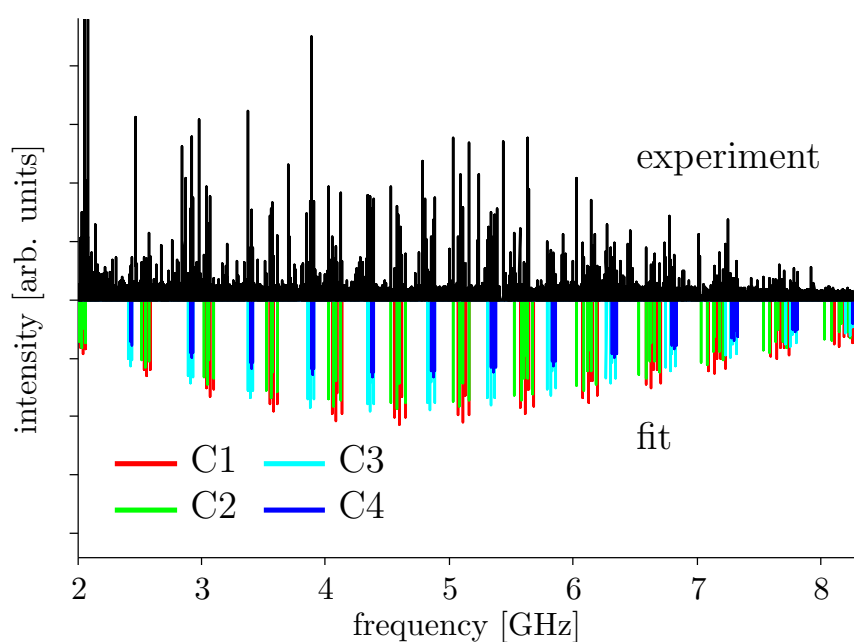
Figure 5.3: *Rotational spectrum of ibuprofen: The upper trace shows the experimental broadband spectrum, and the lower trace represents the results of fitting asymmetric rotor Hamiltonians to the four lowest energy conformers C1-C4 at a temperature of 1.5 K. Known background lines have been removed. The spectrum is dominated by a-type transitions.*

For the ibuprofen conformers, no line splitting due to internal rotation was observed. Quantum chemical calculations of the respective barriers show that they are all higher than 13 kJ/mol, which does not result in resolvable effects for methyl tops in our experiments. The calculated barriers for internal rotational are listed in Table 5.1 and the corresponding bond labels are depicted in Figure 5.4.

For the following discussion of the obtained conformers, the results are compared to quantum chemical calculations at the M06-2X/6-31+G(d,p)

Table 5.1: *Calculated barriers to internal rotation using the M06-2X/6-31+G(d,p) level of theory around five different single bonds in ibuprofen (see Fig. 5.4). Different barriers for each group belong to several minimum positions during a full rotation of the group. All barriers were calculated for the lowest energy conformer C1.*

bond label	rotating group	barrier [kJ/mol]		
1	COOH	32.07	13.73	
2	CH_3	14.11	14.11	14.11
3	isopropyl	36.72	33.62	18.09
4	CH_3	15.95	15.95	15.95
5	CH_3	3.56	3.56	3.56
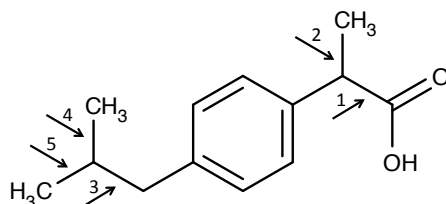
Figure 5.4: *Labels for the calculated barriers to internal rotation around five different single bonds.*

level of theory as implemented in Gaussian09 (see Tab. 5.2). Due to the good agreement between experiment and theory the experimentally identified conformers can directly be assigned to the predicted four lowest energy conformers, which are presented in Figure 5.6 and labeled C1-4 (sorted by increasing energies). The main conclusion is that all conformers show the same orientation of the propanoic acid group but differ in the arrangement of the isobutyl group. Their energies are similar and only differ by less than 0.3 kJ/mol (see Tab. 5.2), explaining the similar intensities in the spectrum (see Fig. 5.5). Other calculated low energy conformers with a different orientation of the COOH group are at least 1.5 kJ/mol higher in energy and are not populated under the cold conditions of our molecular jet. These conformers are depicted in Figure 5.7 and the corresponding calculated parameters are given in Table 5.3.

The stabilization of the carboxyl group is based on the interaction of the hydrogen atom of the α-methyl group with the C=O group via hydrogen bonding. The nature of this interaction can be further illuminated with the help of calculations. They show that the Mulliken charge of the carbonyl oxygen is approximately 0.4 e while that of the hydroxy group as

Table 5.2: *Spectroscopic constants of ibuprofen. The quantum chemical predictions are obtained by DFT calculations (M06-2X/6-31+G(d,p)).*

parameter	C1	calc	C2	calc	C3	calc	C4	calc
A [MHz]	1325.8(9)	1331	1356.1(7)	1355	1555(4)	1576	1523(9)	1536
B [MHz]	260.712(1)	261	261.454(2)	263	245.443(1)	247	244.892(1)	246
C [MHz]	251.179(1)	252	248.310(1)	249	239.754(2)	241	242.101(1)	243
E [kJ/mol]		0		0.15		0.21		0.28
no. lines	66		77		66		52	
error [kHz]	43		45		64		41	
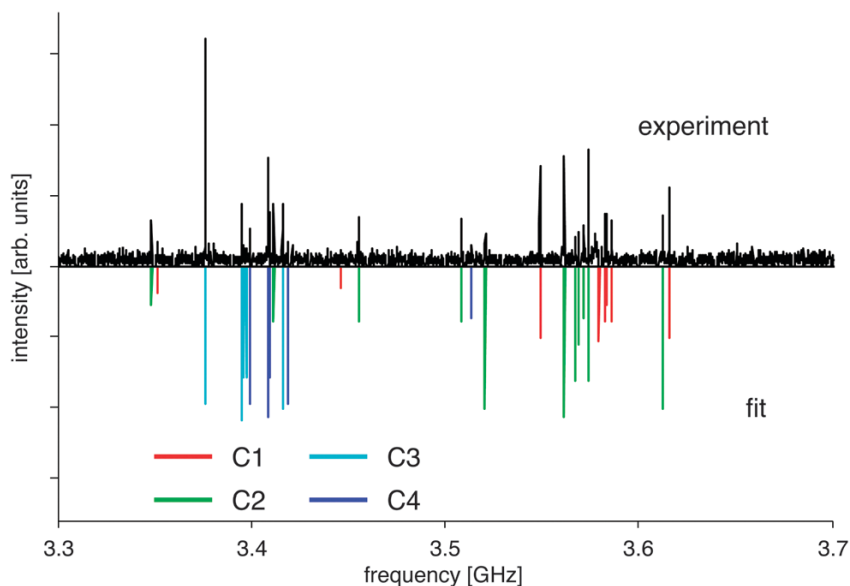
Figure 5.5: *Part of the broadband rotational spectrum of ibuprofen, illustrating the spectral features of the four conformers C1-C4.*

a whole is 0.04 e, so that their electrostatic interaction with the α-methyl hydrogen leads to significantly different energies ($\Delta E \approx 3.9$-5.9 kJ/mol). Interestingly, in contrast to these findings for ibuprofen, the two low-lying conformers of the related NSAID molecule aspirin do differ in the relative orientation of the carboxyl group [43].

Consequently, the conformational richness of ibuprofen arises from the isobutyl group. The first degree of freedom is to adopt a cis- (C1 and C2) or trans-configuration (C3 and C4) with respect to the carboxyl group i.e., being located on the same side or the opposite site of the phenyl ring compared to the carboxylic group. This corresponds to the rotation of the bond connecting the isobutyl group to the phenyl rest (Fig. 5.6). The calculations indicate that a location of both substituents on the same side of the aromatic ring plane is preferred.

Furthermore, a rotation of the isopropyl group around the bond connecting it to the rest of the molecule leads to three additional, nonequivalent minimum configurations (Fig. 5.6). Two of these minima of the potential energy surface are characterized by an elongated carbon chain with one methyl top maximizing the distance to and the other one pointing out of the aromatic ring plane. They differ only by the positioning of the latter methyl top with respect to the rest of the molecule. All observed molecules belong to this class of conformers. In the third possible conformer related
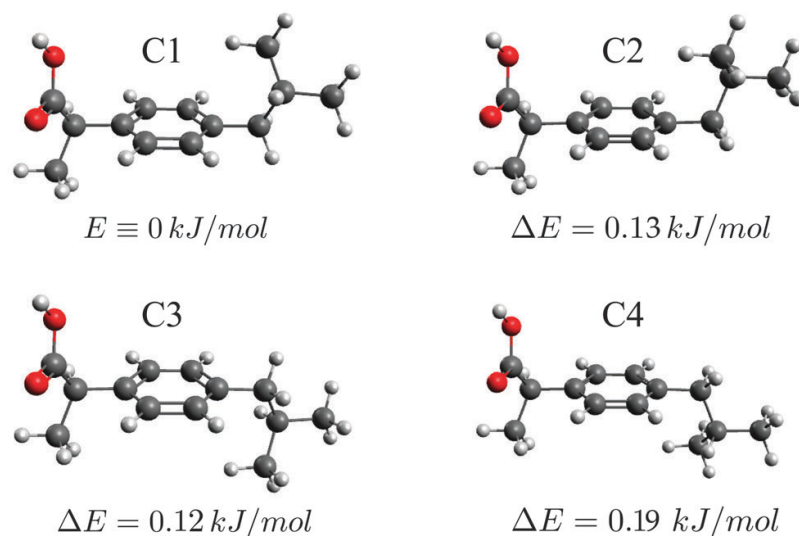
Figure 5.6: *The calculated structures and relative energies (not zero-point corrected) of the four experimentally observed ibuprofen conformers (M06-2X/6-31+G(d,p) theory level). They all show the same orientation of the carboxylic group but differ in the arrangement of the isobutyl group.*

to this rotation, both methyl groups of the isopropyl moiety point out of the aromatic ring plane in a symmetric arrangement. It is significantly higher in energy (ΔE=1.81 kJ/mol) and is not observed in the spectrum. Interestingly, this third conformer was observed in microwave studies of the closely related molecule isobutylbenzene though the associated energy difference is similar [138]. This might be explained by the use of a mixture of helium and neon as backing gas, leading to different occupations of the individual conformers.

Our work agrees with the calculated lowest energy conformers in Reference [131], beside the fact that conformer C2 is not present in their considerations. Note that calculations using B3LYP/6-31+G(d,p) resulted in larger deviations to the experimental rotational constants.

Since the individual conformers only differ in the properties of the isobutyl group and share the same orientation of the carboxyl group they have very similar rotational constants. For example, this becomes apparent in the small spacing between the a-type transition groups of the conformers C1 and C2 or C3 and C4 shown in Figure 5.5. Nevertheless, due to the narrow line widths and the high resolving power of rotational spectroscopy these structurally and energetically very similar molecules can be unambiguously differentiated.
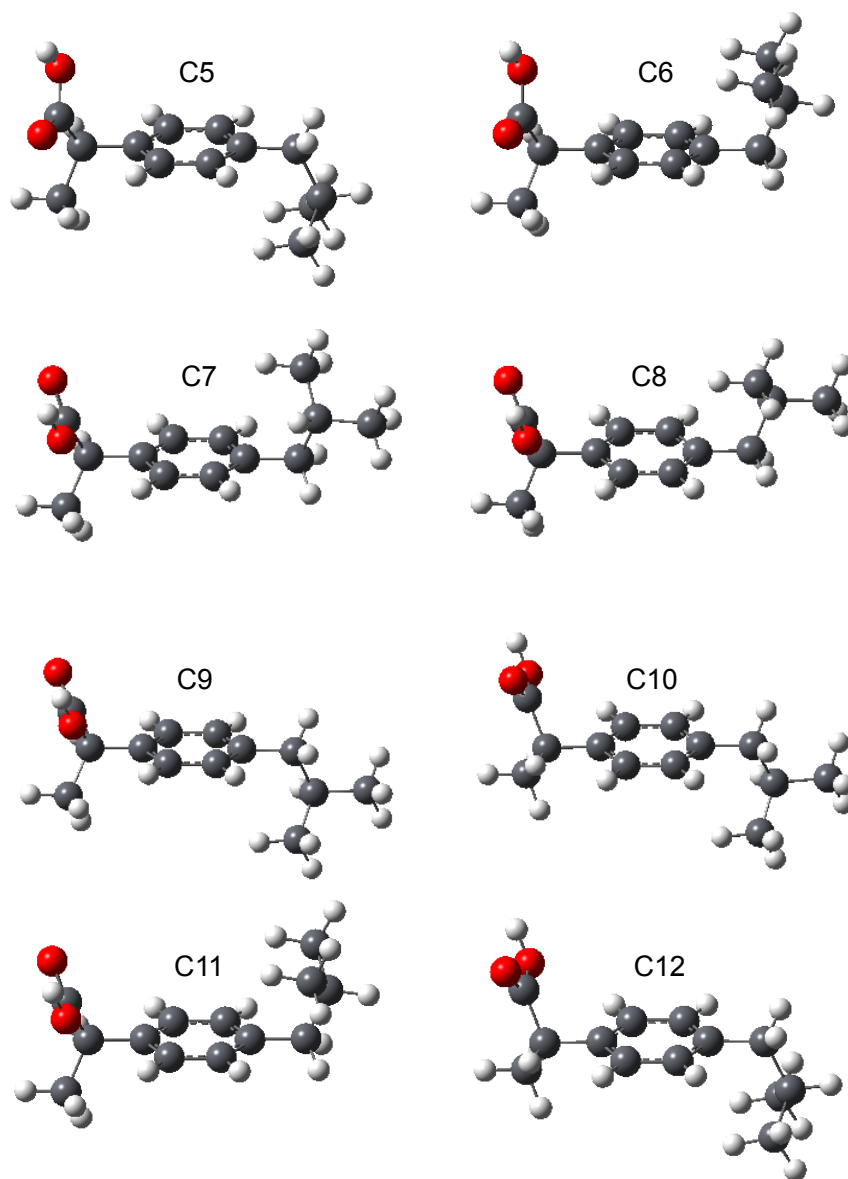
Figure 5.7: *Calculated structures of higher energy conformers of ibuprofen, which are not present in the spectrum. For the calculations the M06-2X/6-31+G(d,p) level of theory was used and the corresponding parameters are given in Table 5.3.*

In supplementary measurements, where the sample was kept at the thermal decomposition temperature of ibuprofen (80 - 100 °C) for a longer time, the spectra of two different, newly observed molecules dominate over

the almost vanishing ibuprofen signal. Their spectra show very clear and strong a-type transitions. We suggest that they correspond to decarboxylation products. This would agree with the fragmentation behavior found before in mass spectrometry studies [139, 140]. Interestingly, both fragments show a pronounced line splitting, which might be due to the internal rotation of the former α-methyl group that is less sterically hindered than in ibuprofen.

5.4   Conclusions

To summarize, in this work four conformers of ibuprofen were identified in the rotational spectrum and assigned to the four lowest energy conformers with the help of quantum chemical calculations. This molecule shows rich conformational flexibility of the isobutyl group that might be needed for the transport of the molecule to the COX enzyme and its subsequent recognition. The structural assignment of the conformers revealed a stabilizing interaction of the α-methyl top with the C=O group of the carboxyl group, which is the same for all observed conformers. This combination of stiffness of the group inserted in the H-bonding network of the COX enzyme and the flexibility of the rest of the molecule indicates that all conformers could adopt to the suitable configuration in order to act as inhibitors. Our results can be used as reference structures to identify structural changes of ibuprofen upon formation of the enzyme-inhibitor complex.

Table 5.3: *Calculated parameters for the twelve lowest energy conformers of ibuprofen using the (M06-2X/6-31+G(d,p) level of theory. The corresponding structures are given in Figure 5.7.*

conformer	A [MHz]	B [MHz]	C [MHz]	μ_A [D]	μ_B [D]	μ_C [D]	μ [D]	E [kJ/mol]
C1	1330.50	261.29	251.80	-1.0689	-0.0409	1.1795	1.5923	0
C2	1354.98	262.89	249.51	-1.1333	-0.4097	1.3425	1.8041	0.13
C3	1576.42	246.96	240.81	1.1494	-0.7773	1.1749	1.8181	0.12
C4	1536.05	246.25	243.49	1.0361	0.2195	1.1643	1.574	0.19
C5	1394.90	269.17	265.67	1.2051	-1.2353	0.3605	1.763	1.81
C6	1191.56	289.62	278.32	-1.2389	-0.4671	1.1602	1.7604	1.85
C7	1331.17	258.77	251.14	-0.8285	-1.1525	-1.3544	1.9619	3.90
C8	1347.50	260.58	249.94	-0.843	-0.7056	-1.4432	1.8908	3.97
C9	1606.47	243.88	238.82	-1.3042	1.5546	0.1805	2.0372	4.23
C10	1577.83	242.51	240.79	-1.303	-0.1272	-1.7303	2.1698	4.27
C11	1180.11	287.56	279.49	-0.8869	-0.6566	-1.6149	1.9559	5.69
C12	1428.70	267.23	261.51	-1.4321	1.5191	0.4832	2.1429	5.88

Chapter 6

Structure determination of *trans*-cinnamaldehyde*

6.1   Introdution

The odorant molecule *trans*-cinnamaldehyde is the major component of cinnamon oil [141] and is responsible for its characteristic smell. The molecule consists of a phenyl ring with an unsaturated aldehyde attached. The structure of the molecule is planar due to the conjugation of the π-electron system, as seen in Figure 6.1. This conjugation causes a change of the typical carbon-carbon bond lengths, which is an interesting effect to study. Since both the structure and the structural flexibility of an odorant molecule are important for molecular recognition by olfactory receptors, a precise experimental molecular structure can be useful for further studies on the structure-odor relationship [142].

The importance of investigating the structure of odorant molecules was already shown before [143, 144], and it is also demonstrated that olfaction is complicated to describe because there are many structures and a vast number of odors. A direct relationship between structure and odor has so far been difficult to establish. One major aim in that research field is to identify common structural features that cause the same odor perception. However, as in many molecular recognition processes, conformational flexibility is known to play a role. A better understanding of this as well as the identification of such common structural features will be an important step also towards predicting the odor of a respective molecule.

---

*This chapter is based on the following publication: S. Zinn, T. Betz, C. Medcraft and M. Schnell. Structure determination of *trans*-cinnamaldehyde. *Physical Chemistry Chemical Physics*, 17:16080-16085, 2015.
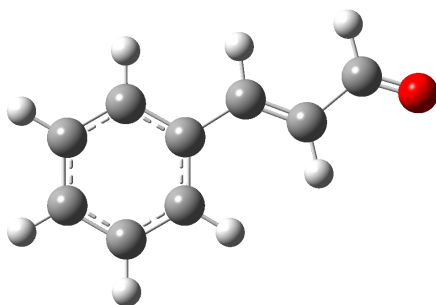
Figure 6.1: *Scheme of the molecular structure of s-trans-trans-cinnamaldehyde ((E)-3-phenylpropenal).*

Cinnamaldehyde was recently found to activate the transient receptor potential ion channel TRPA1, which mediates thermosensation, and thus cinnamaldehyde can be a potential molecular model for studying why noxious cold can be perceived as a burning pain [145]. For this the conformational flexibility of the molecule can be of special interest.

In a photochemical reaction with UV-light *trans*-cinnamaldehyde isomerises to *cis*-cinnamaldehyde [146]. Biochemical reactions with this motif can, for example, also be found in the retina of (human) eyes. Recently, these light-triggered dynamics were studied with femtosecond crystallography on minicrystals of photoactive yellow protein (PYP) [20]. The chromophore of this protein reveals structural similarities with *trans*-cinnamaldehyde, which can be seen as a model system for this photoactive protein in gas-phase studies, another example for the physiological relevance of a detailed structure determination of *trans*-cinnamaldehyde.

Four possible stereoisomers of cinnamaldehyde can exist: two diastereomers, differing in a *cis*- or *trans*-orientation of the carbon-carbon double bond of the side chain. Each of these diastereomers can consist of two conformers, differing by a rotation around the single bond in between the two double bonds. Here we use broadband rotational spectroscopy to study the two conformers of the *trans*-diastereomer, *s-trans-trans*-cinnamaldehyde and the higher energy conformer *s-cis-trans*-cinnamaldehyde that are depicted in Figure 6.2.

This study extends earlier work on *trans*-cinnamaldehyde using low-resolution microwave spectroscopy by Steinmetz et al. [147], in which only one rotational constant could be determined due to low spectral resolution. Here, we report complete sets of rotational constants for both low-energy conformers of *trans*-cinnamaldehyde. We were also able to obtain the rotational constants for all the mono-substituted ^{13}C-isotopologues of the ener-
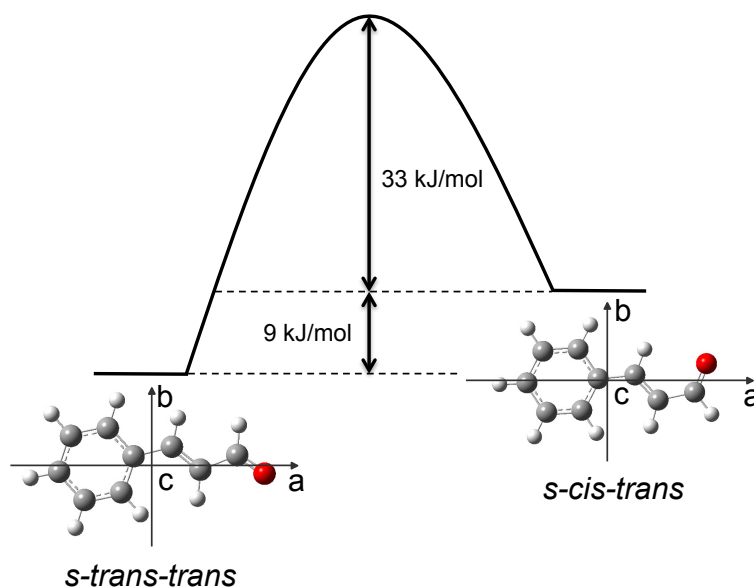
Figure 6.2: *Scheme of the molecular structures of s-trans-trans-cinnamaldehyde ((E)-3-phenylpropenal) and s-cis-trans-cinnamaldehyde in the coordinate system of the molecular moments of inertia and the calculated energy difference and isomerisation barrier of the two conformers, using the MP2 level of theory and the 6-311++G(2d,2p) basis set.*

getically lower conformer in natural abundance and hence to determine its carbon backbone structure using the Kraitchman's equations (r_s-structure) and a mass dependent method (r_m-structure). Different methods to determine the structure from the rotational constants are discussed in Subsection 2.1.4. The obtained structure is compared to a recent gas electron diffraction (GED) study [148]. Such a comparison is also interesting from a conceptional point of view. Typically, gas electron diffraction is performed at the elevated temperatures necessary to generate sufficient vapor pressure of the respective molecules not followed by a supersonic expansion leading to cooling. As a consequence, the molecules can be vibrationally excited and several conformers can be populated, which complicates the analysis. The suitability of the analysis of the experimental data often strongly relies on the quality of the quantum-chemical calculations. A direct comparison between microwave data and GED data will thus be helpful to evaluate the quality of the GED data in the particular case of *trans*-cinnamaldehyde, for which two conformers are present.

6.2   Experimental details

A sample of *trans*-cinnamaldehyde was purchased from Sigma-Aldrich
($\geq$ 95 % purity) and used without further purification. The sample is
a liquid at room temperature and has a reported boiling point of 251 °C.
It has a strong total dipole moment of 5.1 D with the two dipole moment
components of 4.9 D for μ_a and -1.5 D for μ_b. For the measurements, the
sample was heated to 100 °C in a reservoir. Neon was used as a carrier gas
with an absolute backing pressure of 1.8 bar. The gas mixture was super-
sonically expanded into the vacuum chamber via a pulsed nozzle. After
this, the molecules were excited by a 1 μs long microwave pulse, which
was linearly chirped in frequency. Fifty microseconds of the resulting free
induction decay (FID) was recorded, this results in a spectral resolution of
20 kHz. Further experimental details are given in Section 3.2. In total 1.2
million FIDs were recorded and averaged. The rotational spectrum was
obtained by Fourier transforming the experimental data. A Kaiser-Bessel
window function was applied to the spectrum to identify weak transitions
that otherwise, in some cases, could overlap with stronger transitions.

Predictions of the rotational constants for different possible conformers
of cinnamaldehyde were obtained from quantum chemical calculations. Ge-
ometry optimizations were performed using the density-functional theory
(DFT) methods M06-2X and B3LYP as well as the MP2 level of theory, all
with a 6-311++G(2d,2p) basis set as implemented in the program package
Gaussian. The results are listed in Tables 6.1 and 6.2.

The spectra were fit using an asymmetric rotor Hamiltonian (Watson
S-Reduction in I$_r$ representation, Table 2.1 [149]) as implemented in the
PGOPHER program suite, [86].

6.3   Results and Discussion

The experimental spectrum and the corresponding fits for both conform-
ers are shown in Figure 6.3. The experimental spectrum is dominated by
strong a-type transitions, as predicted from the dipole moments. Together
with weaker b-type transitions they could be assigned to *s-trans-trans*-
cinnamaldehyde by comparison to the rotational parameters obtained from
ab initio calculations and to the results of the previous low-resolution mi-
crowave study [147].

In addition, the spectrum of the second conformer, *s-cis-trans*-cinnam-
aldehyde, could be assigned, which is about 40 times weaker. A zoom into
the measured spectrum, illustrating the spectral features of *s-cis-trans*-
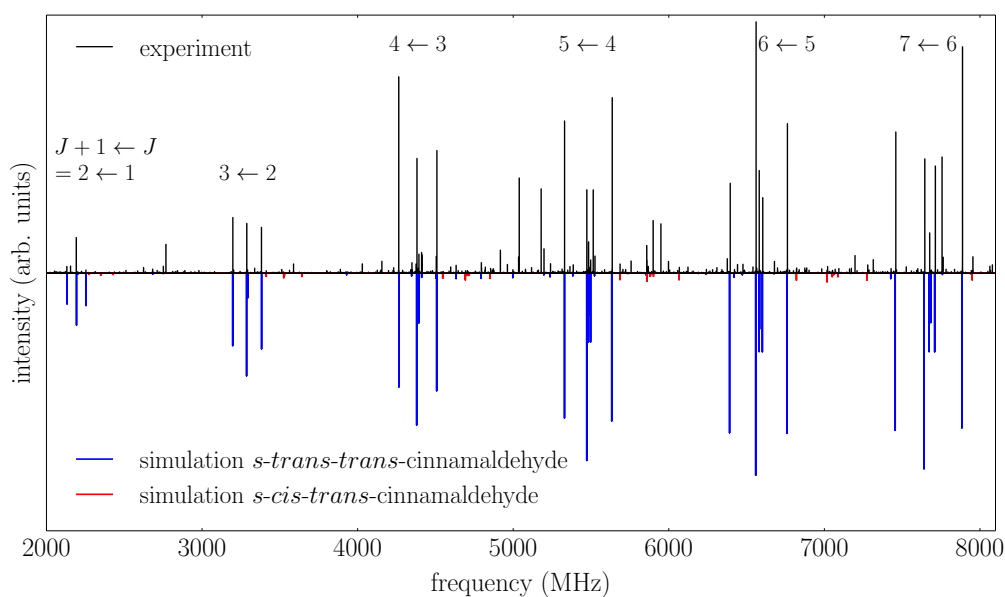
Figure 6.3: *The rotational spectrum of s-trans-trans- (blue trace) and s-cis-trans-cinnamaldehyde (red trace). The upper trace shows the experimental data and the lower trace represents the result of fitting asymmetric rotor Hamiltonians for both conformers to the spectrum. Additional transitions seen in the spectrum may arise from complexes of water and cinnamaldehyde but are not assigned yet.*

cinnamaldehyde, is depicted in Figure 6.4. The two conformers differ in the orientation of the terminal aldehyde group with respect to the C-C double bond of the alkenyl side chain, as depicted in Figure 6.2. The most abundant conformer *s-trans-trans*-cinnamaldehyde is calculated to be about 9 kJ/mol lower in energy than *s-cis-trans*-cinnamaldehyde (MP2/6-311++G(2d,2p)). They are separated by an isomerisation barrier of 33 kJ/mol (see Fig. 6.2), in accordance with the significant intensity difference. The higher energy of the cis-conformer seems to be caused by steric repulsion of the oxygen and the C3 carbon atom and the two double bonds (C2-C3 and C1-O). The atom labels are given in Figure 6.5.

The obtained energies are very similar to those found for acrolein ($H_2CCHCHO$), which is the simplest member in the group of α,β-unsaturated aldehydes. Using microwave spectroscopy [150], the structures of both the *s-cis-* and the *s-trans*-conformer of acrolein were obtained, with a calculated energy difference of 8.5 kJ/mol and a calculated barrier height of 29.3 kJ/mol (CCSD(T)/CBS+CV) [151]. This similarity might be a hint to the dominance of the local electronic environment in the side chain

of *trans*-cinnamaldehyde.

The structural isomer *cis*-cinnamaldehyde, which is the product of a photochemical reaction of *trans*-cinnamaldehyde, was not observed. Furthermore, no spectroscopic indications for internal dynamics, such as rotation around single bonds, were found.

In the following the results of the individual conformers are discussed in more detail.

s-trans-trans-cinnamaldehyde

The experimentally determined spectroscopic constants for *s-trans-trans*-cinnamaldehyde and a comparison to calculated parameters are given in Table 6.1. In total, 93 rotational transitions (52 a- and 41 b-type transitions) could be assigned with an average error of the fit of 6.5 kHz. Anharmonic calculations were carried out using the B3LYP functional of theory using a 6-311++G(2d,2p) basis set. The fitted distortion constants are comparing well with the ones from these calculations. Comparing the rotational constants, the MP2 level of theory agrees best with the experimental values, with deviations of 0.5% and less. For this rather rigid molecule an excellent agreement of the predicted rotational constants using quantum chemical calculations to the experimental determined values can be found. However, in the case of the weakly bound complexes glycolaldehyde dimer and diphenylether methanol (Ch. 7 and 8) a precise prediction of the strength of intermolecular interaction is still challenging with theoretical approaches.

In earlier studies of *trans*-cinnamaldehyde, where the molecule was regarded as a near symmetric top molecule, only the sum of B+C could be determined [147]. This value is in good agreement with the one determined in our high-resolution study, with a deviation of less than 1 % (Tab. 6.1).

The inertial defect Δ of the molecule, calculated from the obtained rotational constants, is rather small. Its value is a scale for the deviation of the molecular structure from planarity ($\Delta = 0$ for planar molecules) and will be discussed in more detail below.

Table 6.1: *Experimentally determined and calculated spectroscopic constants of s-trans-trans-cinnamaldehyde. For all calculations the 6-311++G(2d,2p) basis set was used.*

parameter	experiment	B3LYP	M06-2X	MP2	Steinmetz et al. [147]
A [MHz]	4866.3795(13)	4915.85	4926.28	4884.51	
B [MHz]	579.05960(17)	578.73	582.94	579.03	
C [MHz]	517.81608(16)	517.78	521.26	517.67	
B+C [MHz]	1096.87568(33)	1096.51	1104.20	1096.70	1106.3(1)
D_K [kHz]	1.72(12)	1.2			
D_{JK} [kHz]	0.076(10)	0.08			
D_J [kHz]	0.01005(82)	0.008			
d_1 [kHz]	0.130(32)	0.105			
d_2 [kHz]	0.00123(20)	0.00113			
$|\mu_a|$ [D]		4.73	4.31	4.90	
$|\mu_b|$ [D]		1.17	1.21	1.53	
$|\mu_c|$ [D]		0	0	0	
Δ [u$\mathring{A}^2$]	-0.628				
J_{max}	17				
no. lines	93				
error [kHz]	6.5				

$\Delta = I_c - I_a - I_b$; u is the atomic mass unit

s-cis-trans-cinnamaldehyde

A closer look into the broadband spectrum reveals rotational transitions of the higher-energy conformer *s-cis-trans*-cinnamaldehyde (Fig. 6.4). In total, 33 transitions (19 a-type and 14 b-type) were assigned to this conformer and fit to an asymmetric rotor Hamiltonian with an error of the fit of 5.2 kHz. The experimentally determined constants and calculated values can be found in Table 6.2. Again, the MP2 level of theory gives the best agreement to the experimentally determined rotational constants. The results from the earlier low-resolution study [147] are also in fairly good agreement.

Due to the lower intensity only transitions up to $J = 10$ could be assigned in the spectrum, this leads to less well defined distortion constants for this conformer. The calculated inertial defect is small and of a similar order as for the *s-trans-trans*-conformer.
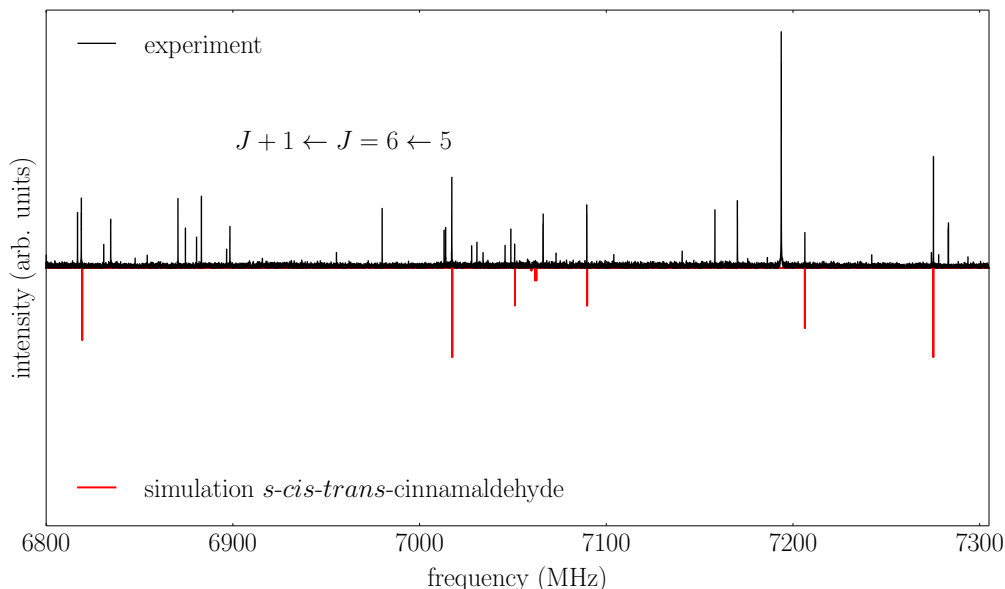
Figure 6.4: *Part of the broadband rotational spectrum (intensity scaled by a factor of 20 compared to Figure 6.3), showing the $J+1 \leftarrow J = 6 \leftarrow 5$ transition of the higher-energy conformer s-cis-trans-cinnamaldehyde (red trace). The upper trace shows the experimental data and the lower trace represents the result of fitting an asymmetric rotor Hamiltonian to it. Additional transitions seen in the spectrum may arise from complexes of water and cinnamaldehyde but are not assigned yet.*

^{13}C-isotopologues of *s-trans-trans*-cinnamaldehyde

For the *s-trans-trans*-conformer, we could also assign rotational transitions arising from all singly substituted ^{13}C-isotopologues. The assignments of these satellite lines for the $J'_{K'_a,K'_c} \leftarrow J_{K_a,K_c} = 7_{1,6} \leftarrow 6_{1,5}$ transition, as an example, are depicted in Figure 6.5.

For each ^{13}C isotopologue, between 12 and 22 rotational transitions could be assigned with an error for the fits between 3 kHz and 9 kHz. From this overall set of 30 rotational constants, the carbon atom positions, and thus the bond lengths and angles, were calculated using Kraitchman's equations for planar molecules (r_s-structure), as implemented in the KRA program [73]. The rotational constants of these fits and the calculated carbon atom positions of the r_s-structure are given in the Tables 6.3 and 6.4.

Table 6.2: *Experimentally determined and calculated spectroscopic constants of s-cis-trans-cinnamaldehyde. For all calculations the 6-311++G(2d,2p) basis set was used.*

parameter	experiment	B3LYP	M06-2X	MP2	Steinmetz et al. [147]
A [MHz]	4494.1094(21)	4526.23	4534.55	4495.56	
B [MHz]	626.04519(27)	625.32	631.43	626.84	
C [MHz]	549.97612(24)	549.42	554.25	550.13	
B+C [MHz]	1176.02131(26)	1174.74	1185.68	1176.96	1179.1(1)
$\vert\mu_a\vert$ [D]		3.58	3.08	3.50	
$\vert\mu_b\vert$ [D]		1.85	1.89	2.17	
$\vert\mu_c\vert$ [D]		0	0	0	
D_K [kHz]	0.40(17)				
D_J [kHz]	0.0058(29)				
Δ [u$\mathring{A}^2$]	-0.801				
J_{max}	10				
no. lines	33				
error [kHz]	5.2				

$\Delta = I_c - I_a - I_b$; u is the atomic mass unit

Table 6.3: *Experimentally determined rotational constants for all nine single ^{13}C substituted species of s-trans-trans-cinnamaldehyde, number of assigned lines and the error of the fit are given in this table. The distortion constants D_J, D_K and D_{JK} of the parent molecule (Tab. 6.1) were used for the fits of the isotopologues.*

Isotopologue	A [MHz]	B [MHz]	C [MHz]	no. lines	error [kHz]
C1	4863.49(83)	571.91382(56)	512.04405(57)	17	7.6
C2	4866.23(81)	576.58248(68)	515.80562(79)	12	7.9
C3	4848.36(59)	578.55109(52)	517.21422(54)	15	6.9
C4	4863.91(32)	578.89400(19)	517.65356(19)	13	2.5
C5	4791.14(67)	577.61341(69)	515.80867(68)	14	8.3
C6	4823.39(69)	573.75216(60)	513.07512(60)	22	8.7
C7	4860.67(70)	572.07195(61)	512.16369(63)	18	8.0
C8	4780.37(85)	575.50095(36)	513.98454(32)	13	4.5
C9	4813.79(61)	578.44614(43)	516.70858(48)	15	6.3
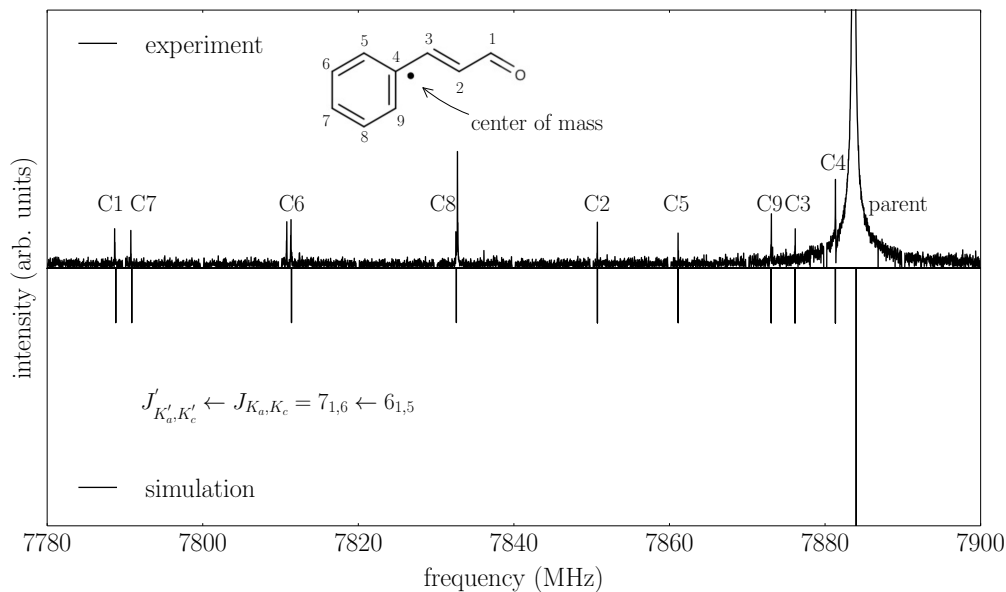
Figure 6.5: *Satellite lines arising from all singly substituted ^{13}C isotopologues of s-trans-trans-cinnamaldehyde and the parent line of the $J'_{K'_a,K'_c} \leftarrow J_{K_a,K_c} = 7_{1,6} \leftarrow 6_{1,5}$ transition. Note that the line shift from the parent transition increases with the distance of the substituted carbon atom to the center of mass of the molecule.*

Table 6.4: *Experimentally determined atom positions, calculated with the substitution method (r_s-structure), are given in this table. The z-coordinate of the molecule is assumed to be zero in the Kraitchman equations for planar molecules.*

Atom number	x	y
C1	3.30890(14)	-0.31446(235)
C2	1.94040(28)	0.23460(401)
C3	0.87748(47)	-0.60873(111)
C4	-0.50070(39)	-0.23877(127)
C5	-1.47934(36)	-1.27512(67)
C6	-2.84562(17)	-0.97925(79)
C7	-3.27169(15)	0.33589(240)
C8	-2.32516(13)	1.37839(33)
C9	-0.96338(36)	1.08289(55)

The calculated inertial defect, $\Delta = I_c - I_a - I_b$, of the experimentally

determined structure has a non-zero value of -0.63 u$\overset{\circ}{A}^{2}$, due to low-lying
out-of-plane vibrations [152], for example at around 60 cm^{-1} (about the
dihedral angle C5-C4-C3-C2, atom labels are given in Fig. 6.5), contribut-
ing to the zero point motion of the molecule in the ground vibrational
state. This inertial defect is neglected in the Kraitchman equations for
planar molecules. Therefore, we carried out a mass-dependent structure-
fit (r$_m^{(1)}$-structure), which is typically closer to the equilibrium geometry
of the molecule as it takes the inertial defect into account [153] (Sub-
sec. 2.1.4). For this a least-square fit of the structure to the rotational
constants was performed, as for example implemented in the STRFIT-
program [73]. Additionally, an adjustable constant was fit, which accounts
for the isotope-dependent rovibrational contribution to the moments of in-
ertia of the molecule [153]. The calculated carbon atom positions of the
r$_m^{(1)}$-structure are given in Table 6.5. The value of the adjustable constant
was determined to be: $c_c = -0.0218(13)$.

A least-square fit of the structure without additional fitting parameters
(r$_0$-structure) led to a poorly defined structure and will not be discussed
further.

Table 6.5: *Experimentally determined atom positions, calculated with
the mass-dependent method (r$_m$-structure), are given in this table. The
z-coordinate of the molecule is assumed to be zero.*

Atom number	x	y
C1	3.3172(88)	-0.310(12)
C2	1.94040(28)	0.23460(401)
C3	0.87748(47)	-0.60873(111)
C4	-0.50070(39)	-0.23877(127)
C5	-1.47934(36)	-1.27512(67)
C6	-2.84562(17)	-0.97925(79)
C7	-3.27169(15)	0.33589(240)
C8	-2.32516(13)	1.37839(33)
C9	-0.96338(36)	1.08289(55)

The comparison of the structural parameters of the carbon backbone of
s-trans-trans-cinnamaldehyde, obtained from these different approaches, is
given in Tables 6.6 and 6.7.

Table 6.6: *Experimentally determined bond lengths of s-trans-trans-cinnamaldehyde (r_s-structure following Kraitchman's approach and the mass dependent r_m-structure) compared to values from ab initio calculations (r_e-structure, MP2/6-311++G(2d,2p)) and a gas electron diffraction (GED, r_g-structure) study [148]. For comparison, the structural parameters of acrolein [150] are given in this table as well.*

bond lengths [Å]	MW r_s	MW $r_m^{(1)}$	MP2 r_e	GED r_g [148]	acrolein [150]
C1-C2	1.4745(18)	1.456(34)	1.465	1.473(8)	1.468(4)
C2-C3	1.3568(26)	1.341(65)	1.349	1.348(1)	1.340(4)
C3-C4	1.4270(7)	1.464(62)	1.460	1.470(8)	
C4-C5	1.4254(11)	1.403(74)	1.404	1.406(1)	
C5-C6	1.3980(5)	1.410(24)	1.394	1.392(1)	
C6-C7	1.3824(24)	1.390(54)	1.395	1.395(1)	
C7-C8	1.4081(18)	1.399(41)	1.398	1.398(1)	
C8-C9	1.3935(4)	1.362(32)	1.391	1.390(1)	
C9-C4	1.4003(13)	1.414(89)	1.405	1.408(1)	

Table 6.7: *Experimentally determined (r_s-structure and r_m-structure) bond angles of s-trans-trans-cinnamaldehyde compared to values from ab initio calculations (r_e-structure, MP2/6-311++G(2d,2p)) and a gas electron diffraction (GED, r_g-structure) study. For comparison, the structural parameters of acrolein [150] are given in this table as well.*

bond angles [°]	MW r_s	MW $r_m^{(1)}$	MP2 r_e	GED r_g [148]	acrolein [150]
C1-C2-C3	119.71(29)	121.3(59)	119.7	115.3(27)	120.4
C2-C3-C4	126.55(16)	127.1(53)	127.3	128.3(26)	
C3-C4-C9	124.32(8)	124.5(54)	122.6	122.0(26)	
C4-C5-C6	121.14(7)	120.5(34)	120.9	121.4(3)	
C5-C6-C7	120.17(9)	120.1(5)	119.9	118.3	
C6-C7-C8	119.81(4)	119.8(13)	119.7	122.1	
C7-C8-C9	120.00(7)	119.5(23)	120.4	118.7	
C8-C9-C4	121.54(4)	123.1(30)	120.5	121.0(3)	
C9-C4-C5	117.35(4)	116.9(35)	118.6	118.6(3)	

The effect of the conjugated π-electron system becomes obvious by evaluating the individual C-C bond lengths (Tab. 6.6). In a conjugated system, the C-C single bonds are shorter compared to non-conjugated C-

C single bonds (typically 1.53 Å), while the C-C double bonds are longer compared to non-conjugated C-C double bonds (typically 1.34 Å), which can be seen in both reported structures.

For this planar molecule the results obtained from the different methods are close, because the rather small inertial defect of the molecules does not lead to large deviations. Nearly all determined structural parameters are in a good agreement with each other and with the *ab initio* values. This is also displayed in Figure 6.6, which is a comparison between the calculated and the experimentally determined carbon backbone structure. It is therefore appropriate to compare the calculated structural parameters (MP2/6-311++G(2d,2p)) for *s-trans-trans*-cinnamaldehyde with the ones for the higher energy conformer *s-cis-trans*-cinnamaldehyde. The steric repulsion between the carbon atom C3 and the oxygen atom as well as between the two π-electron clouds of the double bonds might cause the energy difference between the two conformers. Its occurrence is confirmed by an increase of the C1-C2-C3 angle and an elongation of the C1-C2 single bond in the *s-cis-trans*-conformer compared to the *s-trans-trans*-conformer.

The same behavior can also be found in the experimentally determined values of *s-cis-* and *s-trans*-acrolein [150], which underlines again the similarity of the electronic environment in the side chain of *trans*-cinnamaldehyde and in acrolein. A comparison of these values can be found in Tables 6.8 and 6.9.

Table 6.8: *Comparison of the calculated bond lengths of s-cis-trans- and s-trans-trans-cinnamaldehyde from ab initio calculations using the MP2/6-311++(2d,2p) level of theory to bond lengths of s-cis- and s-trans-acrolein[150].*

bond lengths	cinnamaldehyde		acrolein [150]	
[Å]	*s-trans-trans-*	*s-cis-trans-*	*s-trans-*	*s-cis-*
C1-C2	1.465	1.477	1.468(4)	1.478(6)
C2-C3	1.350	1.348	1.340(4)	1.340(7)
C3-C4	1.460	1.460		
C4-C5	1.403	1.404		
C5-C6	1.394	1.394		
C6-C7	1.395	1.395		
C7-C8	1.398	1.398		
C8-C9	1.391	1.391		
C9-C4	1.405	1.404		

Table 6.9: *Comparison of the calculated bond angles of s-cis-trans- and s-trans-trans-cinnamaldehyde from ab initio calculations using the MP2/6-311++(2d,2p) level of theory to bond angles of s-cis- and s-trans-acrolein[150].*

bond lengths	cinnamaldehyde		acrolein [150]	
[°]	*s-trans-trans-*	*s-cis-trans-*	*s-trans-*	*s-cis-*
C1-C2-C3	119.67	120.76	119.7(3)	121.5(6)
C2-C3-C4	127.32	127.13		
C3-C4-C5	118.73	118.50		
C4-C5-C6	120.89	120.92		
C5-C6-C7	119.94	119.98		
C6-C7-C8	119.69	119.66		
C7-C8-C9	120.38	120.38		
C8-C9-C4	120.46	120.53		
C9-C4-C5	118.63	118.54		
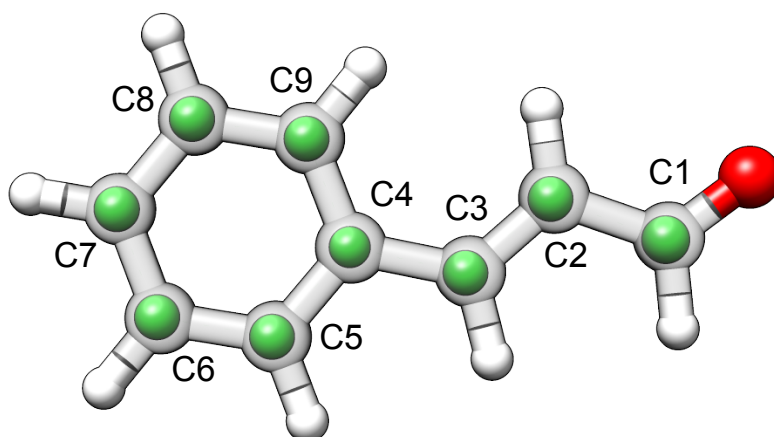
Figure 6.6: *Comparison of the calculated and the experimentally determined (green dots) carbon backbone of s-trans-trans-cinnamaldehyde. The calculated atom positions are obtained from MP2/6-311++G(2d,2p) calculations, while the experimentally determined values originate from the substitution method (r_s-structure).*

The structural parameters obtained in the GED study [148] performed at 165 °C differ from the *ab initio* calculations and from the ones determined in this work (Tab. 6.6 and 6.7) for the values of the side chain. In that study the authors could only identify the *s-trans-trans-*conformer

to be the most dominant species in their 165 °C sample and could not unambiguously identify the presence of the second conformer, *s-cis-trans*-cinnamaldehyde. Since GED structures are an average over all populated rovibrational states, the elevated temperature of this study is especially problematic as only a very small fraction of the molecules will be in the ground vibrational state. Therefore the structure obtained is often not representative of the ground vibrational state or the equilibrium structure. This might explain the deviation of the bond angles of the side chain in the GED structure. Furthermore, the analysis of the experimental data also depends on fixing molecular parameters to calculated values and can be complicated by the presence of more than one conformer. For example, in the GED-study on *trans*-cinnamaldehyde reported in Ref. [148] structural constraints based on the theoretical molecular structure were introduced, which might influence the resulting structure.

6.4 Conclusions

Two conformers of the odorant molecule *trans*-cinnamaldehyde were investigated using broadband microwave spectroscopy in the frequency range of 2 - 8.5 GHz. The rotational transitions of the *s-trans-trans*-conformer are about 40 times stronger than the transitions of the higher energy *s-cis-trans*-conformer. The high sensitivity of the spectrometer allowed us to measure the rotational spectra of all ^{13}C-singly substituted species of *s-trans-trans*-cinnamaldehyde and with this to determine the structure and positions of all carbon atoms of this conformer. Different methods to obtain the structure from the experimentally determined values were used giving comparable results, within the given errors. A comparison to a recent gas electron diffraction study could be performed and the structural similarities between *trans*-cinnamaldehyde and acrolein were discussed. The similarities with acrolein showed that the phenyl ring has little influence on the structure of the side chain in *trans*-cinnamaldehyde.

Chapter 7

The smallest sugar dimer: Interplay of hydrogen bonds in the glycolaldehyde dimer*

7.1   Introduction

Many processes relevant in biological systems, such as molecular recognition and protein folding, are controlled by a subtle equilibrium of intermolecular interactions. Among them, hydrogen bonding is exceptional. Hydrogen bonds are rather strong (on the order of 20 kJ/mol) and directional and they profit from cooperativity [154–157]. They are not only responsible for the dramatically higher boiling points of NH_3, H_2O, and HF compared to their heavier analogues PH_3, H_2S, and HCl, respectively, but they are also known to play an essential role in molecular interactions relevant for biological systems. Molecular recognition of carbohydrates, for example, is widespread and highly relevant in nature [13]. It is also influenced by the conformational flexibility of carbohydrates [37, 158], along with the possibility of forming intramolecular, intermolecular and solvent hydrogen bonds [159, 160].

A molecular-level understanding of the interplay between intra- and intermolecular hydrogen bonding in molecular recognition processes is therefore of great interest. Particularly, it is intriguing to investigate dimer formation of molecules exhibiting relatively strong intramolecular hydrogen bonds [161, 162], for which different scenarios are possible upon dimer

formation: The molecules can form a complex while maintaining the intramolecular hydrogen bonds, for example via stacking, or the intramolecular bonds are broken for the sake of intermolecular hydrogen bonding, or some intermediate form. Furthermore, other interaction types such as the less directed dispersion can tip the subtle balance towards one or the other form [163].

Glycolaldehyde is a perfect model system to study molecular recognition in detail when different interaction types are possible, such as to investigate the role of intra- vs. intermolecular hydrogen bonding as well as dispersion. It is the smallest sugar (Fig. 7.1a) and so far the only one detected in interstellar space [164, 165]. Its gas-phase structure was determined more than 40 years ago [166]. Glycolaldehyde provides two characteristic functional groups, a hydroxy group directly neighboring a carbonyl group, so that it can form a relatively strong intramolecular hydrogen bond [167]. Because of its moderate size, high-level quantum-chemical calculations can be performed and used to validate these methods for larger systems of biological relevance. In the solid state, two glycolaldehyde monomers form a chemically bonded six-membered ring (Fig. 7.1b) [168, 169], which decomposes into the monomer units upon heating. In the conditions of a supersonic expansion, non-covalently bound dimers are formed from isolated monomers (Fig. 7.1c and d) [170].
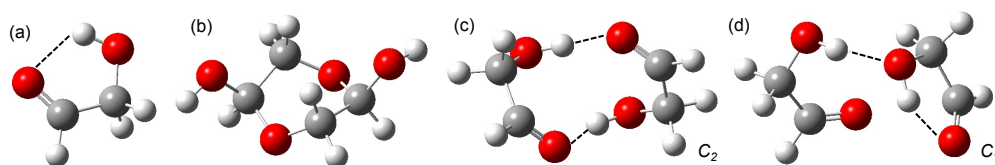
Figure 7.1: *The glycolaldehyde monomer (a) and different structures of the dimer: covalently bound dimer existing in the solid state (b), and the non-covalently bound conformers 1 (c) and 2 (d).*

Recently, Altnöder et al. studied the glycolaldehyde dimer using FTIR- and Raman-spectroscopy under isolated conditions in a supersonic jet [170]. They identified two conformers of the glycolaldehyde dimer, which they assigned to a C_2 symmetric one consisting of two intermolecular hydrogen bonds and a dimer consisting of one inter- and one intramolecular hydrogen bond, which is energetically less favored by about 5 kJ/mol [170]. They compared their vibrational spectra to different theoretical approaches and discussed potential pathways for forming the lowest energy dimer stabilized by two intermolecular hydrogen bonds from the internally stabilized monomer. However, the calculated potential energy surface [170] exhibits

several minima with predicted OH stretching frequencies in comparable frequency ranges. To allow for an unambiguous assignment of the lowest energy conformers of the glycolaldehyde dimer, the authors encouraged a rotational spectroscopy investigation to unambiguously determine their structures and also in view of astrochemical searches.

Here, we use high-resolution broadband chirped-pulse Fourier transform microwave (CP-FTMW) spectroscopy [35] (Sec. 3.2). Structural information, also for molecular clusters, can be obtained because the rotational constants obtained from rotational spectra are directly related to the moments of inertia of the molecules, as shown in Section 2.1. Molecules as heavy as 325 g/mol in the case of $CpRe(CH_3)(CO)(NO)$ has been addressed with CP-FTMW spectroscopy [171]. Quantitative molecular structures can be experimentally determined from an analysis of the rotational spectra of molecular isotopologues, as explained in Subsection 2.1.4. The changes in the moments of inertia of the isotopically substituted species allow for the building up of the substitution structure atom-by-atom using Kraitchman's equations [48] and/or least-squares fits [153] of internal coordinates, for example, as it has been recently exemplified for molecular complexes, such as for the sevoflurane-benzene [172] and the camphor-$(H_2O)_{1-3}$ complexes [26].

In the present study, the high sensitivity of the technique allowed us to record the ^{13}C and ^{18}O isotopologues of the glycolaldehyde dimer in natural abundance. The additional rotational constants were then used to determine its heavy-atom backbone structure. Quantum-chemical calculations were used to support the spectroscopic assignment. In turn, the experimental results help to validate the quality of the theoretical results.

7.2   Experimental details

The rotational spectrum of the glycolaldehyde dimer was recorded in the 2 - 8 GHz frequency range. A detailed description of the setup can be found in Section 3.2. A sample of glycolaldehyde was purchased from Sigma-Aldrich and used without further purification. The sample is a solid at room temperature and has a melting point between 80 and 90 °C. The sample was heated to 80 °C. Neon was used as a carrier gas with an absolute backing pressure of 3.0 bar, and the gas mixture was supersonically expanded into the vacuum chamber via a pulse nozzle. After this, the molecules were excited by a 1 μs long microwave chirp. Forty-five microseconds of the molecular response in form of a free induction decay (FID) were recorded, giving a spectral resolution of 25 kHz. In total 2

million FIDs were recorded and averaged. The rotational spectrum was
obtained by a Fourier transformation of the experimental data. The spec-
tra were fit to an asymmetric rotor Hamiltonian (Watson S-Reduction in I_r
representation [149]) as implemented in the PGOPHER program suite [86].
The additional rotational constants due to isotopic substitution in natural
abundance were used to determine the substitution structure of the lowest
energy conformer 1 using Kraitchman's equations [48] as implemented in
the KRA program package [73].

7.3 Results and Discussion

As displayed in Figure 7.1c and 1d and discussed in Ref. [170], the pre-
dicted lowest energy conformer (conformer 1) consists of two intermolecular
hydrogen bonds connecting the hydroxy- and carbonyl-groups forming a
ten-membered ring. Thus, dimer formation is accompanied by a rearrange-
ment of the hydrogen bonds. The dimer exhibits C_2-symmetry, resulting
in only one non-zero dipole moment component in c-direction, $\mu_c = 3.5$ D
(the axis system is depicted in Fig. 7.4).

The experimental broadband spectrum (top trace) and the correspond-
ing fits to asymmetric rotor Hamiltonians for the two dimer conformers
(bottom traces) are shown in Figure 7.2. For conformer 1 (blue) we only
observe c-type transitions, revealing a congested Q-branch (following the
selection rule $\Delta J = 0$) around 7.8 GHz. We used the computer-assisted
autoassignment program AUTOFIT [89] to get an initial fit of the spec-
trum of conformer 1 followed by further refinement. Finally, 52 c-type
transitions were assigned to this conformer, and the molecular parameters
from experiment and from quantum-chemical calculations (B3LYP-D3 and
MP2) are compared in Table 7.1. Centrifugal distortion constants obtained
from harmonic frequency calculations are also included.

By comparing the experimentally determined rotational constants of
conformer 1 with the ones obtained from quantum-chemical calculations
using the B3LYP-D3 method, we find that for the two different basis sets
(def2-TZVP and aug-cc-pVTZ) the calculated rotational constants A and
B are in good agreement with the experimentally determined values, with
the largest deviation amounting to 3 % (about 20 MHz) for the C rotational
constant. For the MP2 calculations, the agreement is slightly worse. An
interesting comparison is based on the asymmetry parameter $\kappa = (2B -
A - C)/(A - C)$, for which we find a good agreement between experiment
and theory. This relative value often provides additional guidance for the
assignment of conformers based on comparison between experimental and
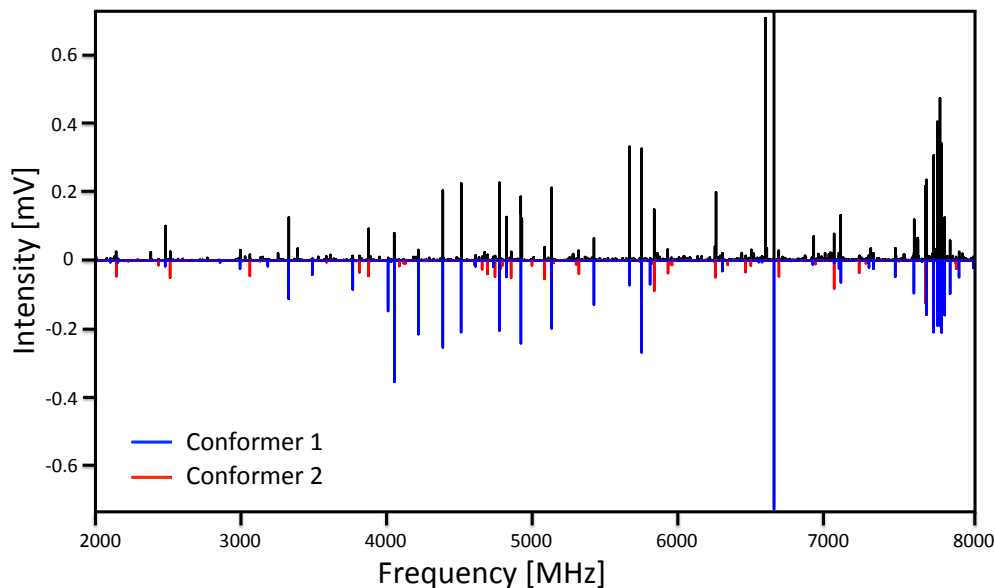
Figure 7.2: *Broadband rotational spectrum of the glycolaldehyde dimer, exhibiting two conformers. The upper trace shows the experimental data. The lower trace shows the simulated spectrum based on fits employing an asymmetric rotor Hamiltonian for the most stable conformer 1 (in blue) and for conformer 2 (in red), which is calculated to be 4.9 kJ/mol higher in energy. Known background lines were removed. Additional spectral lines might be due to impurities or higher order complexes. The noise level of this measurement is 0.2 μV.*

theoretical rotational constants, i.e., when further structural information cannot be extracted such as via isotopic substitution (see below and in Subsec. 2.1.4).

We also recorded and assigned transitions arising from all singly substituted ^{13}C- and ^{18}O-isotopologues of conformer 1. Due to its C_2 symmetry, only four different singly substituted ^{13}C- and ^{18}O- isotopologues exist, with an intensity of about 2.2 % for ^{13}C and 0.4 % for ^{18}O with respect to the parent transitions (i.e., corresponding to twice their natural abundance because of their symmetry). The signal-to-noise (S/N) ratio for the transitions of the ^{18}O isotopologues is about 20:1. An example for the rotational transitions arising from ^{13}C- and ^{18}O-isotopologues is depicted in Figure 7.3. For each rare isotopologue, between 19 and 29 rotational transitions could be assigned and fit. For these fits the distortion constants were fixed to the values of the parent species. The rotational constants of the substituted species can be found in Table 7.2. The data set was

Table 7.1: *Experimentally determined and calculated spectroscopic constants for conformer 1 of the glycolaldehyde dimer. Numbers in parentheses represent error of one standard deviation in units of the last significant figure. The number of assigned lines and the error of the fit are also given.*

	experiment	B3LYP-D3/		MP2/	
		def2-TZVP	aug-cc-pVTZ	def2-TZVP	aug-cc-pVTZ
A [MHz]	2792.67325(87)	2780.962	2783.225	2789.533	2801.957
B [MHz]	1282.99783(41)	1286.011	1283.496	1304.335	1322.20
C [MHz]	1198.16509(39)	1176.691	1166.748	1221.345	1242.145
κ	-0.89	-0.86	-0.86	-0.90	-0.90
D_K [kHz]	1.102(24)	1.140	1.336	1.679	1.336
D_{JK} [kHz]	-0.368(10)	1.951	2.061	0.975	2.061
D_J [kHz]	0.9202(63)	0.747	0.809	0.780	0.804
d_1 [kHz]	0.09567(89)	0.163	0.181	0.128	0.181
d_2 [kHz]	-0.0364(53)	-0.052	-0.055	-0.042	-0.055
$|\mu_a|$ [D]		0	0	0	0
$|\mu_b|$ [D]		0	0	0	0
$|\mu_c|$ [D]		3.4	3.4	3.6	3.6
J_{max}	9				
# lines (a|b|c)	52 (0|0|52)				
error [kHz]	4.9				

then used to determine the precise positions of the carbon and oxygen atoms of conformer 1 using Kraitchman's equations (r_s-structure) [48], as implemented in the KRA program [73]. Experimentally determined atom positions are given in Table 7.3. Due to the symmetry of the molecule the atom positions of C1', C2', O1' and O2' can be determined by mirroring the sign of the a and b coordinate of the atoms C1, C2, O1 and O2.

A comparison of the experimental structural parameters, e.g. bond lengths and bond angles, to the parameters obtained from quantum-chemical calculations is given in Figure 7.4 and in Table 7.4. Note that the quantum-chemical structure represents the equilibrium structure of the complex, while the r_s structure contains zero-point motions in the ground state, which can cause deviations between the experimental and theoretical structures [48, 173]. Although four low-frequency vibrational modes below 100 cm $^{-1}$ were predicted, we do not find a spectroscopic indication of them. The quality of the fits is satisfying for both conformers. Because of the high density of low-intensity transitions, we cannot exclude that spectral features from these low-frequency vibrations might be present.
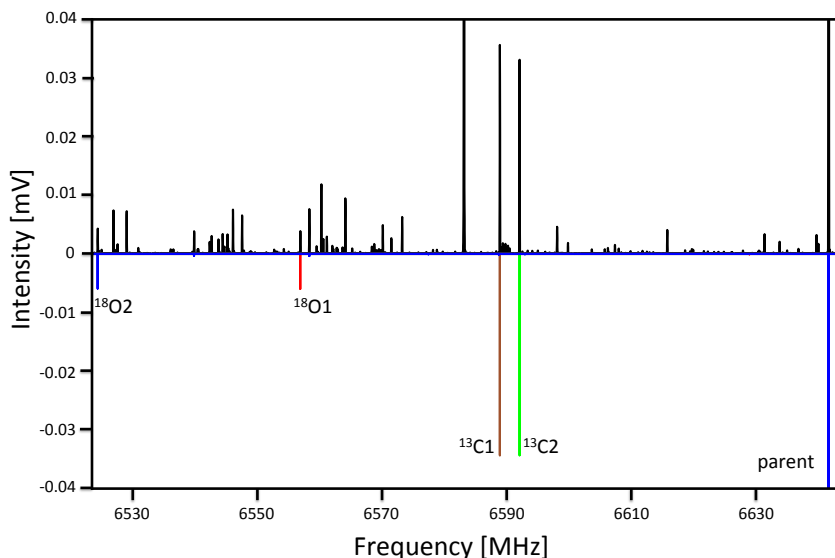
Figure 7.3: $J'_{K'_a,K'_c} \leftarrow J_{K_a,K_c} = 2_{1,1} \leftarrow 1_{0,1}$ *rotational transitions for all singly substituted* ^{13}C *and* ^{18}O *rare isotopologues of conformer 1 in natural abundance and the main isotopologue (see Fig. 7.4 for atom labeling). The signal-to-noise ratio for the* ^{18}O *isotopologues is about 20:1. The large number of unassigned lines may arise from higher order glycolaldehyde clusters or from complexes with water.*

Within the experimental and theoretical uncertainties, the intramolecular geometry parameters are predicted well. Larger deviations are found for the intermolecular parameters and thus for the description of the molecular interactions. This is apparent for the intermolecular carbon-carbon distances C1-C1' and C1-C2' (Fig. 7.4). For both parameters, the experimental bond lengths are clearly shorter than the ones predicted by theory (significantly more than three standard deviations). For α_1, which is the angle between the atoms C1-O1-O2' (see Fig. 7.4 for labeling), a deviation of about 3° (more than three standard deviations) from the experimental values is obtained (Tab. 7.4). This might come along with an overestimation of the dihedral angle τ_1, which is defined between the O1-C1-C2-O2 atoms of one monomer unit.

Calculations using the B3LYP functional, i.e., without the dispersion correction, give a two to three times larger deviation of the rotational constants from the experimentally determined values than the calculations using the B3LYP-D3 functional (compare Tab. 7.5). Without the dispersion correction, the strength of the hydrogen bond seems to be slightly overestimated, which is expressed by a shorter hydrogen bond (1.903 Å

compared to 1.933 Å) and an O1-H-O2′ angle closer to linearity (168° vs.
156°) compared to the structure when including dispersion (B3LYP-D3)
and compared to experimental values. Therefore, the precise prediction of
the intermolecular interaction and with this of the respective changes for
the two interacting moieties highly relies on the correct consideration of
dispersion.

It is also intriguing to discuss the structural changes of the glycolalde-
hyde itself upon dimer formation. For this, we included the respective
structural parameters of the glycolaldehyde monomer in Table 7.6 and 7.7,
as determined in a recent CP-FTMW spectroscopy study [174]. The C1-
C2 and the C1-O1 bonds are affected the most by the dimer formation.
In the complex, the C1-C2 bond is clearly elongated by 0.01 Å, while the
C1-O1 bond neighbouring the hydroxy group is shortened by almost 0.03
Å. The carbonyl C2-O2 bond, on the other hand, is only slightly longer in
the complex than in the monomer.
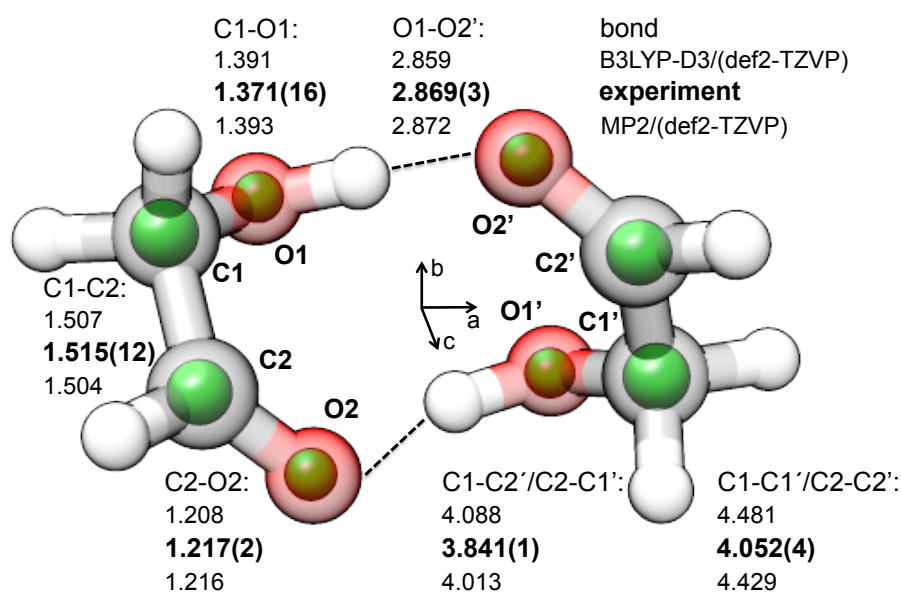
**Figure 7.4:** *Overlay of the experimentally determined structure (green
dots) and the calculated structure using the MP2/def2-TZVP method. Fur-
thermore, a comparison of calculated bond lengths, using the B3LYP-D3
and MP2 functionals, to the experimental values is integrated. Numbers in
parentheses represent the error propagated from the errors in the rotational
constants in Tables 7.1 and 7.2.*

The dimer conformer 2 (Fig. 7.1d) is less energetically favored by about 5 kJ/mol (MP2/aug-cc-pVTZ including zero-point correction) and less populated under the cold conditions of our molecular jet. The broadband rotational spectrum and the corresponding fit (in red) are included in Figure 7.2. In total, 42 transitions (29 b-type and 13 c-type) were assigned to this conformer and fitted to an asymmetric rotor Hamiltonian. The experimentally determined constants and calculated values are given in Table 7.8. For this conformer, the rotational constants obtained at different levels of theory deviate significantly from each other and from the experimental values. Interestingly, density functional theory employing the B3LYP-D3 level of theory seems to provide slightly worse predictions than the MP2 level of theory, while both approaches worked equally well for conformer 1. Furthermore, the different theoretical approaches give varying results for the dipole moment components. In all calculations, μ_b is predicted to be the strongest dipole moment component (in agreement with our experimental findings of recording strong b-type transitions), but they differ significantly in the prediction of μ_a and μ_c. We assigned b- and c-type transitions with an experimentally determined ratio of the dipole moment components of about 5 : 1. No a-type transitions could be identified in the spectrum. This ratio of the dipole moment components is only properly predicted by the MP2/aug-cc-pVTZ level of theory. Thus, even though the rotational constants are rather similar, small changes in the arrangement of the two monomers and especially of the polar groups (hydroxy and carbonyl) with respect to each other can lead to a nearly complete cancellation of the dipole moments along certain directions. By comparing the structures resulting from the different calculations, only minor changes of the angles between the two monomer units are visible. However, the calculated potential energy surface (Fig. 1 in Ref. [170]) of the glycolaldehyde dimer shows a broad minimum for conformer 2, which might explain the slightly different structures obtained using different quantum-chemical methods and basis sets.

Calculations employing the B3LYP functional without dispersion corrections (compare Tab. 7.9) show large deviations, up to 370 MHz, from the experimentally determined rotational constants. Without the dispersion correction the structure of the complex opens up. For example, the dihedral angle between all four carbon atoms (C2-C1-C2'-C1') is increased by 20° when omitting dispersion. This might be caused by an underestimation of attraction.

To obtain further insight into the differences between conformer 1 and conformer 2, a zeroth-order symmetry adapted perturbation theory (SAPT) calculation [175] was performed to decompose the energy contri-

butions to the intermolecular binding forces. Starting from the optimized structures (B3LYP-D3/def2-TZVP), we performed SAPT(0)/jun-cc-pVDZ [176] calculations, which correspond to a reduced aug-cc-pVDZ basis set (without diffuse functions on hydrogen and without diffuse d functions on heavy atoms). This is part of the Psi4 electronic structure package,[177] and the results are presented in Table 7.10.

The total interaction energy is vastly different for both conformers, $\Delta(\Delta E)$=-16.1 kJ mol^{-1}. The largest differences are calculated for the electrostatic interaction, ΔE_{elst}, as well as the repulsion due to quantum-mechanical exchange, ΔE_{exch}. The difference in dispersion energy arises to about 4 kJ mol^{-1}. This relatively small number is somewhat surprising when considering the large changes to the molecular structure of conformer 2 when omitting dispersion.

Due to the lower intensity of the spectrum compared to conformer 1 and a high number of unassigned lines of similar intensity, which might be arising from higher order clusters and clusters with water, for example, it was not possible to make any confident assignment of ^{13}C or even ^{18}O isotopologues for conformer 2. Therefore, structural information is limited to a comparison of the determined molecular parameters with calculated values as given in Table 7.8.

A comparison with the glycolaldehyde-water complex [178] is also of interest here. Under similar experimental conditions as in this study, i.e., employing a supersonic expansion using neon as carrier gas resulting in similar conformational cooling, only one conformer could be identified. The water complex is formed by giving up the intramolecular hydrogen bond of the glycolaldehyde monomer and by forming two intermolecular hydrogen bonds, as in the glycolaldehyde conformer 1. Both the glyco-laldehyde dimer 1 and the water complex seem to gain stability by giving up the intramolecular hydrogen bond of the monomer and by generating two newly formed intermolecular hydrogen bonds. However, the water complex is supported by cooperativity. Such a cooperativity effect is also present for the glycolaldehyde conformer 2.

7.4   Conclusions

In summary, two conformers of the glycolaldehyde dimer were investigated using broadband microwave spectroscopy in the frequency range between 2 - 8 GHz. While the glycolaldehyde monomer is characterized by a moderately strong intramolecular hydrogen bond, this is given up upon formation of the lowest energy dimer, conformer 1. It consists of two inter-

molecular hydrogen bonds, forming a ring of eight heavy atoms, i.e., non-hydrogen atoms, in agreement with a previous molecular jet FTIR spectroscopy study [170]. The initial assignment of the broadband spectrum was achieved using the computer-assisted assignment program AUTOFIT. The high sensitivity of our spectrometer allowed us to also record the rotational signatures of all singly substituted ^{13}C- and ^{18}O-isotopologues in natural abundance for the lowest energy conformer 1 and with this to determine its heavy-atom backbone structure, confirming the structural assignment.

The second dimer conformer maintains one intramolecular hydrogen bond between the hydroxy and the neighboring carbonyl group and forms two new, but less directed intermolecular hydrogen bonds. It is energetically less favored compared to conformer 1 by about 5 kJ/mol. The quantum-chemical calculations employed, which include corrections for dispersion (B3LYP-D3) or explicitly treat dispersion (MP2), show clear deviations of the predicted molecular parameters from the experimental ones. The largest differences were found for the predicted dipole moment components, which demonstrate one of the challenges in quantum-chemical calculations of molecular complexes. Small changes in intermolecular interactions and thus the intermolecular arrangement can result in clearly different molecular parameters that are easily identified by microwave spectroscopy.

Table 7.2: *Experimentally determined rotational constants for all single ^{13}C and ^{18}O substituted species of the glycolaldehyde dimer conformer 1, number of assigned lines and the error of the fit. The distortion constants D_J, D_K, D_{JK}, d_1 and d_2 of the parent molecule, given in Table 7.1, were used for the fits of the isotopologues.*

Isotopologue	A [MHz]	B [MHz]	C [MHz]	no. lines	error [kHz]
C1/C1'	2788.17377(61)	1268.03810(44)	1184.32811(39)	28	6.8
C2/C2'	2777.13504(43)	1270.67055(26)	1187.78323(22)	29	4.6
O1/O1'	2736.03773(46)	1262.95756(34)	1184.40926(26)	19	4.3
O2/O2'	2727.37605(55)	1276.63146(41)	1183.59639(41)	21	4.9

Table 7.3: *Experimentally determined atom positions for conformer 1, calculated with the substitution method.*

Atom number	a	b	c
C2	1.80264(83)	0.6623(23)	0.7704(20)
C1	2.15830(70)	-0.5423(28)	-0.076(20)
O2	0.8378(18)	1.3755(11)	0.5658(27)
O1	1.3592(11)	-0.7493(20)	-1.1701(13)
C2'	-1.80264(83)	-0.6623(23)	0.7704(20)
C1'	-2.15830(70)	0.5423(28)	-0.076(20)
O2'	-0.8378(18)	-1.3755(11)	0.5658(27)
O1'	-1.3592(11)	0.7493(20)	-1.1701(13)

Table 7.4: *Experimentally determined bond angles and dihedral angles of conformer 1 (r_s-structure following Kraitchman's approach) compared to values from quantum-chemical calculations.*

		B3LYP-D3/		MP2/	
bond angles [°]	experiment r_s	def2-TZVP	aug-cc-pVTZ	def2-TZVP	aug-cc-pVTZ
α_1=C1-O1-O2'	89.79(50)	86.94	91.40	87.85	87.00
α_2=C2-C1-O1	115.42(31)	114.60	115.44	114.80	114.58
α_3=C1-C2-O2	123.94(46)	124.72	125.35	124.93	124.71
α_4=C2-O2-O1'	125.51(15)	125.09	125.71	124.87	125.08
τ_1=O1-C1-C2-O2	3.96(1.04)	5.52	5.29	5.58	5.43
τ_2=C2-O2-O1'-C1'	107.30(24)	107.14	106.16	107.14	107.10
τ_2=O1-O2'-C2'-C1'	13.72(61)	14.21	11.03	13.78	14.30

Table 7.5: *Experimentally determined rotational constants for conformer 1 of the glycolaldehyde dimer compared to quantum-chemical calculations using the B3LYP level of theory with and without dispersion correction.*

	exp r_s	B3LYP-D3	B3LYP
		(aug-cc-pVTZ)	
A [MHz]	2792.679	2783.225	2814.590
B [MHz]	1282.999	1283.496	1197.345
C [MHz]	1198.154	1166.748	1038.073

Table 7.6: *Experimentally determined bond lengths of the glycolaldehyde dimer (conformer 1) (r_s-structure following Kraitchman's approach) compared to values from quantum-chemical calculations for the dimer (also depicted in Fig. 7.4) and to experimental values for the glycolaldehyde monomer [174].*

bond	exp r_s	B3LYP-D3/		MP2/		monomer exp [174]
		def2-TZVP	aug-cc-pVTZ	def2-TZVP	aug-cc-pVTZ	
C1-C2	1.515(12)	1.504	1.507	1.504	1.503	1.5012(29)
C1-O1	1.371(16)	1.395	1.392	1.393	1.395	1.3996(32)
C2-O2	1.217(2)	1.218	1.208	1.216	1.218	1.2102(36)
O1-O2'	2.869(3)	2.848	2.860	2.872	2.848	

Table 7.7: *Experimentally determined bond angles and dihedral angles of the glycolaldehyde dimer (conformer 1) (r_s-structure following Kraitchman's approach) compared to experimental values for the glycolaldehyde monomer [174]. Values from quantum chemical calculations are given in Table 7.4.*

bond	exp r_s	monomer exp [174]
C1-O1-O2'	89.79(50)	
C2-C1-O1	115.42(31)	112.28(31)
C1-C2-O2	123.94(46)	121.90(43)
C2-O2-O1'	125.51(15)	
O1-C1-C2-O2	3.96(104)	
C2-O2-O1'-C1'	107.30(24)	
O1-O2'-C2'-C1'	13.72(61)	

Table 7.8: *Experimentally determined and calculated spectroscopic constants of the higher energy glycolaldehyde dimer conformer 2. Numbers in parentheses represent error of one standard deviation in units of the last significant figure. The number of assigned lines and the error of the fit are also given.*

	experiment	B3LYP-D3/			MP2/	
		def2-TZVP	aug-cc-pVTZ	def2-TZVP	aug-cc-pVTZ	
A [MHz]	2938.823326(40)	2780.678	2780.709	2868.851	2909.259	
B [MHz]	1170.31969(17)	1243.932	1233.166	1251.113	1248.777	
C [MHz]	964.30907(18)	1015.574	1012.799	1010.304	1009.973	
κ	-0.79	-0.74	-0.75	-0.74	-0.75	
D_K [kHz]	19.777(41)	12.975	12.618	11.192	11.271	
D_{JK} [kHz]	-9.4496(81)	-6.403	-6.608	-5.046	-4.784	
D_J [kHz]	2.1772(32)	1.933	2.047	1.529	1.418	
d_1 [kHz]	-0.021866(22)	-0.027	-0.026	-0.022	-0.021	
d_2 [kHz]	-0.391601(56)	-0.273	-0.331	-0.310	-0.295	
$|\mu_a|$ [D]		0.1	0.4	0.2	0.03	
$|\mu_b|$ [D]		1.6	1.0	0.9	1.0	
$|\mu_c|$ [D]		0.2	0.04	0.01	0.2	
J_{max}	8					
no. lines (a|b|c)	42 (0|29|13)					
error [kHz]	1.9					

Table 7.9: *Experimentally determined rotational constants for con-
former 2 of the glycolaldehyde dimer compared to quantum-chemical calcu-
lations using the B3LYP level of theory with and without dispersion cor-
rection.*

	exp r_s	B3LYP-D3 (aug-cc-pVTZ)	B3LYP
A [MHz]	2938.824	2780.709	3312.079
B [MHz]	1170.32	1233.166	878.4456
C [MHz]	964.309	1012.799	781.5959

Table 7.10: *Energy decompositions (kJ mol^{-1}) from a SAPT(0)/jun-cc-
pVDZ analysis of the two observed conformers of glycolaldehyde dimer.
The calculations are based on the B3LYP-D3/def2-TZVP optimized struc-
ture.*

	ΔE_{elst}[a]	ΔE_{ind}[b]	ΔE_{disp}[c]	ΔE_{exch}[d]	ΔE_{tot}
conformer 1	-89.6	-26.5	-22.9	75.2	-40.9
conformer 2	-64.8	-18.7	-19.0	58.8	-24.8
$\Delta(\Delta E)$[e]	-24.8	-7.8	-3.9	16.4	-16.1

[a]ΔE_{elst} is the electrostatic or Coulombic exchange.
[b]ΔE_{ind} corresponds to the induction and charge-transfer interactions.
[c]ΔE_{disp} accounts for the dispersive interactions.
[d]ΔE_{exch} represents the repulsion due to quantum-mechanical exchange.
[e]$\Delta(\Delta E)$ is the energy difference $\Delta E_{conformer1} - \Delta E_{conformer2}$.

Chapter 8

The diphenylether-methanol complex: Aromatic embedding wins over classical hydrogen bonding*†

8.1 Introduction

Molecular recognition is driven by the interplay between various intermolecular forces like hydrogen bonding or dispersion interactions. Although molecular recognition phenomena were already known by 1894 when Emil Fischer developed his lock-and-key principle [179], non-covalent molecular recognition is still not well understood on a quantitative level [180].

This study is aimed at elucidating how the various intermolecular interaction energies compete or cooperate with each other. Studying the methanol-diphenylether (DPE) complex involves the interplay of various intermolecular interactions and intramolecular dynamics. In comparison to the glycolaldehyde dimer, presented in Chapter 7, the two phenyl rings of DPE with their delocalized π-electron systems provide powerful dispersion centers. Therefore, they can act as hydrogen bond acceptors for methanol. Beside this, the ether oxygen of DPE also provides an attrac-

---

*This chapter is based on the following manuscript: C. Medcraft, S. Zinn, M. Schnell, A. Poblotzki, J. Altnöder, M. Heger, M. A. Suhm, D. Bernhard, A. Stamm, F. Dietrich, M. Gerhards. Aromatic embedding wins over classical hydrogen bonding - a multi-spectroscopic approach for the diphenyl ether-methanol complex. In preparation.

†The results of quantum chemical calculations, given in Tables 8.3 and 8.2 were performed in the group of Prof. Suhm at the University of Göttingen.

tive hydrogen docking position for the methanol, but the attached phenyl rings might tip the balance between different intermolecular interactions towards π binding.

The rotational spectrum of methanol itself has been the subject of extensive studies as it is an important molecule for many fields of research such as astrophysics and atmospheric science, and it is also an industrially important molecule [181, 182]. The spectrum is complicated by the large amplitude motion of the methyl rotor, as shown in Subsection 2.1.3. The methanol dimer forms a linear chain with one molecule as a H donor and one as the acceptor [183]. A similar motif is seen in the water-methanol complex where water is the H donor [184].

Diphenylether (DPE) belongs to the group of bridged biphenyls that are known to be structurally very flexible. The two phenyl rings are connected via single bonds to the ether oxygen and thus can perform large-amplitude motions. Due to the symmetry of the molecule itself and the phenyl rings, three different tunneling pathways connecting three different frameworks are possible. DPE was spectroscopically investigated previously using resonance-enhanced multi-photon ionization [185]. They observed three vibrational progressions that they attributed to three different conformers of DPE. Furthermore, torsional coupling seems to play a role. The authors used quantum chemical calculations and group theory to support their spectroscopic results.

DPE provides a number of plausible binding sites for methanol, like for example hydrogen bonding to the ether oxygen or to the aromatic rings. Additional stability of the complex might be gained by CH-π or CH-O interactions. Via precise structure determination, rotational spectroscopy can elucidate what type of bonding is most preferred. The flexibility of the monomers may also provide insights into the degree of structural changes upon complex formation.

This is the first complex in a planned series of studies on ROH-DPE complexes (where R=H, CH_3, CH_2CH_3 etc) which will examine the preference for hydrogen bonding over dispersion interactions. This series should provide a valuable collection of data to benchmark various theoretical methods.

8.2   Experimental details

Diphenylether (stated purity 99%) and methanol were purchased from Sigma-Aldrich and used without further purification. DPE is a solid at room temperature, with a melting point of 25-26°C. The boiling point is

258°C at standard conditions. The microwave spectrum was measured using the COMPACT instrument, as mentioned in Section 3.2. In this arrangement, the sample of DPE was placed in a sample reservoir inside the nozzle and heated to 85°C. The methanol sample was placed in a reservoir on a separate section of tubing outside of the vacuum chamber. To compensate for the high vapor pressure of methanol only a fraction of the neon carrier gas (2 bar backing pressure) was diverted to flow over the methanol. The molecules were seeded into a supersonic expansion using a pulse nozzle (Parker General Valve, Series 9) operating at 2 Hz. After supersonic expansion into vacuum, the ensemble of molecules was polarized with a 3 μs chirp spanning 2 -8 GHz. For each spectrum 40 μs of the FID were recorded, yielding a frequency resolution of 25 kHz in the rotational spectra obtained. A total of 3.3 million FIDs were coadded and Fourier transformed with a Kaiser window function to produce the spectrum.

8.3   Results

In the following the results for the DPE monomer and the methanol-DPE complex are discussed. The measured broadband spectrum, of the DPE and methanol mixture is depicted in Figure 8.1.

8.3.1   DPE monomer

The pure rotational spectrum of the DPE monomer shows a clear signature of torsional large-amplitude motion and every transition is split into three components (see Subsec. 2.1.3). Within our frequency range approximately 40 triplets from DPE were identified. Each component of these triplets (labeled as I, II, III) could be fit reasonably well to rigid rotor Hamiltonians (see Fig. 8.2).

The calculated minimum structure of DPE has a chiral conformation (Fig. 8.3) with a twisted arrangement of the two phenyl rings. It is assumed that the splitting in the spectrum arises from tunneling from one twist configuration to the next equivalent one through the potential energy barrier of the skew structure, which has one imaginary frequency based on our calculations and thus is a saddle point first order on the potential energy surface. A scan of the potential energy surface (PES), which also has been calculated previously by various researchers using different levels of theory [185], is depicted in Figure 8.3, calculated on the B3LYP/cc-pDVZ level of theory. A 180° periodicity can be seen for both dihedral angles due to the symmetry of the molecule.
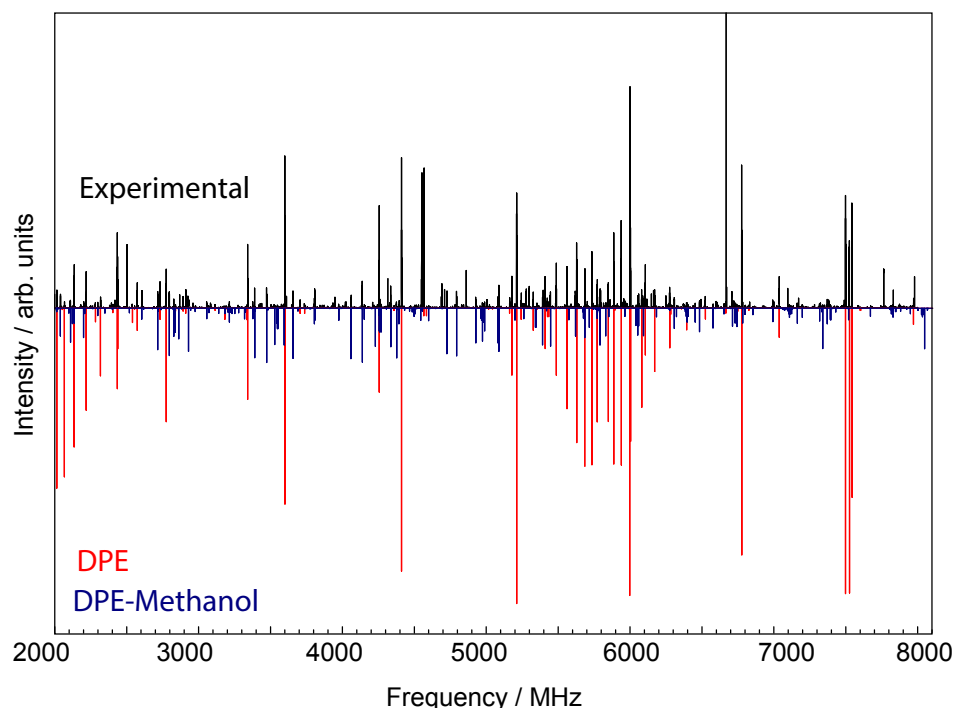
Figure 8.1: *Broadband spectrum of diphenylether and methanol. The top trace shows the experimental results. In the bottom trace, the simulated spectra based on fit parameters for different species are given. The data also contains rotational transitions from both monomers and the methanol dimer. The blue lines (bottom trace) correspond to the assigned DPE-MeOH complex (OH-π conformer).*

The planar and the gable structure are saddle points on the PES while the twist structures is a true minimum. The potential well around the minimum structure is extremely shallow. It can be seen that the two dihedral angles can each be rotated by up to $\approx 15°$ with the calculated energy changing by less than 0.05 kJ/mol. This shallow well also suggests that DPE can easily change shape upon the binding of another molecule.

The rotational constants obtained from the individual fits of the split DPE transitions are given in Table 8.1. A satisfying global fit of all three components for diphenylether is still in progress.

8.3.2   DPE-methanol complex

Quantum chemical calculations using the B3LYP-D3(BJ)/def2-TZVP level of theory result in five low energy conformers of the DPE methanol com-
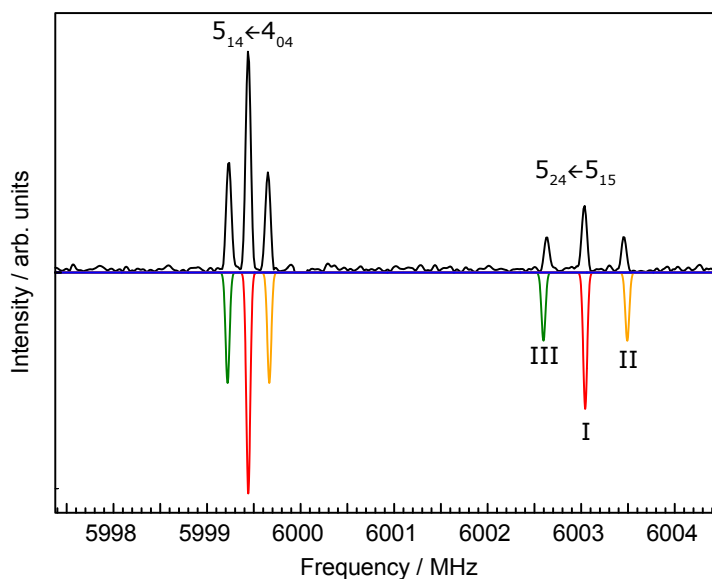
Figure 8.2: *Zoom to the experimental rotational spectrum (top trace), revealing the characteristic splitting for the DPE monomer due to large-amplitude motion into three components. An individual fit for the three components is displayed in the bottom trace.*

plex within an energy range of 5 kJ/mol (Fig. 8.4). Two of them show an OH-O hydrogen bond of the methanol to the ether oxygen (Fig. 8.4 a and b). Additionally, the more stable one of these two conformers, forms a CH-O interaction from one phenyl ring to the methanol oxygen. The other three calculated low energy conformers show am OH-π-interaction from the hydroxy group the the aromatic π-system of one phenyl ring. In the case of the highest energy conformer (Fig. 8.4 e), the pure OH-π-interaction presses the DPE into the less favored skew arrangement of the two phenyl rings (compare Fig. 8.3). Due to the high energy of this conformer (Fig. 8.4 e), it is not expected to be populated under the cold conditions of a supersonic expansion. The other two stable OH-π-structures compete for the global energy minimum (Fig. 8.4 c and d). Beside the OH-π-interaction, both of them show an additional CH-O interaction from the other phenyl ring to the methanol oxygen, which stabilizes these structures. They only differ in the orientation of the methyl group, resulting in an energy difference of 0.5 kJ/mol. The corresponding calculated spectroscopic parameters are given in Table 8.2.

The broadband rotational spectrum obtained from the DPE/MeOH mixture with neon as carrier gas is shown in Figure 8.1. For the DPE-

Table 8.1: *Experimentally determined constants for the three components of a DPE transition obtained from individual fits to rigid rotor Hamiltonians.*

	I	II	III
A [MHz]	2362.08810(292)	2362.25659(110)	2361.83521(86)
B [MHz]	437.99503(135)	437.99079(52)	437.98453(45)
C [MHz]	412.40787(112)	412.44816(45)	412.44331(34)
Δ_J [kHz]	-0.02694(309)	0.03241(170)	0.01907(140)
Δ_{JK} [kHz]	-0.180(51)	1.3887(111)	0.5948(97)
Δ_K [kHz]	14.446(223)	8.874(99)	-18.321(68)
δ_J [kHz]	-3.62(176)	-2.71(53)	-1.60(44)
δ_K [kHz]	12.14(51)	-0.318(151)	0.116(123)
no. lines	59	61	68
error [kHz]	1.31	3.62	1.23

Table 8.2: *Calculated spectroscopic parameters for the lowest energy conformers of DPE-MeOH, performed at the B3LYP-D3(BJ)/def2-TZVP level of theory. The relative energies are zero-point corrected. The corresponding structures are depicted in Figure 8.4. These calculations were performed in the group of Prof. Suhm at the University of Göttingen.*

|	(c) OH-π	(d) OH-π'	(a) OH-O	(b) OH-O$'$	(e) OH-πp
A [MHz]	1022.18	1004.28	858.91	745.16	1035.27
B [MHz]	381.68	398.26	413.38	416.12	364.46
C [MHz]	329.16	330.05	318.78	292.07	314.44
$|\mu_a|$	0.84	0.56	0.19	0.49	2.09
$|\mu_b|$	0.48	0.23	2.69	2.58	1.68
$|\mu_c|$	0.18	1.93	1.25	1.3	0.23
κ	-0.85	-0.80	-0.65	-0.45	-0.86
ΔE	0.0	0.4	1.8	3.2	5.1
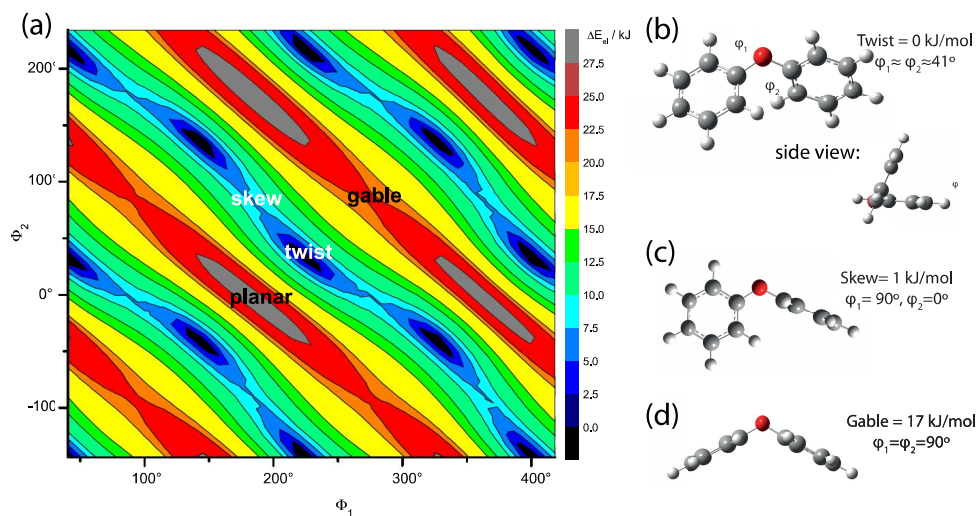
Figure 8.3: *(a) The relaxed scan of the torsional energy surface of DPE calculated at the B3LYP-D3(BJ)/def2-TZVP level. Deep troughs for geared rotation of the two phenyl groups are separated by ridges in which ortho hydrogens come into close contact. Due to the symmetry of DPE, a 180° periodicity is observed for both angles. On the right, selected, optimized structures of DPE are given. The twist structure is a true minimum on the potential energy surface.*

MeOH complex, 120 lines (70 a-type, 50 b-type, and no c-type) could be successfully fit to Watson's S-reduced asymmetric rotor Hamiltonian using the PGOPHER software package [86].

Most of the assigned lines of the DPE-MeOH dimer spectrum show an obvious doublet splitting, the pattern of which suggests a methyl rotor type large amplitude motion (Fig. 8.5). Contrary to the DPE monomer, for which we recorded the characteristic triplet splitting pattern due to the large-amplitude motion of the phenyl rings (Fig. 8.2), we observe no further splittings besides the described doublet pattern in the DPE-methanol spectrum. This indicates that the large amplitude motion of the phenyl rings has been quenched in the cluster. The assigned lines in the rigid rotor fit were attributed to the A-state, and the easily identifiable E-state lines due to methyl group internal rotation were subsequently assigned (Subsec. 2.1.3).

These assignments were exported to the XIAM program [71] in order to perform a global fit. Table 8.3 summarizes the experimentally determined molecular parameters compared to the results obtained from a quantum-

(a) OH–O (1.8)　　　　　(b) OH–O′ (3.2)

(c) OH–π (0.0)　　　　(d) OH–π′ (0.4)　　　　(e) OH–πp (5.1)
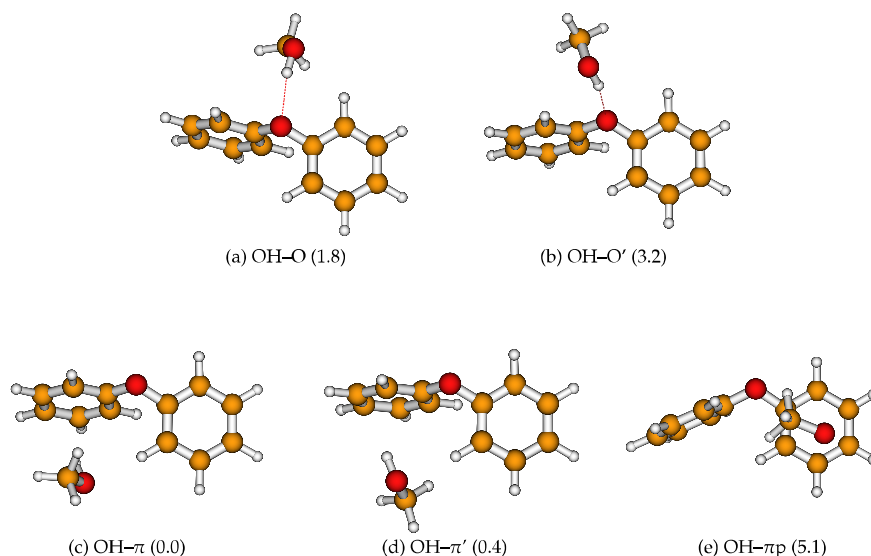
Figure 8.4: *Structures of the most stable DPE-methanol dimers at the B3LYP-D3(BJ)/def2-TZVP level with relative zero-point corrected energies in kJ/mol in parentheses. These calculations were performed in the group of Prof. Suhm at the University of Göttingen.*

chemical calculation (B3PLYP-D3/def2-TZVP) for which also the centrifugal distortion constants and the barrier heights were determined.

For the XIAM fits, starting values for the angles between the methyl rotor of the methanol moiety and the inertial axis (δ and ε) were predicted from the calculated structure. The starting value for F, the rotational constant of the internally rotating methyl top, is less clear. Typical literature values for a methyl top on a rigid frame are around 5.3 cm^{-1}, however, the value for methanol is 27.6 cm^{-1} due to interactions with the large amplitude motion of the OH group. The value of F in methanol-containing complexes is dependent on the amplitude of the OH libration and thus depends on the strength of interaction between methanol with its binding partner (Tab. 8.4). As a consequence, F is determined to be somewhere between that of free methanol (27.6 cm^{-1}) and the value of just the methyl top (5.26 cm^{-1}) for molecular complexes involving methanol. In previous studies on methanol complexes F often has been fixed to 5.3 cm^{-1} (Tab. 8.4). This has been shown to cause a significant underestimation of the barrier height (V_3) [186]. Indeed, when we fix F to 5.3 cm^{-1} the fitted barrier height is 250.74(65) cm^{-1} ('Fit 1' in Tab. 8.3), lower than both free methanol (373 cm^{-1}) and the predicted value from relaxed potential
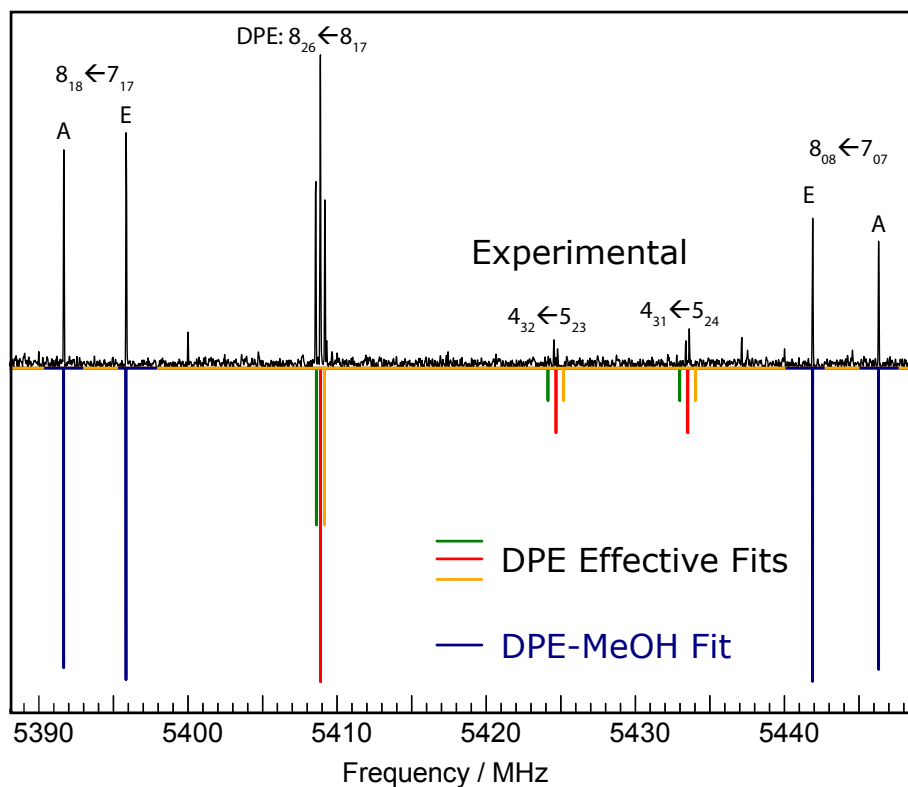
Figure 8.5: *Zoom to the broadband rotational spectrum, illustrating the characteristic triplet splitting pattern for the DPE monomer due to large-amplitude motion of the phenyl rings as well as the observed A-E splitting of the DPE-MeOH dimer, arising from the internal motion of the CH_3 group of the methanol moiety. For the DPE-MeOH dimer, the transitions corresponding to A and E symmetry are fit jointly to an effective Hamiltonian (Tab. 8.3).*

energy scans (435-470 cm^{-1}).

To obtain more realistic values we fit F simultaneously with all the parameters. However, since F is highly correlated with the barrier height V_3 there are significant errors in both parameters (F=10.2(2) cm^{-1} and V_3=480(12)cm^{-1}). This fit is shown in Table 8.3 as 'Fit 2'. It has a lower standard deviation compared to 'Fit 1' where F is fixed. The fitted value of F agrees well with the assumption that the methanol molecule is in an environment somewhere between the strongly bound case and free methanol. Likewise the barrier height agrees with calculated barrier heights. The

Table 8.3: *Molecular parameters of DPE-MeOH: Result of the fit to the experimental rotational spectrum and comparison to results from quantum-chemical calculations for the OH-π dimer (structure (c) in Fig. 8.4). The two fits differ in the treatment of the rotational constant of the internally rotating methyl group F (see text).*

	Fit 1	Fit 2	B3PLYP-D3/ def2-TZVP
A [MHz]	997.9813(30)	997.98324(101)	1019.662
B [MHz]	380.73116(85)	380.73236(28)	382.73
C [MHz]	326.78987(77)	326.79163(26)	333.03
D_J [kHz]	0.029(4)	0.0281(12)	0.014
D_{JK} [kHz]	0.861(28)	0.8232(95)	0.372
D_K [kHz]	-0.234(136)	-0.169(46)	-0.051
d_1 [kHz]	0.008(3)	0.00157(94)	0.00053
d_2 [kHz]	-0.006(2)	-0.00321(54)	-0.00023
κ	-0.839	-0.839	-0.855
λ_a [a]	-0.252(2)	0.0626(8)	
λ_b	-0.385(17)	0.1695(73)	
λ_c	0.888(18)	0.7679(78)	
F_0 [cm^{-1}]	5.3	10.16(27)	
V_3 [cm^{-1}]	250.74(65)	480(12)	445[b]
A states (a/b/c)	120 (70/50/0)	120 (70/50/0)	
E states (a/b/c)	48 (33/15/0)	48 (33/15/0)	
$|\mu_a|/|\mu_b|/|\mu_c|$			0.59/0.60/0.18
error [kHz]	36	12	

[a] Direction cosines were fit as the polar coordinates of the methyl rotor axis with respect to the inertial axes and converted internally to the direction cosines.
[b] Obtained from a relaxed potential energy scan using the B2PLYP-D3 functional and a def2-SVP basis set.

higher barrier compared to the one observed in the methanol monomer is a strong indication that the CH$_3$ group is involved in an intermolecular interaction with the π system, as also visible from Figure 8.4.

Comparison of the rotational constants obtained from this fit with values predicted from quantum-chemical calculations (Tab. 8.3) could not unambiguously identify the geometry of the observed conformer. The calculated rotational constants for the OH-π and OH-π' conformers in Figure 8.4 c and d are within about 10 MHz. Often, quantum-chemical calcula-

Table 8.4: *Barrier heights V_3 for methyl rotation in some methanol-containing complexes.*

	V_3 [cm^{-1}]	F [cm^{-1}]	s^a	Reference
MeOH monomer	373	27.63	6.00	[181]
DPE-MeOH	479.31	10.11	21.08	
DPE-MeOH	250.74	5.3^b	21.03	
MeOH dimer	201	5.4	16.53	[183]
MeOH-formamide	231.01	5.86	17.53	[187]
MeOH-Ar	68.466	5.3	5.74	[188]
MeOH-HCl	74	5.3	6.21	[189]
MeOH-SO$_2$	128.665	5.3	10.79	[190]
MeOH-trimethylamine	174	5.30	14.59	[191]
MeOH-CO	183	5.76	14.12	[192]
MeOH-phenol	170	5.0	15.11	[193]

^{a} reduced dimensionless barrier height $s = 4V_3/9F$
^{b} fixed

tions show larger deviations in the absolute values of rotational constants from the experimentally determined data, but relative values, such as the differences between rotational constants (like $B - C$ as well as the asymmetry parameter κ) are predicted more quantitatively. The experimental values are $B - C = 54$ MHz and κ = -0.839. For the OH-π conformer (Fig. 8.4 c), the predicted values are $B - C = 52$ MHz, and κ = -0.85, while for the OH-π' conformer (Fig. 8.4 d), values of $B - C = 68$ MHz, and κ = -0.80 are predicted (B3LYP-D3(BJ)/def2-TZVP level of theory, Tab. 8.2). This gives a strong indication that indeed the lowest energy conformer, namely the OH-π conformer, is spectroscopically observed.

Unambiguous assignment could be achieved from evaluation of the observed types of rotational transitions, i.e., a-, b-, or c-type, in comparison with the calculated dipole moment components (μ_a, μ_b, and μ_c). No c-type transitions are observed for the DPE-MeOH complex (Tab. 8.3), indicating that μ_c is quite small. This analysis strongly suggests the OH-π conformer, for which the predicted dipole-moment components are μ_a=0.84 D, μ_b=0.48 D, and μ_c=0.18 D (B3LYP-D3(BJ)/def2-TZVP, see Table 8.2, resembling very well the observed ratio of rotational transitions, given in Table 8.3. For the OH-π' conformer, however, the predicted dipole-moment components are μ_a=0.56 D, μ_b=0.23 D, and μ_c=1.93 D (B3LYP-D3(BJ)/def2-TZVP, see Table 8.2, so that we would expect to observe mainly a- and c-type and no b-type transitions.

8.4   Conclusions

The investigated complex of diphenylether and methanol turns out to be an ideal example to study the close competition between hydrogen-bonding to an ether oxygen atom as well as π-bonding to an aromatic ring. According to DFT calculations the experimental structure can be assigned to a π-bonded arrangement, revealing an OH-π interaction. This structure is additionally stabilized by an CH-O contact from the other phenyl ring. Furthermore, evidence for methyl group rotational hindrance and for the quenching of the torsional dynamics of the DPE moiety is collected. The findings are in full agreement with dispersion-corrected hybrid density functional predictions for the mixed dimers, and they fit qualitative expectations about secondary interactions stabilizing the primary OH-π hydrogen bond by CH-O interactions.

Chapter 9

Summary and Outlook

This thesis focuses on the investigation of intermolecular interaction and conformational flexibility of molecules and molecular complexes in the gas phase. These properties are of particular relevance also to biomolecular recognition processes. The fundamental understanding of these processes on a molecular level can be useful, for example, for drug development.

The technique used in this work is chirped-pulse Fourier transform microwave spectroscopy (CP-FTMW). The high accuracy and sensitivity of the spectrometer allows for a precise structure determination of molecules and molecular complexes of biological relevance, but also information on internal dynamics and the bond characters in the molecules can be obtained. In rotational spectroscopy, the obtained molecular parameters are directly related to structural parameters, like bond lengths and angles. Slight changes of the molecular structure, such as a rotation around a single bond to form another conformer, can be identified with this technique, since the rotational spectrum is like a fingerprint of the structure. Additional hyperfine structure in the spectrum might be caused by large amplitude motions, internal rotation or nuclear quadrupole coupling. Information about barrier heights for internal rotation or the electronic surrounding of the quadrupole containing nuclei can be obtained from the analysis of these additional spectral features.

The experimental setup developed within this study is presented in Chapter 3. The CP-FTMW spectrometer is equipped with a laser ablation source for bringing fragile molecules into the gas phase, and a time-of-flight mass spectrometer for fast and efficient beam diagnostics (Sec. 3.3).

Experimental results of molecules and complexes of different complexity are presented in Chapter 4 - 8. The analysis of the electronic structure in 4-aminobenzonitrile, the conformational flexibility of the widespread drug ibuprofen and a precise structure determination of the odorant molecule

116

trans-cinnamaldehyde are discussed. This group of aromatic molecules, with different substituents, provides interesting insights towards structural properties, like for example conformational flexibility. Following, the studies of two different kinds of molecular complexes are presented. The aggregation of the smallest sugar, glycolaldehyde, was investigated to learn about the interplay between inter- and intramolecular hydrogen bonding. Furthermore, the complex formation of diphenylether and methanol shone light onto the different contributions of hydrogen bonding and dispersion interaction upon complex formation.

In 4-amonibenzonitrile two chemically distinct nitrogen atoms of the respective amino and nitrile groups lead to a hyperfine structure of each rotational transition due to nuclear quadrupole coupling, as shown in Chapter 4. Determining their individual quadrupole interactions is complicated by the combined effects of the two nuclei. The determined nuclear quadrupole coupling constants allow for the analysis of the electronic environment of the nitrogen atoms, which is of particular interest when comparing ABN to other para-substituted benzonitriles. By determining the occupancies of the hybrid orbitals of the amino-group nitrogen from the experimental nuclear quadrupole coupling constants, it is shown that there is a significantly lower charge density in ABN compared to other para-substituted benzonitriles like DMABN. This result is particularly interesting with respect to the occurrence of dual fluorescence because it can be interpreted as a possible barrier to charge-transfer states.

In Chapter 5 investigations of the conformational flexibility of the widespread drug ibuprofen are presented. Ibuprofen reveals two flexible side chains, an isobutyl and a propanoic acid group in para position. Four conformers were identified in the rotational spectrum and assigned to the lowest energy conformers obtained from quantum chemical calculations. These four conformers only differ by 0.3 kJ/mol and all of them show the same configuration for the propanoic acid group, while the isobutyl group can adopt different orientations. In a comparison of this result to a crystal structure of ibuprofen binding the COX enzyme, where it inhibits the development of pain, it can be seen that this configuration of the carboxy group is essential for binding to the active side. The isobutyl group has more space at the active site and its orientation is rather flexible in terms of the recognition process.

For the odorant molecule *trans*-cinnamaldehyde two stable conformers were found in the rotational spectrum (Ch. 6). The molecule is planar due to the conjugated π-electron system, which includes all heavy atoms. In this study the precise structure of the carbon backbone of the molecule was determined solely based on the experimental results. For the most stable

118

conformer, all singly substituted ^{13}C species could be identified in the spectrum in natural abundance. From these additional information, the carbon atom positions can be calculated using for example the Kraitchman equations. The precise structure can then be used to benchmark quantum-chemical calculations.

The interplay between intra- and intermolecular hydrogen bonding upon aggregation of glycolaldehyde is discussed in Chapter 7. Glycolaldehyde is the smallest and, so far, only sugar that has been detected in interstellar space. It is a perfect model system to study molecular recognition, since cooperative effects of hydrogen bonding and influences of dispersion interaction can be studied. Furthermore, high-level quantum-chemical calculations are still feasible for this complex size. Two different glycolaldehyde dimer conformers could be identified in the rotational spectrum in agreement with previous FTIR studies. The lowest energy conformer reveals C_2 symmetry, by giving up the strong intramolecular hydrogen bond of the monomer unit and by building up two intermolecular hydrogen bonds. The second conformer is about 5 kJ/mol higher in energy. Upon complex formation it keeps one intramolecular and forms one intermolecular hydrogen bond. For the lowest energy conformer a precise structure could be determined from the additional spectroscopic constants of all singly substituted ^{13}C and ^{18}O species in natural abundance. From a detailed comparison of the experimental results to quantum chemical calculations it becomes obvious that already small changes in intermolecular interactions and thus the intermolecular arrangement can result in clearly different molecular parameters that are easily identified by microwave spectroscopy but still be challenging for theoretical approaches.

The aim to elucidate how various intermolecular interactions compete or cooperate with each other is presented in Chapter 8. Compared to the glycolaldehyde dimer the complex formation between diphenylether and methanol provides several possible binding scenarios. In this case dispersion interaction might dominant the formation, since the aromatic rings with their delocalized π electron systems provide powerful dispersion centers. Diphenylether and methanol are flexible molecules, which show large amplitude motions in their monomer spectra. It is interesting to study the change of this flexibility upon complex formation. One stable complex formation is found in the rotational spectrum. It shows a combined interaction of a hydrogen and a π-bonded arrangement, with a dominance of the π-bonding. Internal rotation of the methyl top of the methanol molecule is still feasible, while the large amplitude motion in the diphenylether is locked upon complex formation. This study is a start of a series of investigations between diphenylether and alcohols with increasing size. It should

allow for an investigation of the competition between dispersion forces, hydrogen bonding and steric effects. Furthermore, the data can be used to benchmark theoretical methods.

Further studies of biomolecular complexes in the gas phase will provide a fundamental understanding of the ways how complexes are formed and which intermolecular forces are dominating. The knowledge obtained from model complexes can be transferred towards larger systems and quantum chemical calculations can be improved by a comparison to precise experimentally determined structures.

Bibliography

[1] F. Yamamoto, T. Clausen, H.and White, J. Marken, and S. Hakomori, "Molecular genetic basis of the histo-blood group ABO system," *Nature* **345**, 229 (1990).

[2] J. Milland and M. S. Sandrin, "ABO blood group and related antigens, natural antibodies and transplantation," *Tissue Antigens* **68**, 459 (2006).

[3] A. Kobata, E. F. Grollman, and V. Ginsburg, "An enzymatic basis for blood type B in humans," *Biochem. Biophys. Res. Commun.* **32**, 272 (1968).

[4] A. Kobata, E. F. Grollman, and V. Ginsburg, "An enzymatic basis for blood type A in humans," *Arch. Biochem. Biophys.* **124**, 609 (1968).

[5] C. Rademacher, N. Landstrom, J.and Sindhuwinata, M. M. Palcic, G. Widmalm, and T. Peters, "NMR-based exploration of the acceptor binding site of human blood group B galactosyltransferase with molecular fragments," *Glycoconj. J.* **27**, 349 (2010).

[6] J. Angulo, B. Langpap, A. Blume, T. Biet, B. Meyer, N. R. Krishna, H. Peters, M. M. Palcic, et al., "Blood group B galactosyltransferase: insights into substrate binding from NMR experiments," *J. Am. Chem. Soc.* **128**, 13529 (2006).

[7] L. L. Lairson, B. Henrissat, G. J. Davies, and S. G. Withers, "Glycosyltransferases: structures, functions, and mechanisms," *Annu. Rev. Biochem.* **77**, 521 (2008).

[8] M. L. Sinnott, "Catalytic mechanisms of enzymic glycosyl transfer," *Chem. Rev.* **90**, 1171 (1990).

[9] A. Varki, R. D. Cummings, J. D. Esko, H. H. Freeze, P. Stanley, C. R. Bertozzi, G. W. Hart, and M. E. Etzler, *Essentials of Glycobiology 2nd edition* (CSH Press, 2008).

[10] R. S. Haltiwanger and J. B. Lowe, "Role of glycosylation in development," *Annu. Rev. Biochem.* **73**, 491 (2004).

[11] F. London, "Zur Theorie und Systematik der Molekularkräfte," *Z. Phys.* **63**, 245 (1930).

[12] S. Elgavish and B. Shaanan, "Structures of the Erythrina corallodendron lectin and of its complexes with mono- and disaccharides," *J. Mol. Biol.* **277**, 917 (1998).

[13] R. A. Dwek, "Glycobiology: Toward Understanding the Function of Sugars," *Chem. Rev.* **96**, 683 (1996).

[14] K. Wüthrich, "The way of NMR structures of proteins," *Nat. Struct. Biol.* **8**, 923 (2001).

[15] L. E. Kay, "NMR studies of protein structure and dynamics," *J. Magn. Reson.* **173**, 193 (2005).

[16] R. R. Ernst, "Nuclear Magnetic Resonance Fourier Transform Spectroscopy (Nobel Lecture)," *Angew. Chem. Int. Ed.* **31**, 805 (1992).

[17] D. C. Hodgkin, "The X-ray analysis of complicated molecules," *Nobel Lecture* (1964).

[18] J. M. Bijvoet, A. F. Peerdeman, and A. J. van Bommel, "Determination of the Absolute Configuration of Optically Active Compounds by Means of X-Rays," *Nature* **168**, 271 (1951).

[19] R. J. D. Miller, "Femtosecond Crystallography with Capturing Chemistry in Action," *Science* **343**, 1108 (2014).

[20] J. Tenboer, S. Basu, N. Zatsepin, K. Pande, D. Milathianaki, M. Frank, M. Hunter, S. Boutet, et al., "Time-resolved serial crystallography captures high-resolution intermediates of photoactive yellow protein," *Science (New York, N.Y.)* **346**, 1242 (2014).

[21] L. M. G. Chavas, L. Gumprecht, and H. N. Chapman, "Possibilities for serial femtosecond crystallography sample delivery at future light sources," *Struct. Dyn.* **2**, 041709 (2015).

[22] S. Melandri, M. E. Sanz, W. Caminati, P. G. Favero, and Z. Kisiel, "The hydrogen bond between water and aromatic bases of biological interest: An experimental and theoretical study of the 1:1 complex of pyrimidine with water," *J. Am. Chem. Soc.* **120**, 11504 (1998).

[23] S. Melandri, D. Consalvo, W. Caminati, and P. G. Favero, "Hydrogen bonding, structure ,and dynamics of benzonitrile-water," *Chem. Phys.* **111**, 3874 (1999).

[24] S. Blanco, J. C. Lopéz, J. L. Alonso, P. Ottaviani, and W. Caminati, "Pure rotational spectrum and model calculations of indole-water," *J. Chem. Phys.* **119**, 880 (2003).

[25] C. Pérez, J. L. Neill, M. T. Muckle, D. P. Zaleski, I. Peña, J. C. Lopez, J. L. Alonso, and B. H. Pate, "Water-Water and Water-Solute Interactions in Microsolvated Organic Complexes," *Angew. Chem. Int. Ed.* **53**, 993 (2014).

[26] C. Pérez, A. Krin, A. L. Steber, J. C. López, Z. Kisiel, and M. Schnell, "Wetting Camphor: Multi-Isotopic Substitution Identifies the Complementary Roles of Hydrogen Bonding and Dispersive Forces," *J. Phys. Chem. Lett.* **7**, 154 (2016).

[27] W. Gordy, "Microwave spectroscopy," *Rev. Mod. Phys.* **20**, 668 (1948).

[28] C. H. Townes, "The Ammonia Spectrum and Line Shapes Near 1.25 cm Wave Length," *Phys. Rev.* **70**, 665 (1946).

[29] W. E. Good, "Inversion Spectrum of Ammonia," *Phys. Rev.* **70**, 213 (1946).

[30] B. P. Dailey, R. L. Kyhl, M. W. P. Stranberg, J. H. van Vleck, and E. B. Wilson Jr, "The Hyperfine Structure of the Microwave Spectrum of Ammonia and the Existence of a Quadrupole Moment in ^{14}N," *Phys. Rev.* **70**, 984 (1946).

[31] J. P. Gordon, H. J. Zeiger, and C. H. Townes, "Molecular Microwave Oszillator and New Structure in the Microwave Spectrum of NH_3," *Phys. Rev.* **99**, 282 (1954).

[32] J. P. Gordon, H. J. Zeiger, and C. H. Townes, "The Maser-New Type of Microwave Amplifier, Frequency Standard and Spectrometer," *Phys. Rev.* **99**, 1264 (1955).

[33] T. J. Balle and W. Flygare, "Fabry-Perot cavity pulsed Fourier transform microwave spectrometer with a pulsed nozzle particle source," *Rev. Sci. Instrum.* **52**, 33 (1981).

[34] J.-U. Grabow, W. Stahl, and H. Dreizler, "A multioctave coaxially oriented beam-resonator arrangement Fourier-transform microwave spectrometer," *Rev. Sci. Instrum.* **67**, 4072 (1996).

[35] G. G. Brown, B. C. Dian, K. O. Douglass, S. M. Geyer, S. T. Shipman, and B. H. Pate, "A Broadband Fourier Transform Microwave Spectrometer Based on Chirped Pulse Excitation," *Rev. Sci. Instrum.* **79** (2008).

[36] A. Lesarri, S. Mata, J. C. López, and J. L. Alonso, "A laser-ablation molecular-beam Fourier-transform microwave spectrometer: The rotational spectrum of organic solids," *Rev. Sci. Instrum.* **74**, 4799 (2003).

[37] E. J. Cocinero, A. Lesarri, P. Ècija, F. J. Basterretxea, J.-U. Grabow, J. A. Fernàndez, and F. Castaño, "Ribose Found in the Gas Phase," *Angew. Chem. Int. Ed.* **51**, 3119 (2012).

[38] A. Lesarri, S. Mata, E. J. Cocinero, S. Blanco, J. C. López, and J. L. Alonso, "The structure of neutral proline," *Angew. Chem. Int. Ed.* **41**, 4673 (2002).

[39] A. Lesarri, E. J. Cocinero, J. C. López, and J. L. Alonso, "The shape of neutral valine," *Angew. Chem. Int. Ed.* **43**, 605 (2004).

[40] S. Blanco, A. Lesarri, J. C. López, and J. L. Alonso, "The gas-phase structure of alanine," *J. Am. Chem. Soc.* **126**, 11675 (2004).

[41] J. L. Alonso, I. Peña, J. C. López, and V. Vaquero, "Rotational spectral signatures of four tautomers of guanine," *Angew. Chem. Int. Ed.* **48**, 6141 (2009).

[42] J. L. Alonso, V. Vaquero, I. Peña, J. C. López, S. Mata, and W. Caminati, "All Five Forms of Cytosine Revealed in the Gas Phase," *Angew. Chem. Int. Ed.* **52**, 2331 (2013).

[43] C. Cabezas, J. L. Alonso, J. C. López, and S. Mata, "Unveiling the shape of aspirin in the gas phase," *Angew. Chem. Int. Ed.* **51**, 1375 (2012).

[44] C. Cabezas, M. Varela, I. Peña, J. C. López, and J. L. Alonso, "The microwave spectrum of neurotransmitter serotonin," *Phys. Chem. Chem. Phys.* **14**, 13618 (2012).

[45] I. Peña, A. M. Daly, C. Cabezas, S. Mata, C. Bermúdez, A. Niño, J. C. Lopéz, J.-U. Grabow, et al., "Disentangling the Puzzle of Hydrogen Bonding in Vitamin C," *J. Phys. Chem. Lett.* **4**, 65 (2013).

[46] M. Varela, C. Cabezas, J. C. López, and J. L. Alonso, "Rotational Spectrum of Paracetamol," *J. Phys. Chem. A* **117**, 13275 (2013).

[47] T. Betz, S. Zinn, and M. Schnell, "The shape of ibuprofen in the gas phase," *Phys. Chem. Chem. Phys.* **17**, 4538 (2015).

[48] J. Kraitchman, "Determination of Molecular Structure from Microwave Spectroscopic Data," *Am. J. Phys* **21**, 17 (1953).

[49] B. C. Dian, G. G. Brown, K. O. Douglass, and B. H. Pate, "Measuring picosecond isomerization kinetics via broadband microwave spectroscopy," *Science* **320**, 924 (2008).

[50] B. C. Dian, G. G. Brown, K. O. Douglass, F. S. Rees, J. E. Johns, P. Nair, R. D. Suenram, and B. H. Pate, "Conformational isomerization kinetics of pent-1-en-4-yne with 3,330 cm^{-1} of internal energy measured by dynamic rotational spectroscopy," *P. Natl. Acad. Sci. USA* **105**, 12696 (2008).

[51] D. Patterson, M. Schnell, and J. M. Doyle, "Enantiomer-specific detection of chiral molecules via microwave spectroscopy," *Nature* **497**, 475 (2013).

[52] V. A. Shubert, D. Schmitz, D. Patterson, J. M. Doyle, and M. Schnell, "Identifying Enantiomers in Mixtures of Chiral Molecules with Broadband Microwave Spectroscopy," *Angew. Chem. Int. Ed.* **52**, 1 (2013).

[53] S. Lobsiger, C. Perez, L. Evangelisti, K. K. Lehmann, and B. H. Pate, "Molecular Structure and Chirality Detection by Fourier Transform Microwave Spectroscopy," *J. Phys. Chem. Lett.* **6**, 196 (2015).

[54] "European Southern Observatory - Atacama Large Millimeter/submillimeter Array," (2014).

[55] C. Qi, K. I. Öberg, D. J. Wilner, P. D'Alessio, E. Bergin, S. M. Andrews, G. A. Blake, M. R. Hogerheijde, et al., "Imaging of the CO snow line in a solar nebula analog," *Science* **341**, 630 (2013).

[56] J. K. Jørgensen, R. Visser, N. Sakai, E. A. Bergin, C. Brinch, D. Harsono, J. E. Lindberg, E. F. van Dishoeck, et al., "A Recent Accretion Burst in the Low-Mass Protostar Iras 15398-3359: Alma Imaging of Its Related Chemistry," *Astrophys. J.* **779**, L22 (2013).

[57] A. Belloche, R. T. Garrod, H. S. P. Müller, and K. M. Menten, "Detection of a branched alkyl molecule in the interstellar medium: *iso*-propyl cyanide," *Science* **233**, 232 (2014).

[58] S. M. Fortman, J. P. McMillan, C. F. Neese, S. K. Randall, A. J. Remijan, T. Wilson, and F. C. De Lucia, "An analysis of a preliminary ALMA Orion KL spectrum via the use of complete experimental spectra from the laboratory," *J. Mol. Spec.* **280**, 11 (2012).

[59] M. J. Travers, M. C. McCarthy, P. Kalmus, C. A. Gottlieb, and P. Thaddeus, "Laboratory Detection of the Linear Cyanopolyyne $HC_{11}N$," *Astrophys. J.* **469**, L65 (1996).

[60] J. P. Wagner and P. R. Schreiner, "London Dispersion in Molecular ChemistryReconsidering Steric Effects," *Angew. Chem. Int. Ed.* **54**, 12274 (2015).

[61] M. Born and R. Oppenheimer, "Zur Quantentheorie der Moleküle," *Ann. Phys.* **84**, 457 (1927).

[62] F. Merkt and M. Quack, "Molecular Quantum Mechanics and Molecular Spectra, Molecular Symmetry, and Interaction of Matter with Radiation," in *Handbook of High-resolution Spectroscopy*, Vol. 1, edited by M. Quack and F. Merkt (John Wiley & Sons, Ltd, New York, 2011) pp. 1–56.

[63] C. H. Townes and A. L. Schawlow, *Microwave spectroscopy*, 2nd ed. (Courier Dover Publications, Mineola, 1975).

[64] G. W. King, R. M. Hainer, and P. C. Cross, "The Asymmetric Rotor I. Calculation and Symmetry Classification of Energy Levels," *J. Chem. Phys.* **11**, 27 (1943).

[65] J. K. G. Watson, "Determination of Centrifugal Distortion Coefficients of Asymmetric Top Molecules," *J. Chem. Phys.* **46**, 1935 (1967).

[66] J. K. G. Watson, "Simplification of the molecular vibration-rotation Hamiltonian," *Mol. Phys.* **15**, 479 (1968).

[67] W. Gordy and R. Cook, *Microwave Molecular Spectra* (John Wiley & Sons, New York, 1970).

[68] A. Bauder, "Fundamentals of Rotational Spectroscopy," in *Handbook of High-resolution Spectroscopy*, Vol. 1, edited by M. Quack and F. Merkt (John Wiley & Sons, Ltd, New York, 2011) pp. 57–116.

[69] C. H. Townes and B. P. Dailey, "Determination of Electronic Structure of Molecules from Nuclear Quadrupole Effects," *J. Chem. Phys.* **17**, 782 (1949).

[70] H. M. Pickett, "The fitting and prediction of vibration-rotation spectra with spin interactions," *J. Mol. Spec.* **148**, 371 (1991).

[71] H. Hartwig and H. Dreizler, "The Microwave Spectrum of trans-2,3-Dimethyloxirane in Torsional Excited States," *Z. Naturforsch.* **51a**, 923 (1996).

[72] P. Groner, "Effective rotational Hamiltonian for molecules with two periodic large-amplitude motions," *J. Chem. Phys.* **107**, 4483 (1997).

[73] Z. Kisiel, "PROSPE. Programs for Rotational Spectroscopy. http://info.ifpan.edu.pl/~kisiel/orospe.htm," (2015).

[74] J. Liévin, J. Demaison, M. Herman, A. Fayt, and C. Puzzarini, "Comparison of the experimental, semi-experimental and ab initio equilibrium structures of acetylene: influence of relativisitic effects and of the diagonal Born-Oppenheimer corrections," *J. Chem. Phys.* **134**, 64119 (2011).

[75] C. Møller and M. S. Plesset, "Note on an Approximation Treatment for Many-Electron Systems," *Phys. Rev.* **46**, 618 (1934).

[76] D. R. Hartree, "The Wave Mechanics of an Atom with a Non-Coulomb Central Field. Part II. Some Results and Discussion," *Math. Proc. Cambridge* **24**, 111 (1928).

[77] D. R. Hartree, "The Wave Mechanics of an Atom with a Non-Coulomb Central Field. Part I. Theory and Methods," *Math. Proc. Cambridge* **24**, 89 (1928).

[78] V. Fock, "Näherungsmethode zur Lösung des quantenmechanischen Mehrkörperproblems," *Z. Phys.* **61**, 126 (1930).

[79] R. G. Parr, "Density Functional Theory," *Annu. Rev. Phys. Chem.* **34**, 631 (1983).

[80] A. D. Becke, "A new mixing of Hartree-Fock and local density-functional theories," *J. Chem. Phys.* **98**, 1372 (1993).

[81] Y. Zhao and D. G. Truhlar, "The M06 suite of density functionals for main group thermochemistry, thermochemical kinetics, noncovalent interactions, excited states, and transition elements: two new functionals and systematic testing of four M06-class functionals and 12 other functionals," *Theor. Chem. Acc* **120**, 215 (2008).

[82] S. Grimme, S. Ehrlich, and G. Goerigk, "Effect of the Damping Function in Dispersion Corrected Density Functional Theory," *J. Comput. Chem.* **32**, 1456 (2011).

[83] R. Ditchfield, W. J. Hehre, and J. A. Pople, "Self-Consistent Molecular-Orbital Method. IX. An Extended Gaussian-Type Basis for Molecular-Orbital Studies of Organic Molecules," *J. Chem. Phys.* **54**, 724 (1971).

[84] R. Krishnan, J. S. Binkley, R. Seeger, and J. A. Pople, "Self-consistent molecular orbital methods . XX . A basis set for correlated wave functions," *J. Chem. Phys.* **72**, 650 (1980).

[85] T. H. Dunning Jr, "Gaussian basis sets for use in correlated molecular calculations. I. The atoms boron through neon and hydrogen," *J. Chem. Phys.* **90**, 1007 (1989).

[86] C. M. Western, "PGOPHER, a Program for Simulating Rotational Structure, University of Bristol, http://pgopher.chm.bris.ac.uk," (2015).

[87] J. K. G. Watson, "Indeterminacies of Fitting Parameters in Molecular Spectroscopy," in *Handbook of High-resolution Spectroscopy*, Vol. 1, edited by M. Quack and F. Merkt (John Wiley & Sons, Ltd, New York, 2011) pp. 587–606.

[88] S. A. Cooke and P. Ohring, "Decoding Pure Rotational Molecular Spectra for Asymmetric Molecules," *J. Spectrosc.* **2013**, 1 (2013).

[89] N. A. Seifert, F. I. A., P. C., Z. D. P., N. J. L., S. A. L., S. R. D., L. A., et al., "AUTOFIT, an automated fitting tool for broadband rotational spectra, and applications to 1-hexanal," *J. Mol. Spectrosc.* **312**, 13 (2015).

[90] N. F. Ramsey, *Molecular Beams* (Oxford University Press, Oxford, 1985).

[91] N. F. Ramsey, "Thermal Beam Sources," in *Experimental Methods in the Physical Sciences - Atomic, Molecular, and Optical Physics: Atoms and Molecules*, Vol. 29, edited by F. Dunning and R. G. Hulet (Academic Press, Waltham, 1996) Chap. 1, pp. 1–20.

[92] M. D. Morse, "Supersonic Beam Sources," in *Experimental Methods in the Physical Sciences - Atomic, Molecular, and Optical Physics: Atoms and Molecules*, Vol. 29, edited by F. Dunning and R. G. Hulet (Academic Press, Waltham, 1996) Chap. 2, pp. 21–47.

[93] D. R. Miller, "Free Jet Sources," in *Atomic and Molecular Beam Methods*, Vol. 1, edited by G. Scoles (Oxford University Press, Oxford, 1988) Chap. 2, pp. 14–53.

[94] E. J. Campbell, L. W. Buxton, T. J. Balle, M. R. Keenan, and W. H. Flygare, "The gas dynamics of a pulsed supersonic nozzle molecular source as observed with a Fabry-Perot cavity microwave spectrometer," *J. Chem. Phys.* **74**, 829 (1981).

[95] J.-U. Grabow, "Fourier Transform Microwave Spectroscopy Measurement and Instrumentation," in *Handbook of High-resolution Spectroscopy*, Vol. 2, edited by M. Quack and F. Merkt (John Wiley & Sons, Ltd, New York, 2011) pp. 723–800.

[96] S. G. Kukolich and L. C. Sarkozy, "Design, construction, and testing of a large-cavity, 1-10 GHz Flygare-Balle spectrometer," *Rev. Sci. Instrum.* **82**, 094103 (2011).

[97] D. Schmitz, V. A. Shubert, T. Betz, and M. Schnell, "Multi-resonance effects within a single chirp in broadband rotational spectroscopy: The rapid adiabatic passage regime for benzonitrile," *J. Mol. Spectrosc.* **280**, 77 (2012).

[98] C. Weickhardt, F. Moritz, and J. Grotemeyer, "Time-of-flight mass spectrometry: State-of the-art in chemical analysis and molecular science," *Mass Spectrom. Rev.* **15**, 139 (1996).

[99] Z. R. Grabowski, K. Rotkiewicz, and W. Rettig, "Structural changes accompanying intramolecular electron transfer: focus on twisted intramolecular charge-transfer states and structures," *Chem. Rev.* **103**, 3899 (2003).

[100] E. Lippert, W. Lüder, F. Moll, W. Nägele, H. Boos, H. Prigge, and I. Seibold-Blankenstein, "Umwandlung von Elektronenanregungsenergie," *Angew. Chem.* **73**, 695 (1961).

[101] E. Lippert, W. Lüder, and H. H. Boos, *Proceedings of the Fourth International Meeting on Advances in Molecular Spectroscopy 1959*, edited by A. Mangini (Pergamon, Oxford, 1962) pp. 443–457.

[102] W. Rettig and V. Bonačić-Koutecký, "On a possible mechanism of the multiple fluorescence of p-N,N'-dimethylaminobenzonitrile and related compounds," *Chem. Phys. Lett.* **62**, 115 (1979).

[103] K. Rotkiewicz, K. Grellmann, and Z. Grabowski, "Reinterpretation of the anomalous fluorescense of p-N,N'-dimethylamino-benzonitrile," *Chem. Phys. Lett.* **19**, 315 (1973).

[104] W. Rettig, "Charge Separation in Excited States of Decoupled Systems - TICT Compounds and Implications Regarding the Development of New Laser Dyes and the Primary Process of Vision and Photosynthesis," *Angew. Chem. Int. Ed.* **25**, 971 (1986).

[105] U. Leinhos, W. Kuehnle, and K. A. Zachariasse, "Intramolecular charge transfer and thermal exciplex dissociation with p-aminobenzonitriles in toluene," *J. Phys. Chem.* **95**, 2013 (1991).

[106] I. Gómez, M. Reguero, M. Boggio-Pasqua, and M. A. Robb, "Intramolecular charge transfer in 4-aminobenzonitriles does not necessarily need the twist," *J. Am. Chem. Soc.* **127**, 7119 (2005).

[107] E. Gibson, A. Jones, and D. Phillips, "Laser-induced fluorescence of jet-cooled 4-Aminobenzonitrile," *Chem. Phys. Lett.* **146**, 1 (1988).

[108] A. J. Fleisher, R. G. Bird, D. P. Zaleski, B. H. Pate, and D. W. Pratt, "High-Resolution Electronic Spectroscopy of the Doorway States to Intramolecular Charge Transfer," *J. Phys. Chem. B* **117**, 4231 4240 (2013).

[109] G. Berden, J. van Rooy, W. Meerts, and K. A. Zachariasse, "Rotationally resolved electronic spectroscopy of 4-aminobenzonitrile," *Chem. Phys. Lett.* **278**, 373 (1997).

[110] D. Borst, T. Korter, and D. Pratt, "On the additivity of bond dipole moments. Stark effect studies of the rotationally resolved electronic spectra of aniline, benzonitrile, and aminobenzonitrile," *Chem. Phys. Lett.* **350**, 485 (2001).

[111] R. G. Bird, J. L. Neill, V. J. Alstadt, J. W. Young, B. H. Pate, and D. W. Pratt, "Ground state ^{14}N quadrupole couplings in the microwave spectra of N,N'-dimethylaniline and 4,4'-dimethylaminobenzonitrile," *J. Phys. Chem. A* **115**, 9392 (2011).

[112] E. M. Gibson, A. C. Jones, A. G. Taylor, W. G. Bouwman, D. Phillips, and J. Sandell, "Laser-induced fluorescence spectroscopy of 4-aminobenzonitrile, 4-(N,N-dimethylamino)benzonitrile, and their van der Waals complexes in a supersonic jet," *J. Phys. Chem.* **92**, 5449 (1988).

[113] H. Yu, E. Joslin, B. Crystall, T. Smith, W. Sinclair, and D. Phillips, "Spectroscopy and dynamics of jet-cooled 4-aminobenzonitrile (4-ABN)," *J. Phys. Chem.* **97**, 8146 (1993).

[114] G. Varsányi, *Assignments for vibrational spectra of seven hundred benzene derivatives* (Wiley, New York, 1974).

[115] K. Sakota, N. Yamamoto, K. Ohashi, M. Saeki, S. Ishiuchi, M. Sakai, M. Fujii, and H. Sekiya, "IR-dip and IR-UV hole-burning spectra of jet-cooled 4-aminobenzonitrile-(H$_2$O)$_1$. Observation of π-type and σ-type hydrogen-bonded conformers in the CN site," *Chem. Phys.* **283**, 209 (2002).

[116] E. Alejandro, C. Landajo, A. Longarte, J. A. Fernández, and F. Castaño, "Influence of the aliphatic chain on the (hydrogen-bonded) p-aminobenzonitrile complexes with methanol and ethanol," *J. Chem. Phys.* **119**, 9513 (2003).

[117] U. Spoerel and W. Stahl, "The Aniline-Water Complex," *J. Mol. Spectrosc.* **190**, 278 (1998).

[118] D. Lister, J. Tyler, J. Høg, and N. Larsen, "The microwave spectrum, structure and dipole moment of aniline," *J. Mol. Struct.* **23**, 253 (1974).

[119] K. Wohlfart, M. Schnell, J.-U. Grabow, and J. Küpper, "Precise dipole moment and quadrupole coupling constants of benzonitrile," *J. Mol. Spectrosc.* **247**, 119 (2008), arXiv:0709.2984 .

[120] A. Hatta, M. Suzuki, and K. Kozima, "Nuclear Quadrupole Effects in the Microwave Spectrum and Dipole Moment of Aniline," *Bull. Chem. Soc. Jpn.* **46**, 2321 (1973).

[121] C. Tanjaroon, R. Subramanian, C. Karunatilaka, and S. G. Kukolich, "Microwave Measurements of ^{14}N and D Quadrupole Coupling for (Z)-2-Hydroxypyridine and 2-Pyridone Tautomers," *J. Phys. Chem. A* **108**, 9531 (2004).

[122] WHO, "Model Lists of Essential Medicines, www.who.int/medicines/publications/essentialmedicines/en/," (2013).

[123] S. Offermanns and W. Rosenthal, *Encyclopedic Reference of Molecular Pharmacology*, Vol. 1 (Springer Verlag, 2004).

[124] K. Aktories, U. Förstermann, F. Hofmann, and K. Starke, *Allgemeine und spezielle Pharmakologie und Toxikologie*, 11th ed. (Elsevier, Munich, 2013).

[125] F. D. Hart and E. C. Huskisson, "Non-steroidal anti-inflammatory drugs. Current status and rational therapeutic use," *Drugs* **27**, 232 (1984).

[126] G. Dannhardt and W. Kiefer, "Cyclooxygenase inhibitors - current status and future prospects," *Eur. J. Med. Chem.* **36**, 109 (2001).

[127] H. Hao, G. Wang, and J. Sun, "Enantioselective pharmacokinetics of ibuprofen and involved mechanisms," *Drug Metab. Revi.* **37**, 215 (2005).

[128] G.-Q. Lin, Q.-D. You, and J.-F. Cheng, *Chiral Drugs: Chemistry and Biological Action* (John Wiley & Sons, Hoboken, New Jersey, 2011).

[129] A. Jubert, M. L. Legarto, N. E. Massa, L. L. Tévez, and N. B. Okulik, "Vibrational and theoretical studies of non-steroidal anti-inflammatory drugs Ibuprofen [2-(4-isobutylphenyl)propionic acid]; Naproxen [6-methoxy-α-methyl-2-naphthalene acetic acid] and Tolmetin acids [1-methyl-5-(4-methylbenzoyl)-1H-pyrrole-2-acetic acid]," *J. Mol. Struct.* **783**, 34 (2006).

[130] M. L. Vueba, M. E. Pina, and L. A. E. Batista de Carvalho, "Conformational stability of ibuprofen: assessed by DFT calculations and optical vibrational spectroscopy," *J. Pharm. Sci.* **97**, 845 (2008).

[131] Z. Fu, X. Li, and K. M. Merz, "Accurate assessment of the strain energy in a protein-bound drug using QM/MM X-ray refinement and converged quantum chemistry," *J. Comput. Chem.* **32**, 2587 (2011).

[132] L. Liu and H. Gao, "Molecular structure and vibrational spectra of ibuprofen using density function theory calculations," *Spectrochim. Acta. A. Mol. Biomol. Spectrosc.* **89**, 201 (2012).

[133] B. S. Selinsky, K. Gupta, C. T. Sharkey, and P. J. Loll, "Structural Analysis of NSAID Binding by Prostaglandin H 2 Synthase: Time-Dependent and Time-Independent Inhibitors Elicit Identical Enzyme Conformations," *Biochemistry (Mosc.)* **40**, 5172 (2001).

[134] A. Viegas, J. Manso, M. C. Corvo, M. M. B. Marques, and E. J. Cabrita, "Binding of ibuprofen, ketorolac, and diclofenac to COX-1 and COX-2 studied by saturation transfer difference NMR," *J. Med. Chem.* **54**, 8555 (2011).

[135] V. Limongelli, M. Bonomi, L. Marinelli, F. L. Gervasio, A. Cavalli, E. Novellino, and M. Parrinello, "Molecular basis of cyclooxygenase enzymes (COXs) selective inhibition," *PNAS* **107**, 5411 (2010).

[136] A. L. Blobaum and L. J. Marnett, "Structural and functional basis of cyclooxygenase inhibition," *J. Med. Chem.* **50**, 1425 (2007).

[137] S. T. Shipman, J. L. Neill, R. D. Suenram, M. T. Muckle, and B. H. Pate, "Structure Determination of Strawberry Aldehyde by Broadband Microwave Spectroscopy: Conformational Stabilization by Dispersive Interactions," *Journal of Physical Chemistry Letters* **2**, 443 (2011).

[138] G. Churchill, R. Hassey, K. Utzat, J. Fournier, R. K. Bohn, and H. H. Michels, "Two Conformers Observed and Characterized in Isobutylbenzene," *J. Phys. Chem. A* **114**, 1029 (2010).

[139] M. A. Zayed, M. F. Hawash, M. A. Fahmey, and A. M. M. El-Gizouli, "Investigation of ibuprofen drug using mass spectrometry, thermal analyses, and semi-empirical molecular orbital calculation," *J. Therm. Anal. Calorim.* **108**, 315 (2012).

[140] G. Caviglioli, P. Valeria, P. Brunella, C. Sergio, A. Attilia, and B. Gaetano, "Identification of degradation products of Ibuprofen arising from oxidative and thermal treatments," *J. Pharm. Biomed. Anal.* **30**, 499 (2002).

[141] R. Scharnow, *Codiertes Handbuch der Güter des Seetransports* (1986).

[142] J. C. Brookes, A. P. Horsfield, and A. M. Stoneham, "Odour character differences for enantiomers correlate with molecular flexibility," *J. R. Soc. Interface* **6**, 75 (2009).

[143] H. Mouhib, W. Stahl, M. Lüthy, M. Büchel, and P. Kraft, "Cassis Odor through Microwave Eyes: Olfactory Properties and Gas- Phase Structures of all the Cassyrane Stereoisomers and its Dihydro Derivatives," *Angew. Chem. Int. Ed.* **50**, 5576 (2011).

[144] H. Mouhib and W. Stahl, "Conformational Analysis of Green Apple Flavour: The Gas-Phase Structure of Ethyl Valerate Validated by Microwave Spectroscopy," *ChemPhysChem* **13**, 1297 (2012).

[145] M. Bandell, G. Story, S. Hwang, V. Viswanath, S. Eid, M. Petrus, T. Earley, and A. Patapoutian, "Noxious Cold Ion Channel TRPA1 Is Activated by Pungent Compounds and Bradykinin," *Neuron* **41**, 849 (2004).

[146] J. Dennis and T. Y. Shibamoto, "Photochemical Products of Trans-Cinnamic Alcohol: Possible Formation of Skin Irritants and Allergens," *J. Toxicol. Cutaneous Ocul. Toxicol.* **9**, 149 (1990).

[147] W. E. Steinmetz, "The Application of Low-Resolution Microwave Spectroscopy to Conformational Analysis," *J. Am. Chem. Soc.* , 685 (1973).

[148] T. Egawa, R. Matsumoto, D. Yamamoto, and H. Takeuchi, "Molecular structure of trans-cinnamaldehyde as determined by gas electron diffraction aided by DFT calculations," *J. Mol. Struct.* **892**, 158 (2008).

[149] J. Watson, *Vibrational Spectra and Structure* (Elsevier, 1977) p. 1.

[150] C. Blom, G. Grassi, and A. Bauder, "Molecular Structure of s-cis- and s-trans-Acrolein Determined by Microwave Spectroscopy," *J. Am. Chem. Soc.* **106**, 7427 (1984).

[151] C. Puzzarini, E. Penocchio, M. Biczysko, and V. Barone, "Molecular Structure and Spectroscopic Signatures of Acrolein: Theory Meets Experiment," *J. Phys. Chem. A* **118**, 6648 (2014).

[152] T. Oka, "On negative inertial defect," *J. Mol. Struct.* **352/353** (1995).

[153] J. Watson, A. Roytburg, and W. Ulrich, "Least-Squares Mass-Dependence Molecular Structures," *J. Mol. Spectrosc.* **196**, 102 (1999).

[154] G. C. Pimentel and A. L. McClellan, "HYDROGEN BONDING," *Annu. Rev. Phys. Chem.* **22**, 347 (1971).

[155] T. Steiner, "The Hydrogen Bond in the Solid State," *Angew. Chem. Int. Ed.* **41**, 48 (2002).

[156] C. L. Perrin and J. B. Nielson, "STRONG HYDROGEN BONDS IN CHEMISTRY AND BIOLOGY," *Annu. Rev. Phys. Chem.* **48**, 511 (1997).

[157] S. Scheiner, "AB INITIO STUDIES OF HYDRGOGEN BONDS: The Water Dimer Paradigm," *Annu. Rev. Phys. Chem.* **45**, 23 (1994).

[158] E. J. Cocinero, A. Lesarri, P. Ècija, A. Cimas, B. G. Davis, F. J. Basterretxea, J. A. Fernàndez, and F. Castaño, "Free Fructose is conformationally locked," *J. Am. Chem. Soc.* **135**, 2845 (2013).

[159] P. Çarçabal, R. A. Jockusch, I. Hünig, L. C. Snoek, R. T. Kroemer, B. G. Davis, D. P. Gamblin, I. Compagnon, et al., "Hydrogen bonding and cooperativity in isolated and hydrated sugars: mannose, galactose, glucose, and lactose," *J. Am. Chem. Soc.* **32**, 11414 (1976).

[160] J. Screen, E. C. Stanca-Kaposta, D. P. Gamblin, B. Liu, N. A. Macleod, L. C. Snoek, B. G. Davis, and J. P. Simons, "IR-Spectral Signatures of Aromatic-Sugar Complexes: Probing Carbohydrate-Protein Interactions," *Angew. Chem. Int. Ed.* **46**, 6648 (2007).

[161] A. Zehnacker and M. A. Suhm, "Chirality Recognition between Neutral Molecules in the Gas Phase," *Angew. Chem. Int. Ed.* **47**, 6970 (2008).

[162] T. B. Adler, N. Borho, M. Reiher, and M. A. Suhm, "Chirality-Induced Switch in Hydrogen-Bond Topology: Tetrameric Methyl Lactate Clusters in the Gas Phase," *Angew. Chem. Int. Ed.* **45**, 3440 (2006).

[163] M. Albrecht, A. Borba, K. Le Barbu-Debus, R. Dittrich, B. ans Fausto, S. Grimme, A. Mahjoub, M. Nedìc, U. Schmitt, et al., "Chirality influence on the aggregation of methyl mandelate," *New J. Chem.* **34**, 1266 (2010).

[164] J. M. Hollis, F. J. Lovas, and P. R. Jewell, "Interstellar Glycolaldehyde: The First Sugar," *Astrophys. J.* **540**, 107 (2000).

[165] J. K. Jørgensen, C. Favre, S. E. Bisschop, T. L. Bourke, E. F. Van Dishoeck, and M. Schmalzl, "Detection of the simplest sugar, glycolaldehyde, in a solar-type protostar with ALMA," *Astrophysical Journal Letters* **757**, 1 (2012).

[166] K.-M. Marstokk and H. Møllendal, "Microwave spectra of isotopic glycolaldehydes, substitution structure, intramolecular hydrogen bond and dipole moment," *J. Mol. Struct.* **16**, 259 (1973).

[167] H. H. Jensen, H. Møllendal, and E. Nilssen, "An ab initio study of internal hydrogen bonding and conformational properties of glycolaldehyde," *J. Mol. Struct.* **30**, 145 (1976).

[168] H. Michelsen and P. Klaboe, "Spectroscopic studies of glycolaldehyde," *J. Mol. Struct.* **4**, 293 (1969).

[169] Y. Kobayashi, H. Takahara, H. Takahashi, and K. Higasi, "Infrared and Raman studies of the structure of crystalline glygolaldehyde," *J. Mol. Struct.* **32**, 235 (1976).

[170] J. Altnöder, J. J. Lee, K. E. Otto, and M. A. Suhm, "Molecular Recognition in Glycolaldehyde, the Simplest Sugar: Two Isolated Hydrogen Bonds Win Over One Cooperative Pair," *Chemistry Open* **1**, 269 (2012).

[171] C. Medcraft, R. Wolf, and M. Schnell, "High-resolution spectroscopy of the chiral metal complex [CpRe(CH$_3$)(CO)(NO)]: a potential candidate for probing parity violation," *Angew. Chem. Int. Ed.* **53**, 11656 (2014).

[172] N. A. Seifert, D. P. Zaleski, C. Pérez, J. L. Neill, B. H. Pate, M. Vallejo-López, A. Lesarri, E. J. Cocinero, et al., "Probing the C-H...π Weak Hydrogen Bond in Anesthetic Binding: The Sevoflurane-Benzene Cluster," *Angew. Chem. Int. Ed.* **53**, 3210 (2014).

[173] S. Zinn, C. Medcraft, T. Betz, and M. Schnell, "Structure determination of trans-cinnamaldehyde by broadband microwave spectroscopy," *Phys. Chem. Chem. Phys.* **17**, 16080 (2015).

[174] P. B. Carroll, B. McGuire, D. Zaleski, J. Neill, B. Pate, and S. Widicus Weaver, "The pure rotational spectrum of glycolaldehyde isotopologues observed in natural abundance," *J. Mol. Spectrosc.* **284**, 21 (2013).

[175] B. Jeziorski, R. Moszynski, and K. Szalewicz, "Perturbation Theory Approach to Intermolecular Potential Energy Surfaces of van der Waals Complexes," *Chem. Rev.* **94**, 1887 (1994).

[176] T. M. Parker, L. A. Burns, R. M. Parrish, A. G. Ryno, and C. D. Sherrill, "Levels of Symmetry Adapted Perturbation Theory (SAPT). I. Efficiency and Performance for Interaction Energies," *J. Chem. Phys.* **140**, 094106 (2014).

[177] J. M. Turney, A. C. Simmonett, R. M. Parrish, E. G. Hohenstein, F. A. Evangelista, J. T. Fermann, B. J. Mintz, L. A. Burns, et al., "Psi4: An Open-Source Ab Initio Electronic Structure Program," *Wiley Interdiscip. Rev. Comput. Mol. Sci.* **2**, 556 (2012).

[178] J.-R. Aviles-Moreno, J. Demaison, and T. R. Huet, "Conformational Flexibility in Hydrated Sugars: the Glycolaldehyde-Water Complex," *J. Am. Chem. Soc.* **128**, 10467 (2006).

[179] E. Fischer, "Einfluss der Configuration auf die Wirkung der Enzyme," *Chem. Ber.* **27**, 2985 (1894).

[180] J. Lehn, "Supramolecular chemistry," *Science* **260**, 1762 (1993).

[181] R. M. Lees and J. G. Baker, "Torsion-Vibration-Rotation Interactions in Methanol. I. Millimeter Wave Spectrum," *J. Chem. Phys.* **48**, 5299 (1968).

[182] R. M. Lees, F. J. Lovas, W. H. Kirchhoff, and D. R. Johnson, "Microwave Spectra of Molecules of Astrophysical Interest: III. Methanol," *J. Phys. Chem. Ref. Data* **2**, 205 (1973).

[183] F. Lovas and H. Hartwig, "The Microwave Spectrum of the Methanol Dimer for K = 0 and 1 States," *J. Mol. Spectrosc.* **185**, 98 (1997).

[184] P. A. Stockmana, G. A. Blake, F. J. Lovas, and R. D. Suenram, "Microwave rotation-tunneling spectroscopy of the water-methanol dimer: Direct structural proof for the strongest bound conformation," *J. Chem. Phys.* **107**, 3782 (1997).

[185] A. Paiva, P. Kistemaker, and T. Weeding, "A REMPI investigation of the minimum energy conformations of diphenyl ether," *Int. J. Mass Spectrom.* **221**, 107 (2002).

[186] G. Fraser, F. Lovas, and R. Suenram, "On the Apparent Methyl Internal-Rotation Barrier Decrease in Weakly Bound Methanol Complexes," *J. Mol. Spectrosc.* **167**, 231 (1994).

[187] F. J. Lovas, R. D. Suenram, G. T. Fraser, C. W. Gillies, and J. Zozom, "The microwave spectrum of formamide-water and formamide-methanol complexes," *J. Chem. Phys.* **88**, 722 (1988).

[188] X.-Q. Tan, L. Sun, and R. Kuczkowski, "The Methanol-Ar Complex: Apparent Reduction of the Methyl Group Internal Rotation Barrier," *J. Mol. Spectrosc.* **171**, 248 (1995).

[189] X.-Q. Tan, I. I. Ioannou, and R. L. Kuczkowski, "The methanol-HCl complex: structure and methyl group internal rotation barrier," *J. Mol. Struct.* **356**, 105 (1995).

[190] L. Sun, X.-Q. Tan, J. J. Oh, and R. L. Kuczkowski, "The microwave spectrum and structure of the methanol-SO_2 complex," *J. Chem. Phys.* **103**, 6440 (1995).

[191] X.-Q. Tan, I. I. Ioannou, K. B. Foltz, and R. L. Kuczkowski, "The Methanol-Trimethylamine Complex: Structure and Large Amplitude Motions," *J. Mol. Spectrosc.* **193**, 181 (1996).

[192] F. Lovas, S. Belov, M. Tretyakov, J. Ortigoso, and R. Suenram, "The Microwave Spectrum and Structure of the CH_3OH CO Dimer," *J. Mol. Spectrosc.* **167**, 191 (1994).

[193] M. Schmitt, J. Küpper, D. Spangenberg, and A. Westphal, "Determination of the structures and barriers to hindered internal rotation of the phenol-methanol cluster in the S_0 and S_1 states," *Chem. Phys.* **254**, 349 (2000).

Danksagung

An dieser Stelle möchte ich mich bei allen bedanken, die zum gelingen dieser Arbeit beigetragen haben.

Ganz besonders möchte ich meiner Betreuerin Melanie Schnell danken, die mich mit Ihrer positiven Art in der Gruppe aufgenommen hat und meine Arbeit immer mit größtem Interesse und Vertrauen begleitet hat.

Herrn Prof. Weller danke ich für die Co-Betreuung meiner Arbeit und für die Übernahme des Zweitgutachtens.

Vielen Dank an Dr. Thomas Betz für die Zusammenarbeit in meinen ersten beiden Jahren und die Einweisung in die Vakuumtechnik.

I would like to thank Dr. Cristóbal Pérez for his continuous work and improvement of the "COMPACT" spectrometer, which built the basis for the study of the weakly bound complexes.

I would like to thank Dr. Chris Medcraft for the successful teamwork on the complex measurements, for proof reading my thesis, and for insights into new sports.

Danke an David Schmitz für die hilfreichen Diskussionen und Ratschläge, für den Kaffee am morgen und die angenehme Sitznachbarschaft.

Many thanks to all members of the CoComol group for the nice working atmosphere. Especially to Sérgio Domingos, Jack Graneek, Chris Medcraft, Simon Merz, David Schmitz, Alvin Shubert, and Amanda Steber for the awesome time I have with you. I will miss our senseless lunch-break discussion, the Friday beer and to beat Jack in playing kicker.

Ein ganz besonderer Dank gilt auch meinen Eltern und meiner ganzen Familie für Ihren unaufhöhrlichen Rückhalt.

Zum Schluss möchte ich vom ganzen Herzen meinem Mann Johannes danken. Deine Geduld und Dein Vertrauen in mich haben diese Arbeit erst möglich gemacht.

Selbständigkeitserklärung

Hiermit erkläre ich an Eides statt, dass ich die vorliegende Dissertationsschrift selbst verfasst und keine anderen als die angegeben Quellen und Hilfsmittel benutzt habe.

Hamburg, den 06. Juni 2016

_____
Unterschrift